POLITECNICO DI TORINO

Corso di Laurea Magistrale
in Automotive Engineering

Master degree thesis

Fuel cell vehicle simulation and optimization based on ADVISOR

Supervisor: Chiar.^{mo} Prof. Ing. Andrea Tonoli

Co-supervisor: Ing. Sara Luciani

Applicant: Lin Jianyang

Academic Year 2020/2021

Acknowledgments

Just like the simulation approach of ADVISOR, life can be understood backward but must be lived forward. Upon the completion of the thesis work, looking back at the year spending in Politecnico di Torino, I am grateful for those who offer their generous help.

I would like to express my special thanks to my co-supervisors, Sara Luciani, who gave me many valuable suggestions and continuous help when carrying out the research. My heartfelt gratitude goes to my supervisor, Andrea Tonoli, who has set an example of an excellent engineer, researcher, and professor and influences me a lot.

I would like to take this opportunity to express my love to my family, who have supported me in many ways. I'm also indebted to my fiancee Wu Jingmin, who has accompanied me through the journey of life.

Abstract

Fuel cell vehicles regain their momentum and become the hot topic of hybrid electric vehicle research with the increasingly severe environmental issues and the maturity of relating technologies.

The thesis works aim to investigate the possibility of extending the FCV's driving range by improving the efficiency of the fuel cell and the electric machine based on ADVISOR. The thesis works can be divided into three stages: in the first stage, several control strategies were proposed, including power follower control, discretization method, fuzzy logic control. These proposed control strategies were compared with the power follower control strategy in ADVISOR. The simulations were run over three drive cycles with SUV parameters loaded. The simulated SUV is powered by two energy sources, which are a fuel cell modeled by KTH and a lithium-ion battery. In the second stage, with the goal of increasing the efficiency of the electric machine, a two-speed gearbox was introduced to the driveline. Gear ratio pair and shifting strategy were selected. The impact of the two-speed gearbox on fuel economy was studied. In the third stage, we developed a fuzzy logic controller with driving intention prediction and applied it to the SUV propelled by the Toyota Mirai fuel cell system.

Table of Contents

1.Introduction

1.1 Background

The development of the automobile industry caused a shortage of energy and led to the deterioration of the ecological environment. The environmental deterioration is mainly due to the burning of fossil fuels, where the exhaust gas contains carbon dioxide, nitrogen oxides (NOx), particulate matter (PM), carbon monoxide (CO), and so on. Particulate matter has been proven to cause exacerbation of asthma, respiratory infections, and a significant impact on the development and function of children's lungs. Carbon dioxide is a greenhouse gas, which has been paid attention to for a long time. It is mainly produced by the combustion of carbon, of which 25% comes from automobile exhaust emission. With a large amount of carbon dioxide emissions, the greenhouse effect is becoming more and more severe, and the temperature is rising year by year. Moreover, car emissions have also caused environmental degradation such as acid rain and photochemical smog. So it is vital for the automotive industry to make a shift towards environmentally friendly energy.

Fuel cell vehicles can help cut greenhouse gas emissions by substituting fossil fuels with hydrogen as energy carriers and contribute to achieving a climate-neutral economy. It is strategically important not only for the government but also for car manufacturers to focus on FCVs in transition to sustainable mobility. The advantages of FCVs are apparent. First, Fuel cell vehicles propelled by the electrochemical reaction of hydrogen have zero pollution, and their by-product is pure water. Second, not limited by Carnot cycles, the efficiency of fuel cell is three times the one of internal combustion engine. Third, when comparing with EV, the FCVs outperforms in terms of driving range and charge time.

Supportive policies related to hydrogen and fuel cell can be seen in many countries and regions. EU has support hydrogen power and fuel cell research and development since the second Framework Program (FP2) in 1986. In February 2019, Fuel Cells and Hydrogen Joint Undertaking (FCHJU) released the Hydrogen Roadmap Europe, which proposed a roadmap for hydrogen energy development towards 2030 and 2050 [1]. In China, the Ministry of Science and Technology launched many scientific and technological projects on hydrogen and FCVs from the 10th Five Year Plan to the 13th Five Year Plan. Fiscal subsidy policies for FCVs were introduced by four ministries [2]. Japan Revitalization Strategy and the Strategic Energy Plan considers hydrogen as strategic energy [3][4]. The industry is well planned, which puts Japan in a leading position of this field. The US is the first player in the field of the hydrogen economy. In the 1970s, the International Association for Hydrogen was established. In recent years, tax credits were revised to support and stimulate development. DOE in the US plays a primary role in research and development activities.

1.2 Introduction of energy management system

Hybrid vehicles usually involve two sets of control tasks. One is component-level control (also called low-level control), the second one is called high-level control. This high-level control is referred to the energy management system (EMS). In a conventional vehicle, there is no need for the presence of EMS. The driver decides the instant power delivery through pedal and brakes. The power desired is then translated into low-level controller. Because fuel cell electric vehicles are powered by several energy sources, an EMS is required. Energy management system in hybrid fuel cell vehicle consists in deciding the amount of power delivered by the fuel cell and by the battery or supercapacitor respectively at each instant while meeting the system constraints and achieving some specific goals (for example, sustaining the state of charge of the battery or achieving a better fuel economy).

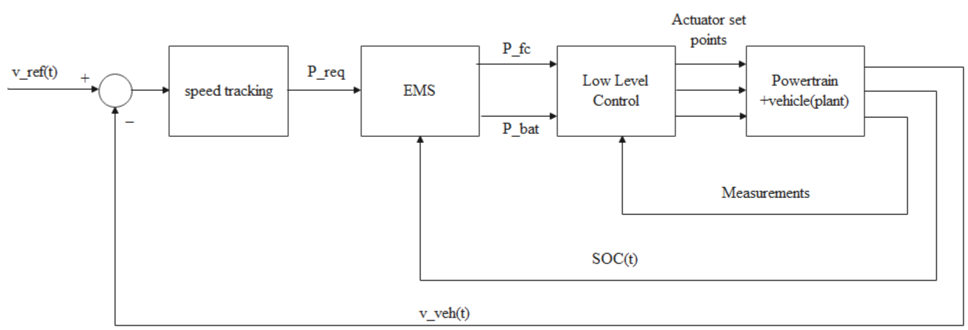

Figure 1.1 Role of EMS

Figure 1.1 shows the roles played by EMS in a FCV. The power request is calculated according to the drive cycle, and then sent to EMS as an input. The EMS decides the power split between onboard energy sources, which are the fuel cell and the battery. P_{fc} and P_{batt} are then sent to the low-level controller so that the actuator set points are determined. The plant feeds back the measurements to the low-level control.

The EMS could be classified into several families, as is shown in Figure 1.2. Two main kinds of control methods could be identified. The first one is rule-based control strategy. The main feature of this kind control strategy is the effectiveness in real-time implementation. Decisions of fuel cell operating points made by this kind of control are based on human knowledge, intuition, or from the information obtained by the offline optimization method. Finally, a set of rules is generated to control the power delivery. The second family is model-based optimization control strategy. This kind of control strategy is optimized by minimizing the cost function designer predefined, leading to a global or local optimal. Due to its computational complexity and requirement of prior knowledge of the drive cycle (for example, dynamic programming), they are limited in practical implementation. However, the model-based control strategy is helpful for benchmarking and generating rules for online implementation.

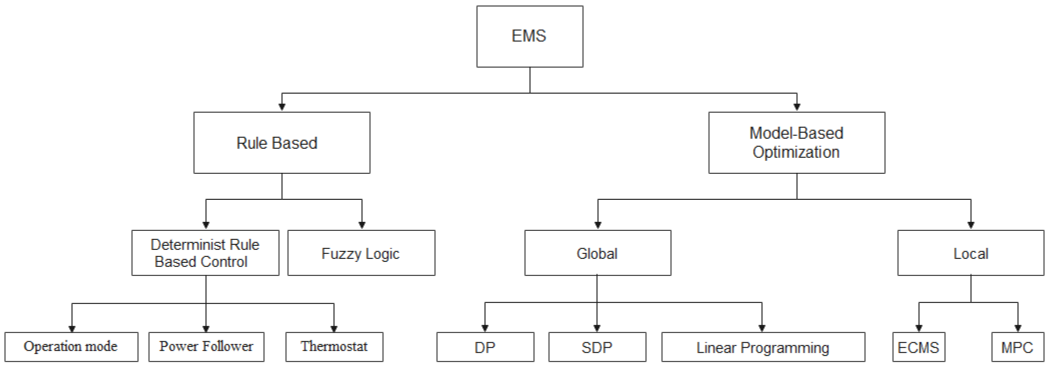

Figure 1.2 Classification of EMS

1.3 Layout of the thesis

FCVs are regaining their momentums with the increasing urges to address the issues posed by pollution. Related policies published by different countries accelerate the development of FCVs. Therefore, works in this thesis were conducted to simulate FCVs and to investigate the fuel consumption and efficiency in ADVISOR. The aim of the paper is to extend the mileage of FCVs by increasing the efficiency of the fuel cell and the electric machine. Simulations were performed based on ADVISOR in Matlab/Simulink environment. Chapter 2 and chapter 3 give information of the fuel cell and the fuel cell vehicle. Modeling techniques of different components in ADVISOR are presented in chapter 4. Different control strategies are proposed and compared with the KTH fuel cell model in chapter 5. The two-speed transmission is introduced to be integrated into the driveline in chapter 6, aiming to improve the efficiency of the electric machine. Fuzzy logic with the prediction of driving intention is implemented in the vehicle propelled by the Toyota Mirai fuel cell in chapter 7.

2. PEMFC structure and theory

2.1 PEMFC basic

The fuel cell is an energy converter that converts chemical energy into electric energy by electrochemical reaction. Compared with batteries, they all consist of anodes, cathodes, and electrolytes. The difference is: when the reaction substance in the battery is completely consumed, it can no longer generate electric energy; And for the fuel cell, as long as fuel and oxidant are fed into fuel cell, electricity can be drawn continuously. PEMFC is short for 'proton exchange membrane fuel cell' or 'polymer electrolyte membrane fuel cell'. The core of a PEM fuel cell is a polymer membrane, which enables the reaction to happen.

The working principle of PEMFC is essentially a reverse process of water electrolysis, shown in Figure 2.1. In the process of water electrolysis, an external power supply is needed to produce hydrogen and oxygen; In the reaction process of PEMFC, hydrogen and oxygen are electrochemically turned into the water with the aid of catalysts, producing electric energy. Electrochemical reactions happen at the surface of the catalyst locating at the interface between the electrolyte and the membrane. Hydrogen is fed on the anode side. Due to the presence of catalysts, hydrogen molecules are decomposed into protons and electrons, as described in equation 2.1.

$$H_2 \rightarrow 2H^+ + 2e^- \quad (2.1)$$

Protons go through the membrane, while the electrons take the path of the collector and external circuit and perform the useful work. On the cathode side, oxygen is supplied. Together with the electrons coming from the external circuit, at the surface of catalysts, the following reaction (2-2) takes place.

$$4H^+ + 4e^- + O_2 \rightarrow 2H_2O \quad (2.2)$$

The water produced in the form of gas or liquid is recycled for humidifying oxygen and hydrogen. Apart from the water and electricity, a large amount of heat is also generated. For keeping the fuel cell at its operating temperature (usually less than 85°C), a cooling system is needed.

So the main process could be described by the following overall equation:

$$H_2 + \frac{1}{2}O_2 \rightarrow H_2O + 286\ kJ \cdot mol^{-1} \quad (2.3)$$

The equation is only validated at 25 °C, the value $286\ kJ \cdot mol^{-1}$ is known as the higher heating value of hydrogen. It is the amount of energy released when 1 mol of hydrogen is completely combusted, and the product is in liquid form. In another case where the product water is in vapor form, less heat is released (i.e., $241\ kJ \cdot mol^{-1}$ known as lower heating value). The difference between higher heating value and lower heating value is the heat evaporation of water at 25°C.

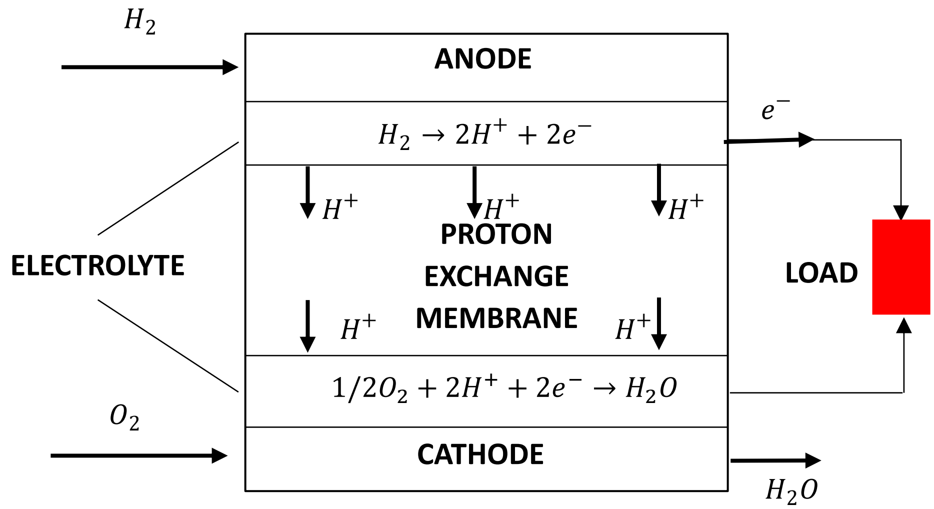

Figure 2.1 Working Principle of Proton Exchange Membrane Fuel Cell

The HHV and LHV are introduced here for these are the maximum energy 1 mol of hydrogen can deliver and are helpful for efficiency calculation. The portion that can be converted to the electricity of this reaction enthalpy is called Gibbs free energy, calculated as:

$$\Delta G = \Delta H - T\Delta S \quad (2.4)$$

Very often, the theoretical efficiency of fuel cell stack can be obtained by simply using ΔG divided by ΔH, that is:

$$\eta = \frac{\Delta G}{\Delta H} \quad (2.5)$$

Speaking of useful electric work, it can be calculated as the product of charge and potential:

$$W_{el} = qE \quad (2.6)$$

Where q is the charge, W_{el} is the useful work, E is the potential.

The amount of charge can then be calculated as:

$$q = nF \quad (2.7)$$

Where n represents the number of electrons per mole of hydrogen, F is Faraday's constant.

And W_{el} corresponds to Gibbs free energy:

$$W_{el} = -\Delta G \quad (2.8)$$

Substituting the equation 2.6 and equation 2.7 into equation 2.8 yields:

$$E = \frac{-\Delta G}{nF} \quad (2.9)$$

The voltage of a single cell of proton exchange membrane fuel cell (PEMFC) is generally between 0.5-1.2V, so the single cell can not be used directly. However, several cells can reach hundreds of volts and hundreds of kilowatts through proper connection. In practical application, according to the demand of power and voltage, several single cells are connected in series to form a stack.

The polarization curve, representing the voltage-current relationship, is critical to evaluate the performance of the fuel cell. We can observe that there are typically three stages in the polarization curve. The voltage decreases rapidly in the low-current and high-voltage region in the first stage. In the second stage, the voltage drops linearly as the current increases. In the last stage, the voltage decreases rapidly. Actually, the presence of these three stages is due to the cell undergoing three different losses: activation losses, ohmic losses and concentration losses.

Activation losses occur when low current is drawn from the fuel cell. The losses are caused by the slowness of the reaction taking place on the surface of the electrodes. Because the electrode, electrolyte and internal connections have their resistance, linear losses occur. As for concentration losses, also denoted as mass transportation losses, they are resulted from insufficient transportation of reactants to the electrode surface. Additionally, another type of loss, called crossover losses, is neglected here, for the value of this kind of loss is small. Figure 2.2 illustrates the phenomenon as mentioned above.

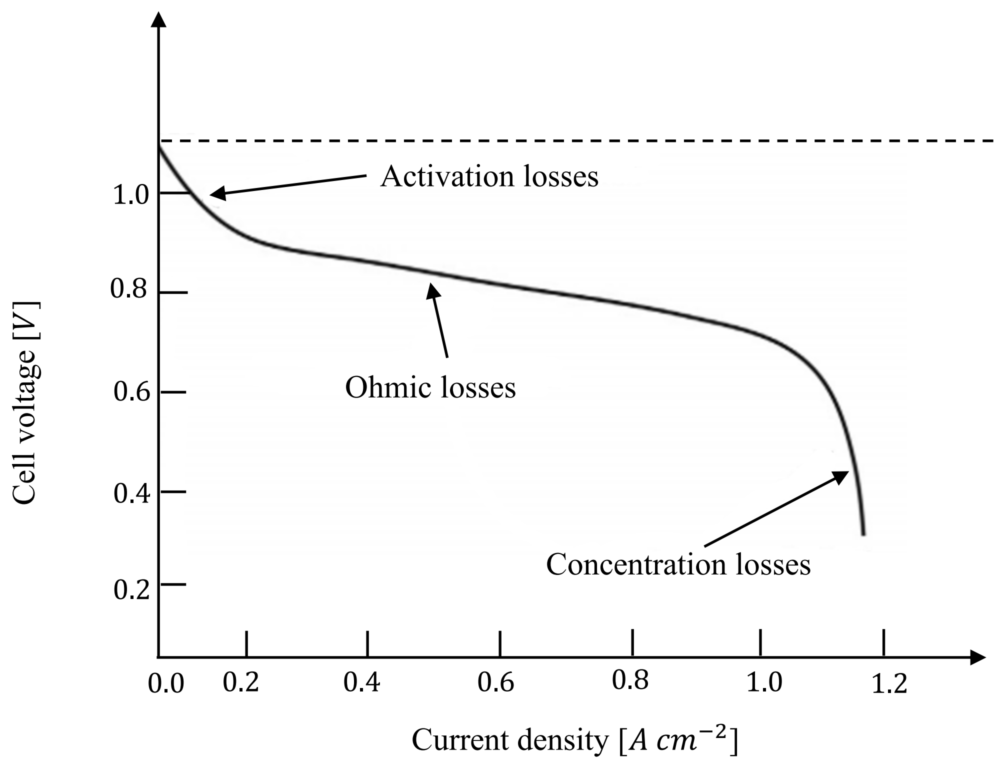

Figure 2.2 Polarization Curve of Fuel cell

2.2 PEMFC structure and its components

MEA (Membrane Electrode Assembly) is the core component of the fuel cell, which is made up of polymer electrolyte membrane, catalyst layers, and gas diffusion layers. Its layout is shown in Figure 2.3.

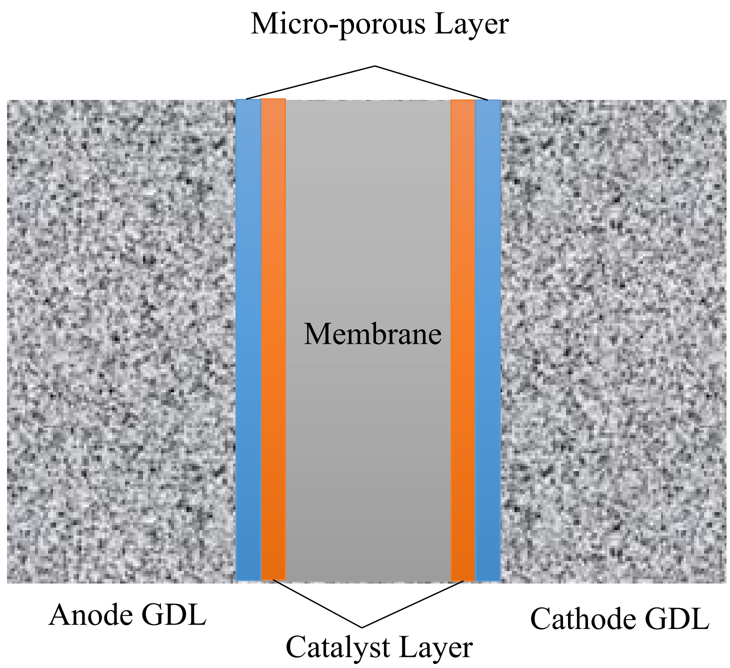

Figure 2.3 Layout of MEA

The polymer electrolyte membrane, also called the proton exchange membrane, conducts the positive ions while blocks the electrons from anode to cathode. So the membrane must present high protonic conductivity, mechanical and chemical stability in the environment of the fuel cell. It also serves as a barrier to keep the hydrogen and oxygen from mixing together. Nafion is the well-known material of membrane, whose structure is displayed in Figure 2.4. The SO_3H group is bonded to the Teflon-like backbone. At the end of the side chain are actually $SO_3{}^{2-}$ and H^+, which is highly hydrophilic. Well-hydrated regions are created around this side chain. The movement of H^+ in this area makes the membrane protonic conductive. To sum up, the conductivity of the proton of the membrane depends on the structure of the membrane and water contents.

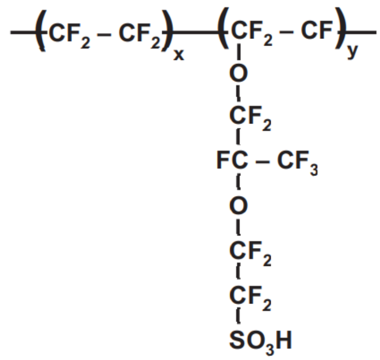

Figure 2.4 Structure of PFSA polymer (Nafion)

Catalyst layers are located on both sides of the membrane. Platinum particles in size of 2-5 nm disperse on the surface of carbon powder support and mix with ion-conducting polymer. Then they are sandwiched between the PEM and GDLs. The catalysts speed up the process of hydrogen molecules splitting into protons and electrons on the anode side. On the cathode side, the catalysts enable the oxygen reduction reaction.

Gas diffusion layers locate outside the catalyst layers. They perform the function of evenly distributing the gas. GDL is typically composed of a sheet of carbon paper and has a porous structure. In many cases, the microporous layer is added to the inner surface of the GDL. It is coated with a thin layer of high-surface-area carbon and mixed with PTFE. The function of GDL can be summarized as follows:

1. The membrane and catalyst layers are filmy, GDLs act as supports to them.
2. GDLs conduct heat generated in the reaction to the bipolar plates.
3. GDLs conduct the electrons to complete the electrical path.
4. GDLs provide a way for reactant gases to get to the catalyst layer and for product water to go out to the flow field channels.

An explosive diagram in Figure 2.5 shows the main components of the fuel cell stack.

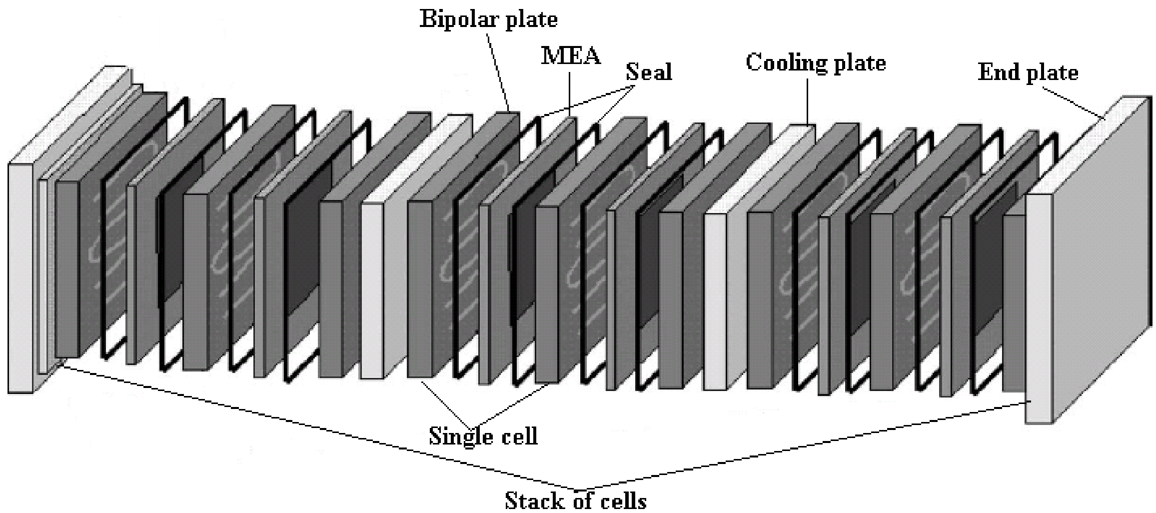

Figure 2.5 Exploded View of Fuel Cell Stack

We can see that the fuel cell stack consists of many single cells. The two plates on each side of the MEA are called bipolar plates. On one side of the bipolar plate it is the anode of a single cell. On another side of the plate, it is the cathode of an adjacent single cell. It is the reason called 'bipolar'. Single cells are connected electrically by the plates. Flow field channels are carved on the surface of each side of bipolar plates, the reactant gases of different cells are separated by these plates. It is worthwhile mentioning that the bipolar plates also play significant roles in cooling. So, one of the requirements for the bipolar plates is having good thermal conductivity.

Seals can be seen beside the GDLs. As mentioned, GDLs have a porous structure. The seal is used here to seal the skirts of GDLs to prevent the gas from leaking out.

Collectors aim to distribute the current evenly. The end plates transmit the pressure of screws, compressing different layers of the fuel cell stack.

2.3 Hydrogen/Oxygen supply system

2.3.1 Hydrogen supply system

One way to store hydrogen on the vehicle is to use a high-pressure tank. Usually, the pressure inside the tank for automotive application is 350 bars and 700 bars. A lightweight tank made of an aluminum body wrapped by composite fiber and resin could achieve the storage density of 5% hydrogen by weight. The second way is to store the hydrogen in liquid form. The tanks used to store the liquid hydrogen must be specially constructed and insulated to minimize the hydrogen's boil-off. This way could achieve a storage density of 14.2% by weight. Another way is to store hydrogen in metal hydrides. Storage efficiency of only 1.0% to 1.4% hydrogen by weight can be achieved in this way because metals are not lightweight materials.

There are two ways for the hydrogen that comes from the tank to be supplied to the fuel cell anode inlet. The first one is the simplest, which is called dead-end mode. This mode only requires a preset pressure regulator to reduce the pressure. It has many drawbacks: first, any impurities, including water vapor in hydrogen, will accumulate in the anode of the fuel cell. Second, impurities may diffuse from the air side. These drawbacks could be overcome by adding hydrogen purge. Due to the dead-end mode is not able to achieve mass balance and its efficiency is too low (excessive hydrogen will flow out of the system), a close loop mode is favored. The close-loop system recycles the hydrogen and separates the water. A humidifier and heat exchanger would be added before the anode to humidify the fuel to 100% and control its temperature.

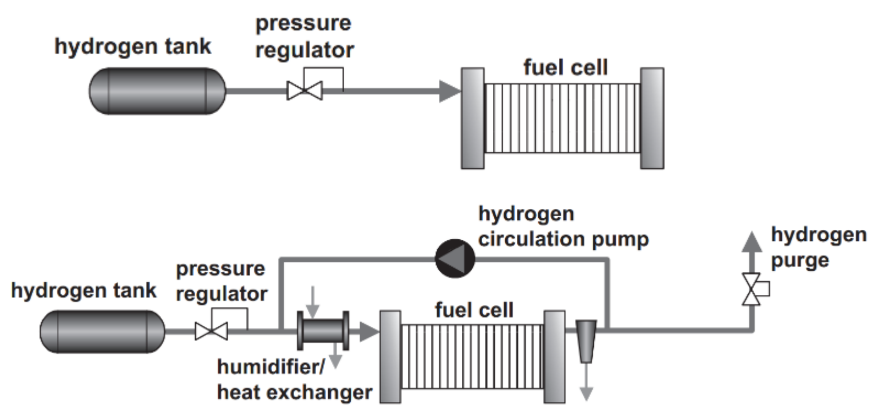

Figure 2.6 Schemes of Hydrogen Supply system (1) Dead-end mode; (2) Close-loop mode

2.3.2 Air supply system

The air supply system has a big impact on the stack performance. To be more exact, the performance varies with the operating pressure and the air stoichiometry which the air supply system is providing. As can be seen in Figure 2.7, the improvement in the voltage does not increase linearly as the air pressure and stoichiometry increase.

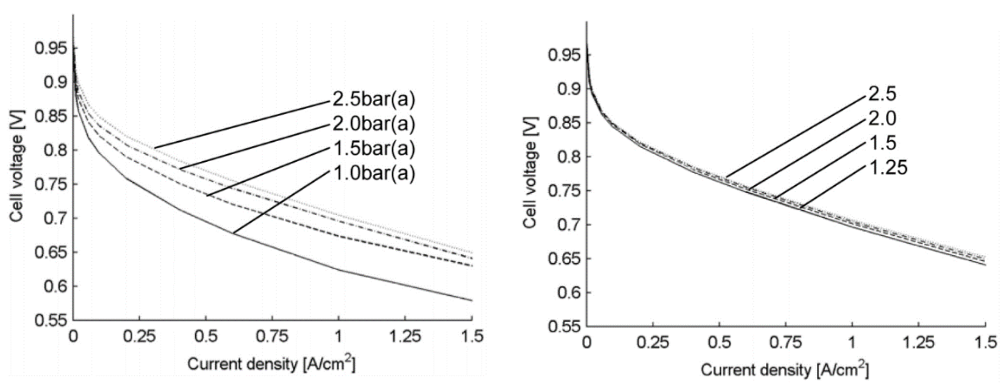

Figure 2.7 Effect of Air Pressure and Air Stoichiometry on the Polarization Curve [5]

The main function performed by the air supply system is to pressurize, humidify, clean the air. The schematic diagram of the air supply system is shown below.

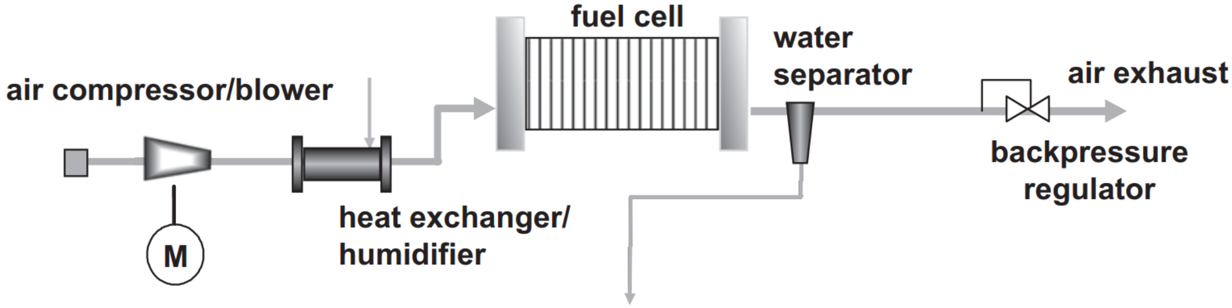

Figure 2.8 Schematic Diagram of Air Supply System [6]

Machines used to pressurize the air have different types: the screw compressor, the scroll compressor, the piston compressor, the turbo compressor, the blower, and so on. The piston compressor has the capability of delivering very high pressure at very low air mass. In the contrary, the blower is able to deliver a very high air mass flow at very low pressure. Each type of machines has a particular pressure-flow characteristic shown in Figure 2.9, which has to be carefully matched when designing a fuel cell system.

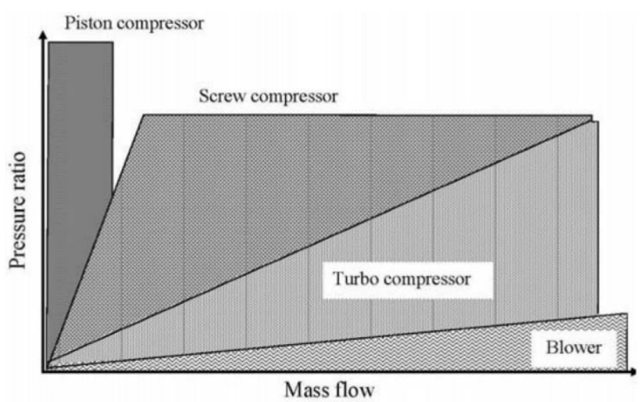

Figure 2.9 Pressure-Flow Characteristic of Air Supply Machine

2.4 Water management system

It is of high importance to take care of the water management issues. At the MEA level, when the current is drawn from the fuel cell, protons move from the anode to the cathode dragging the water molecules. This so-called 'electro-osmotic drag' transport. Together with water produced on the cathode side, this causes water accumulation on the cathode side. However, the water gradient is generated, which will drag the water molecules back to the anode. This is the phenomenon called back diffusion. The electro-osmotic drag will prevail over back diffusion at high currents, resulting in drying out of the anode. There are also other reasons leading the MEA to dry out:

(1) Insufficient humidification: This happens when feeding the cell with low-humidified or dry reactant gases.

(2) At higher cell operating temperatures, water produced at the cathode alone cannot compensate for the lack of water.

On the opposite, a phenomenon called flooding can occur in high current operations due to the rate of water removal being less than the rate of water produced and transported. The flooding areas could be catalyst layers, gas diffusion layers, and flow field channels. Flooding affects the performance of the fuel cell.

Approaches to deal with the above-mentioned issues are classified into many categories.

The first one is by optimizing the structure of the fuel cell. For example, changing the shape of the flow channel [7], optimizing the shape and size of micro pores of cathode GDL[8][9]. By changing structural parameters, the ability of water removal is increased.

The second is to change the material of some components. The hydrophilicity of the membrane can be improved by spraying silica to the proton exchange membrane. More water stays on the membrane eliminating the flooding phenomenon[10].

The third one is through a proper control system, which adjusts the air intake rate, current density, temperature, pressure, and other parameters in the PEMFC. The water content inside the membrane was adjusted to keep the fuel cell from flooding or drying out.

It is necessary to humidify the reactant gases before entering the stack to prevent drying of the membrane. The general approach is through the injection of water or steam. The fuel cell stack of Mirai uses 3D flow field channels, allowing self-humidifying[11].

2.5 Heat management system

The choice of methods to remove excess heat in the fuel cell depends on the size of the fuel cell. Typically, fuel cell cooling methods are cooling by water and cooling by air. The water-cooled method uses a cooling circulating water pump to force the circulating coolant to flow through the stack and remove excess heat. The coolant passes the radiator and transfers the heat to the environment. The air-cooled type usually uses the fuel cell cathode air. The generated heat is directly taken out of the system. There are two ways of air cooling, which are natural cooling and forced cooling. In practical applications, the fuel cell with rated power below 100W can be cooled by natural cooling. This method can provide sufficient airflow to supply oxygen and discharge the generated water without additional fans and other equipment. Fuel cells with a power higher than 100 W need to use an external fan to achieve forced cooling.

It is difficult for the air-cooled system to keep the stack operating within the normal working temperature range. For vehicle application, the cooling by water method is used. PEMFC heat management system includes water pump, radiator, cooling fan, sensors, bypass valve, water tank, and coolant deionizer. The water pump pressurizes the cooling liquid (usually deionized water) and drives the cooling liquid to circulate in the stack. The radiator and bypass valve are the actuators for coolant temperature control. The radiator realizes the heat exchange between the coolant and the environment. The bypass valve is used to ensure that the temperature of the fuel cell can rise rapidly during the cold start and to accurately control the temperature of the fuel cell under different ambient temperatures. The coolant must be deionized so that it loses its electrical conductivity.

The ECU controls the flow of the circulating water pump and the cooling fan's speed according to the temperature. When the conductivity sensor detects the conductivity of the coolant exceeding the limit, the ECU will give an alarm to replace the deionizer. If necessary, the ECU will cut off the supply of hydrogen and air.

3. Powertrain components of FCVs

3.1 Configuration of powertrain

Fuel cell vehicles are often hybridized with an electric energy storage system to cope with frequent start-up or shut-down, rapid variation of power demand. The electric energy storage system refers to a battery, a supercapacitor, or both. An energy storage system could assist the fuel cell by delivering a certain amount of power. Therefore, the fuel cell can avoid rapid varying power demand and operate with higher efficiency. Hybridization also makes capturing regenerative energy possible and enables the designer to downsize the fuel cell. Concerning the application of fuel cells in the automotive field, there are many solutions of powertrain arrangement listed in Figure 3.1.

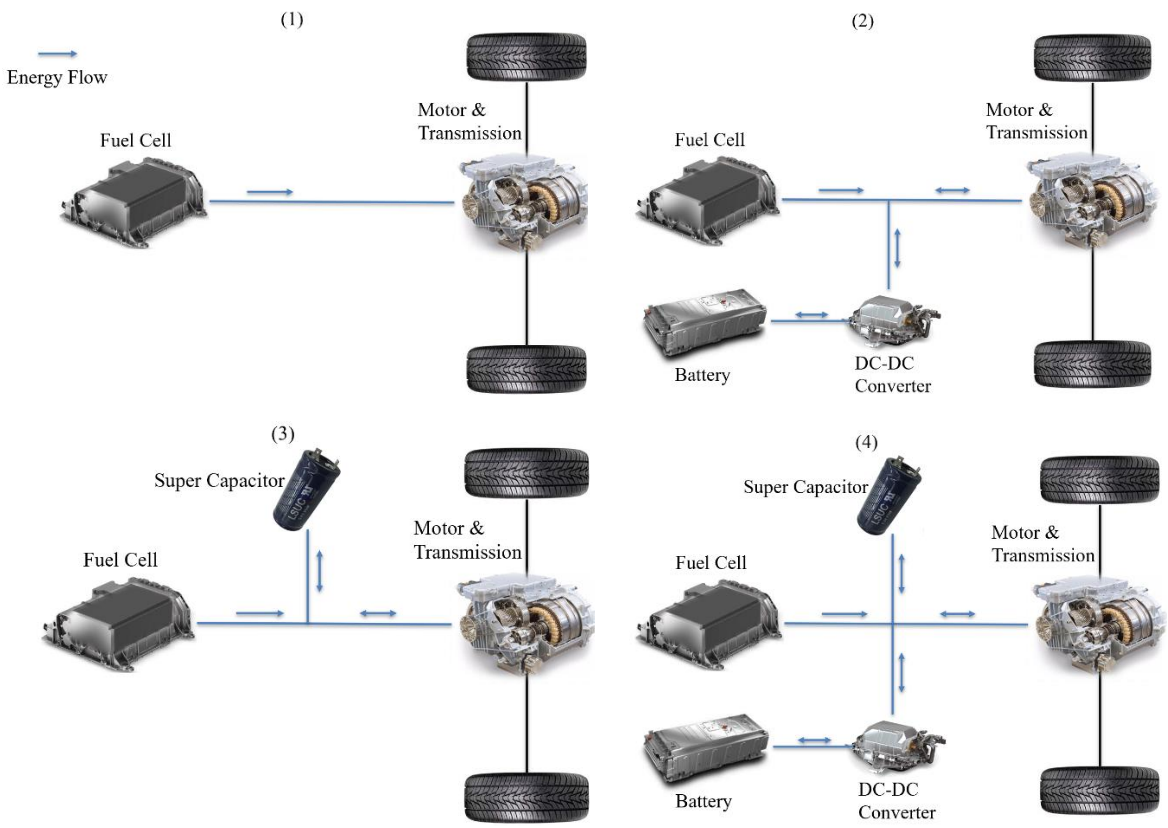

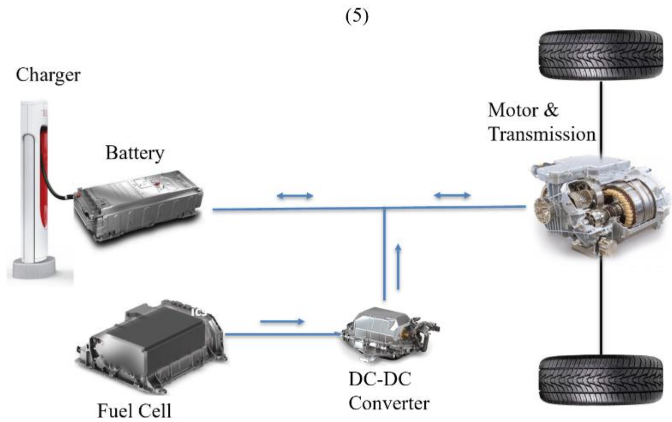

Figure 3.1 Configurations of FCVs: (1) Pure fuel cell with no hybridization;(2) Fuel cell with a battery; (3) Fuel cell with a supercapacitor; (4) Fuel cell with a supercapacitor; (5) Fuel cell with a supercapacitor and a battery

1. Pure fuel cell with no hybridization
   In this configuration, the only power source is the fuel cell. This arrangement has a simple structure and less weight is added to the vehicle. However, due to the fact that the response of fuel cell to transient loads is limited by hydrogen and airflow rates, so it requires a higher power fuel cell stack and fast hydrogen and air supply systems to meet the power needed. Vehicles with this configuration are not able to store braking energy and have a long cold start time. The first research prototype of Ford FCV with this powertrain arrangement was developed in 1999.
2. Fuel cell with a battery
   In this case, a battery is connected with a DC/DC converter. The voltage at the fuel cell output side is the DC-link voltage. The fuel cell acts as a main power source and the battery assists the fuel cell as a secondary power source. The transient power provided by battery is regulated by the DC/DC converter. Adopting the solution of fuel cell with a battery can lower the requirement for fast dynamic response and high rated power of the fuel cell. The cost both in research and in production is reduced. With the help of a battery, the fuel cell could avoid the oxygen starvation phenomenon and prolong its lifetime. Vehicles with this arrangement can start within a shorter time and have the capability to recover the regenerative energy. However, the disadvantages lie in the relatively complicated structure. When the battery is absorbing the energy in regenerative mode, the transient current is high, which is not good for the battery's lifetime. It is worthwhile to mention that this configuration is widely used. Applications could be found in Honda FCX Clarity, Toyota FCHV, GM Fuel Cell Equinox Vehicles, Seicento Elettra, and so on.
3. Fuel cell with a supercapacitor
   Apart from the battery, a supercapacitor can also be used as a secondary power source. The supercapacitor has a larger power density and allows larger charging and discharging currents. The supercapacitor will absorb the regenerative braking energy and provides a fraction of transient power for vehicle acceleration. This configuration is the simplest of

the hybridized powertrain arrangement. So the cost and weight of the vehicle are reduced. Although the advantages are so tempting, supercapacitors have the drawback of low energy density, the discharging time of supercapacitors is limited.

4. Fuel cell with a supercapacitor and a battery
   Based on the configuration of fuel cell with a battery, a supercapacitor is connected parallelly.
   The supercapacitor provides peak current during acceleration and recovers peak current in emergency braking. In this way, the requirements of specific energy and specific power can be separated from each other. That is, specific power requirements for the battery can be lowered. Large current peaks of the battery could be avoided so as to extend battery's life. The configuration has the disadvantages of high cost, control complexity.
5. Plug-in fuel cell
   This configuration can be considered as a PHEV using the fuel cell as the range extender. In this configuration, the battery's state of charge is a factor determining the fuel cell output power. Ford's latest HySeries Drive, Audi A7 Sportback htron quattro adopted this configuration.

3.2 Components of FCV

3.2.1 Electric machine

AC motors are often considered the candidate for HEV rather than DC motors, for HEV requires high efficiency and reliability. A brief comparison among four kinds of motors is presented in this section. The scores of three types of AC motor are listed below according to the literature [12].

Table 3.1 Score of Different Motors[12]

	DC machine	Induction Machine	Permanent Magnet Synchronous Machine	Switched Reluctance Machine
Power density	2	3	5	3
Efficiency	2	3	5	3
Cost	4	5	3	4
Reliability	3	5	4	5
controllability	5	4	5	3
Safety	4	5	3	5
Maturity	5	5	4	3
Total score	25	30	29	26

DC motors' torque-speed characteristic well meets the tractive requirement, and the control is simple. However, due to the presence of the brush, it has drawbacks such as low efficiency, low reliability, and frequent needs of maintenance.

Induction machines are considered one of the most potential candidates for the electric propulsion of HEVs. Induction machines have the advantages of high reliability, low maintenance, low cost, and are capable of working in poor environments. The drawbacks of this type are low efficiency and low power factor, which are more severe at high speed. Dual inverters are introduced to solve this issue, aiming at extending constant power.

The PMSM has a high torque/power density, a high efficiency. The heat of PMSM motor can be removed easily. It is more expensive to manufacture than the induction machines because of the magnets inside the rotor. Over currents or too high temperatures can cause the magnets to be destroyed. An uncontrolled rectification can occur when the speed gets too high. Because of the presence of magnets, this type of machine also has a short constant power region. Thus field weakening might be necessary to be applied to obtain a high speed.

It is well accepted that SRM has great potential for HEV implementation. These motors have many advantages such as high reliability, and outstanding torque–speed characteristics. Comparing with the PMSM, SRM can has a long constant-power range. There are, however, several disadvantages hindering the adoption of this type of machine. These disadvantages are acoustic noise, torque ripple, excessive bus current ripple, and electromagnetic-interference (EMI) noise generation.

Table 3.2 Application of Motor for FCVs

	Types of motor adopted	**Maximum Power**	**Maximum Torque**
Toyota Mirai	Permanent Magnet AC Synchronous	112 kW	335 Nm
Honda Clarity	Permanent Magnet AC Synchronous	129.8 kW	334 Nm
Hyundai NEXO	Permanent Magnet AC Synchronous	120 kW	395 Nm
Hyundai Ix35	Induction Machine	100 kW	300 Nm
Mercedes-Benz F-Cell	Induction Machine	160 kW	375 Nm
Ford Focus FCV	Induction Machine	67 kW	190 Nm

3.2.2 Battery

A battery converts chemical energy to electric energy to power the vehicle and is essential for balancing the energy flow in FCVs. In this subchapter, various kinds of batteries are compared in terms of specific energy, specific power, lifespan and cost. Figure 3.2 illustrates the specific energy and specific power of different batteries.

The lead-acid battery is commonly used as the power source for the starter in conventional vehicles. It has a low specific energy, generally in between 20 and 40 Wh/kg [13]. Besides, the charge and discharge cycle of the lead-acid battery (50-500 cycles) are shorter when compared to other kinds of battery. What's more, this technology is mature and has fully reached its potential. Improvement can be hard to achieve. Thus it is not suitable to supply the traction power for the hybrid vehicle. It may be appropriate to consider the application of lead-acid battery in low performance, small range vehicles for its low cost (USD 100/kWh) [14].

The appearance of the nickel-metal hydride battery was a breakthrough in the battery industry. It has a relatively high energy density (60-80 Wh/kg) [15] and can charge/discharge in large current. The cost (USD 700–800/kWh) is higher than the lead-acid battery but less than lithium-ion battery[14]. Its energy density is considered insufficient for BEV but suitable for HEV. Implementations of such technology can be seen in Toyota Prius, Mirai, and so on.

It is well accepted that lithium-ion battery is the most promising technology. It has a high energy density of up to 165 Wh/kg. It has high efficiency and a long lifespan [16], and its potential to improve is very high. As well as nickel-metal hydride battery, lithium-ion battery is considered as the green battery for it contains no heavy metals. However, despite the advantages, it presents a safety issue. When it is overcharged, the lithium-ion battery is easy to be in a fire or even explode. Therefore, it has high requirements for the battery management system.

The supercapacitor is characterized with high power density, long life cycle but low energy density. Supercapacitor alone can not be the power source but can be implemented with battery or fuel cell to smooth the power demand of the main power source. Because of its features, which are high power density and long life cycle, the industry could focus on improving the battery's specific energy other than making a compromise between specific power and specific energy.

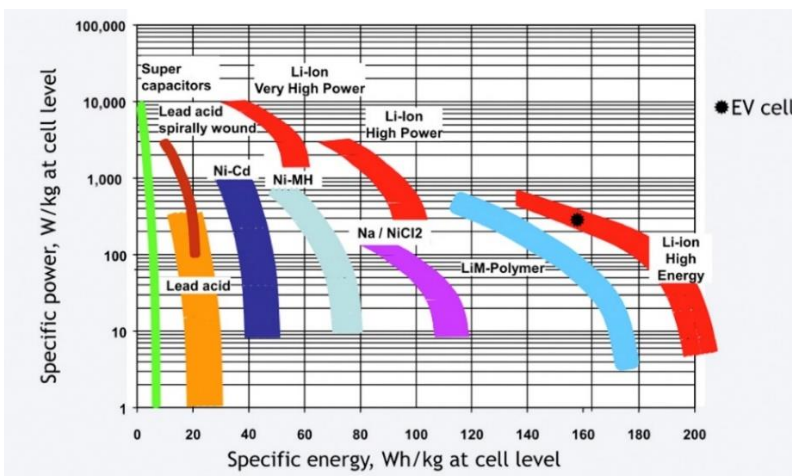

Figure 3.2 Comparison of Different Batteries

4. Advisor modeling

4.1 Introduction

In 1994, The National Renewable Energy Laboratory designed ADVISOR (ADvanced VehIcle SimulatOR). Its goal is to assist the US Department of Energy (DOE) in developing technologies for HEVs. It was published on the internet in September 1998 for free use and attracted many users, including academia, industry expert, and government entities. The main function of ADVISOR is to investigate the vehicle performance and emission, fuel consumption of different powertrain configurations (traditional vehicle with ICE, EV, HEV, and so on).

ADVISOR includes three graphical user interface screens to guide users through the simulation process. In the first GUI screen (vehicle input window), we can select different vehicle configurations (i.e., series, parallel, conventional) and modify various components that composed the powertrain. Users can modify the components' parameters through the editable variable menu in the lower right part. Another option is through modifying the m file of each component that will be loaded in the workspace to obtain the vehicle you intend to simulate and evaluate. In the second GUI screen (simulation setup window), users can define the simulation events of the vehicle. The most important function in this simulation setup window is choosing the drive cycle. We can also define the acceleration and gradeability test conditions in this window. It is worth mentioning the SOC correction function is also made available on this screen. It enables changes in SOC of the battery pack (delta SOC) to convert to equivalent fuel consumption of the fuel converter (linear approximation approach). In the third GUI screen (results window), the results of different components can be chosen and displayed in this window. The results are post-processed and can be time-dependent or integrated. For instance, the fuel flow rate is a function of time, while the distance is an integrated value.

The advantages of this software can be identified and summarized in the following aspects:

1. The simulation model adopted the concept of modular design. The designer of ADVISOR built the simulation model of each component (fuel converter, energy storage system, gearbox, electric machine, final drive, wheel, axle, and so on) by modules, which offered great flexibility and efficiency in extending and modifying each component.
2. The Simulink block diagram and source code are open and available for free. One can access the source code and Simulink block with ease and study the working principles customizing his own models efficiently.
3. ADVISOR adopted a unique simulation approach. The approach combines backward and forward-facing calculation. The backward-facing calculation propagates the power request (in some systems, torque and speed requests) starting from drive cycle. The data flow follows the direction: drive cycle → vehicle →wheels →final drive→ gearbox →electric machine→power bus →energy source. At the same time, a forward-facing approach computes reversely. By modifying control commands to the subsystems, it minimizes the

difference between the driver demand and the response of the system. So it possesses the merits of both forward and backward approaches and can compute faster and provide robust results.

4. ADVISOR is developed in the Matlab/Simulink environment. Since Matlab has many advanced and handy toolboxes, ADVISOR can integrate these toolboxes into the simulation. It can also perform the co-simulation with Saber, Simplorer, VisuaDOC, Sinda/fluint and so on.

The users have to be aware of the limitations of ADVISOR before diving into simulating vehicles through it.

1. The components modeling of ADVISOR is quasi-static. So ADVISOR is not able to predict phenomena within small time scales.
2. ADVISOR is an analysis tool, can not be used as a tool for design.
3. The communication signal between the electrical components is the power rather than voltage or current.

4.2 Vehicle model

The vehicle in ADVISOR is modeled as longitudinal vehicle dynamics with one degree of freedom. Figure 4.1 shows the forces of the vehicle in the longitudinal direction. The balance of forces is expressed as equation 4.1. The vehicle has to overcome four different kinds of forces to meet the speed trace, which are rolling resistance(F_f), road grade force(F_i), acceleration force(F_j), aerodynamic force(F_w).

$$F_t = F_f + F_w + F_i + F_j \quad (4.1)$$

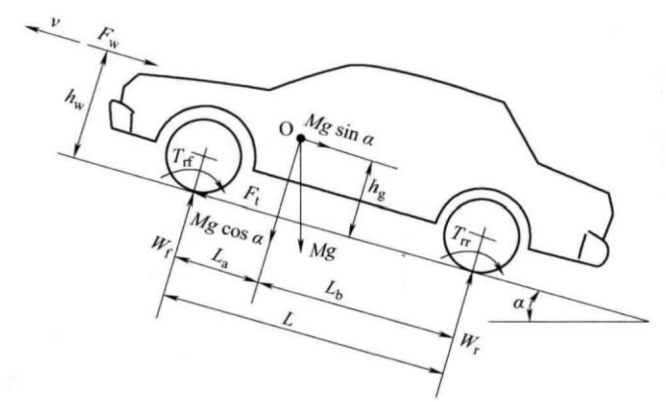

Figure 4.1 Forces of Vehicle in Longitudinal Direction

The energy of deforming the tire is larger than the energy of recovery of the tire, which results in the so-called rolling resistance. The tire undergoes the repeated cycles of deformation and recovery, dissipating the hysteresis energy loss as heat. Figure 4.2 shows the hysteresis cycle of the tire.

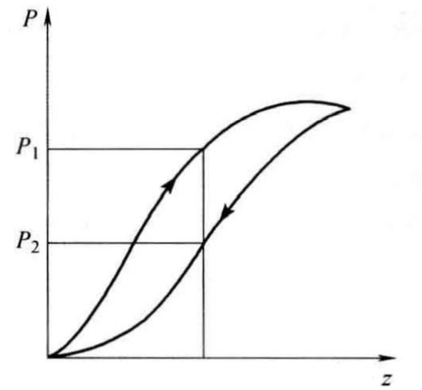

Figure 4.2 Hysteresis Cycle of the Tire

In the figure, P is the force applied to tire, P_1 is the force when subjected to deformation, P_2 is the force in recovery. Z stands for deformation of the tire. Rolling resistance can be simply expressed by:

$$F_f = mgf\cos\alpha \quad (4.2)$$

Where f is the rolling resistance coefficient. f is a coefficient whose value depends on factors such as road conditions, tire conditions (temperature, material, dimension, structure, inflation pressure). Values of the rolling resistance coefficient of different road conditions can be seen in Table 4.1.

Table 4.1 Rolling Resistance Coefficient of different road conditions

Road conditions	Rolling resistance coefficient
concrete, new asphalt, cobbles	0.01 - 0.015
tar or asphalt	0.02
gravel - rolled (new)	0.02
cobbles (large, worn)	0.03
solid sand, gravel (loose, worn), soil (medium-hard)	0.04 - 0.08
loose sand	0.2 - 0.4

The aerodynamic force of a vehicle is a function of vehicle velocity. Equation 4.3 calculates the value.

$$F_W = \frac{1}{2}\rho C_d A u^2 \quad (4.3)$$

Where ρ is the air density, C_d is drag coefficient, A is the frontal area, u is the velocity of the vehicle with respect to air, in the units of m/s. If u is expressed in the units km/h, aerodynamic force is :

$$F_W = \frac{C_d A u^2}{21.15} \quad (4.4)$$

Road grade force is the component of gravity when a vehicle is in a road with an inclination angle of α, it is calculated as:

$$F_i = \ mgsin\alpha \quad (4.5)$$

The product of mass and acceleration is the force caused by acceleration needed to overcome.

$$F_j = m\frac{du}{dt} \quad (4.6)$$

In ADVISOR Simulink vehicle block, these four forces are calculated in the way above mentioned. The Simulink diagram in Figure 4.3 illustrates the calculating procedure.

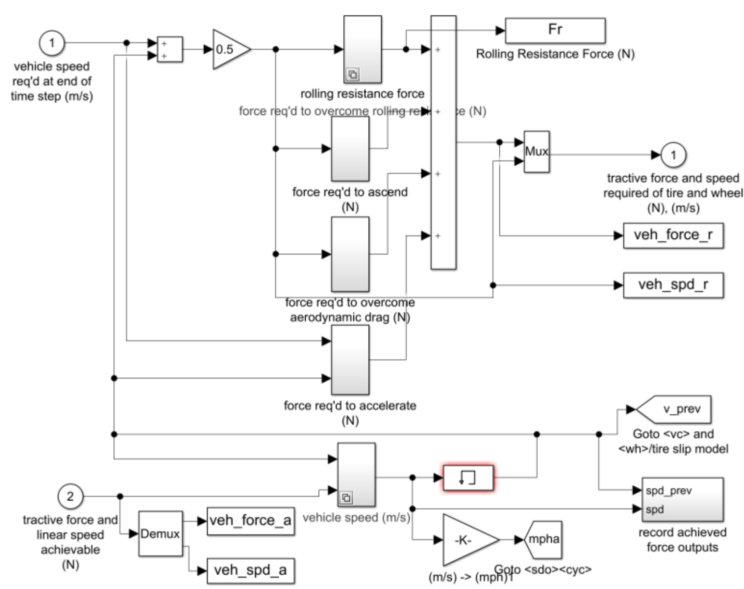

Figure 4.3 Simulink Block Diagram of Vehicle Model

The vehicle that is considered in the paper is an SUV. The parameters of the vehicle are listed as follows:

Table 4.2 Main Vehicle Parameters Considered in Simulation

Parameters	**Values**
Total mass: m	$1961kg$
Drag coefficient: C_d	0.44
Frontal area: A	$2.66\ m^2$
CoG height	$0.7\ m$
Wheel base: l	$2.75\ m$
Effective rolling radius: r	$0.343\ m$
Weight distribution: C_w	0.55

4.3 Fuel cell model

There exist five different types of fuel cell models in ADVISOR. The selection of FC models is important for further simulation. By identifying the features of each model, these five fuel cell models are compared.

The first one is called 'Net model' and is based on power-efficiency maps. An example of power-efficiency map is displayed in Figure 4.4. In this map, the relationship between the fuel cell efficiency and the fuel cell system net power output is described. This model assumes that the fuel cell system can deliver a given net power consuming a corresponding amount of hydrogen independent of the system's complexity. To be more exact, the power request that came from EMS is directly transferred to the output of the fuel cell system and serves as the available net power, if there is no temperature correction. This power request is used to search fuel consumed in a fuel-power map so that fuel consumption is obtained.

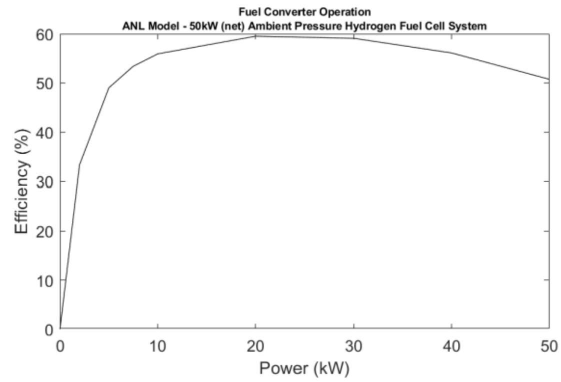

Figure 4.4 Power-Efficiency Map of Fuel cell 'Net model'

The second model of fuel cell is called 'Polarization curve model'. It has a similar approach with the 'Net model'. however, some differences are also noticeable. First, the second model is based on polarization curve of fuel cell rather than the map of power-efficiency. It allows us to define the number of cells and cell active area. Current density of individual cells is found through a lookup table and later is used to determine the cell voltage, fuel use, as is showed in Figure 4.5. Second, the net power of FC system is the gross power of FC stack subtracted by the auxiliary power, described as equation 4.7. The gross power of FC stack is simply the product of voltage, current and the number of cells.

$$P_{net} = P_{gross} - P_{aux} \quad (4.7)$$

Auxiliary system consists of water pump, fuel pump, coolant pump, air compressor, which are all represented by power maps. However, the power consumed by water pump and coolant pump is constant.

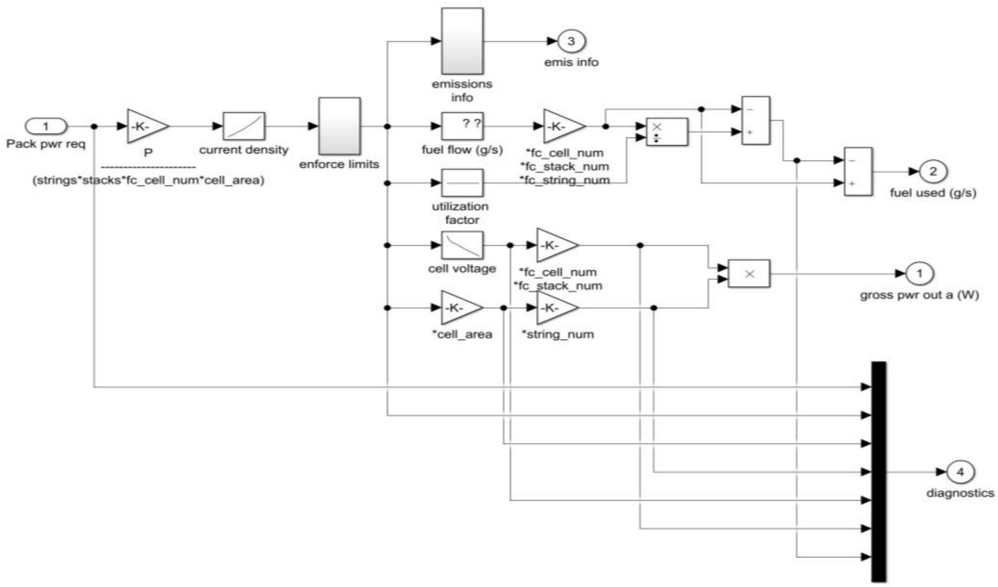

Figure 4.5 Simulink Block of Polarization Curve Model

The third fuel cell system model (GCTool) is included in ADVISOR as a co-simulation option. Since the GCtool does not ship with ADVISOR, it requires a separate download. Its description is omitted.

The VT fuel cell system model (Figure 4.6) is a transient, semi-empirical, polarization curve based model developed by Virginia Tech. Thermal management and the water balance of the fuel cell are considered in this model. The data of compressor maps are from Opcon Autorotor. The user can evaluate the fuel consumption affected by cold-start, the power output affected by temperature. The process of air and hydrogen humidification can also be investigated.

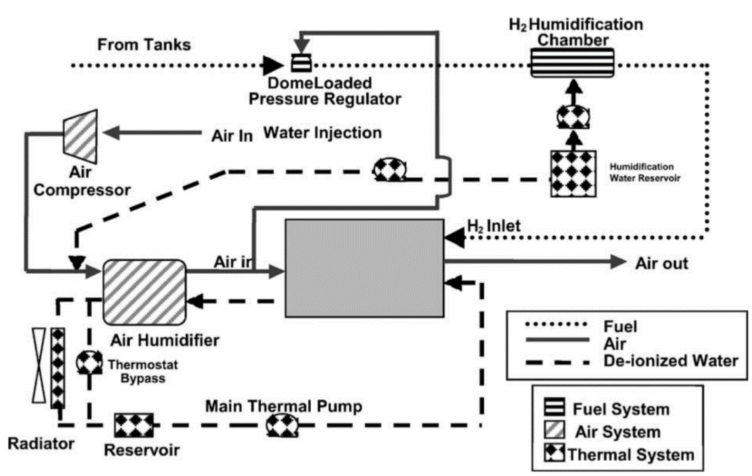

Figure 4.6 Schematic Diagram of VT Model[17]

The KTH fuel cell system model, similar to the VT model, is a semi-empirical model with thermal and water management. Different from VT model, it is a steady-state model, and its stack is modeled theoretically. Users can design the stack by defining the maximum stack output power. The maximum output power is used to determine cell number given the active area and stoichiometric coefficient of reactant. The auxiliary system of this model consists of the pump and fan for cooling, pump for recirculation of water, blower for recirculation of hydrogen, comepressor at cathode inlet. The schematic diagram of the model shows that it allows some amount of hydrogen to be recycled and water produced on the cathode side to be condensed and reused for humidifying the reactant gases. The compressor is modeled using lookup table indexed by mass airflow rate, in which the data comes from Opcon Autorotor. The heat generated in the stack is taken away by coolant and transferred to the environment by the radiator.

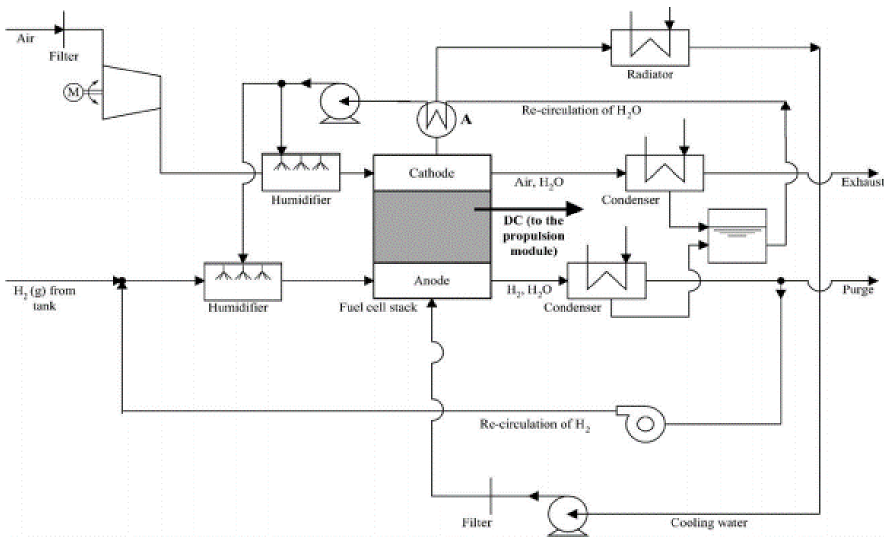

Figure 4.7 Schematic Diagram of KTH Model[18]

4.4 Powertrain components model

4.4.1 Wheel and axle model

Wheel and axle modules play the role in transmitting torque and speed requests from tire to the final drive in backward calculation and also transmitting the actual torque and speed from final drive to tire in forward calculation. In this model, it takes into consideration the drag torque, inertia effect of wheel and axle, tire slip and friction brakes.

4.4.1.1 Backward calculation of wheel and axle

In the path of backward calculation, the torque and speed request of wheel is computed according to the signal from vehicle block. Computation of wheel torque request (wh_trq_r) considers the drag torque (T_loss) and inertial effect ($T\_inertia$), as is described by equation 4.8

$$wh\_trq\_r = (F\_req\_limited - F\_front\_brake\_req) \times wh\_radius + T\_loss + T\_inertia \quad (4.8)$$

Speed request at wheel center (wh_spd_r) is calculated according to the slip ratio equation $s = (\omega r - v/v)$, that is:

$$wh\_spd\_r = (1 + wh\_slip\_r) \times v\_req\_limited/wh\_radius \quad (4.9)$$

where $F\_req\_limited$ is the limited traction force request of the front wheel, $F\_front\_brake\_req$ is the front brake force request, wh_slip_r is slip ratio request of the tire, $v\_req\_limited$ is limited velocity request.

Torque loss is linearly related to total vehicle mass. It is determined through a lookup table. When the wheel is not turning, the torque loss should be zero.

The inertial effect is calculated as the product of inertia and angular speed of the wheel.

The wheel slip ratio (wh_slip_r) is proportional to wh_slip_force_coeff, which is a ratio of tractive force on front tires and vehicle weight on front tires. Thus, $wh\_slip\_force\_coeff$ is used to index the wh_slip.

4.4.1.2 Forward calculation of wheel and axle

In the process of forward calculation of wheel and axle, force achieved by wheel and vehicle speed achieved is calculated according to the torque and speed achieved by final drive. Similarly with backward calculation, calculating achieved force and speed by wheel involves the drag torque and effect of inertia, which is:

$$wh\_force\_a = (wh\_trq\_a - T\_loss - T\_inertia)/wh\_radius + F\_front\_brake + F\_rear\_brake \quad (4.10)$$

Achieved vehicle speed is:

$$veh\_spd\_a = wh\_spd\_a \times wh\_radius/(1 + wh\_slip\_a) \quad (4.11)$$

4.4.2 Electric machine model

Electric machine model refers to motor/controller block in ADVISOR. The motor/controller block calculates the electric power request to the power bus in backward process and defines the available torque and speed to the gearbox. It is made up of three parts:

1. Power request of electric machine to power bus.

2. Available torque and speed of electric machine computation.

3. Temperature effect on emotor.

4.4.2.1. Power requested from the electric machine to power bus

When computing the power request, the block considers rotor's inertia, torque limit, torque capability dependent on torque and speed. According to the speed request of the rotor(outputted by gearbox) $mc\_spd\_out\_r$, the block estimates the rotational speed of the electric machine (mc_spd_est) and computes rotor inertia and torque. The power requested from the motor ($mc\_pwr\_in\_r$) is computed by indexing in the motor's power map.

mc_spd_est is estimated according to the blocks in Figure 4.8. The requested motor speed is replaced by an estimate of the motor's previous speed whenever the vehicle missed the trace by more than 2 mph.

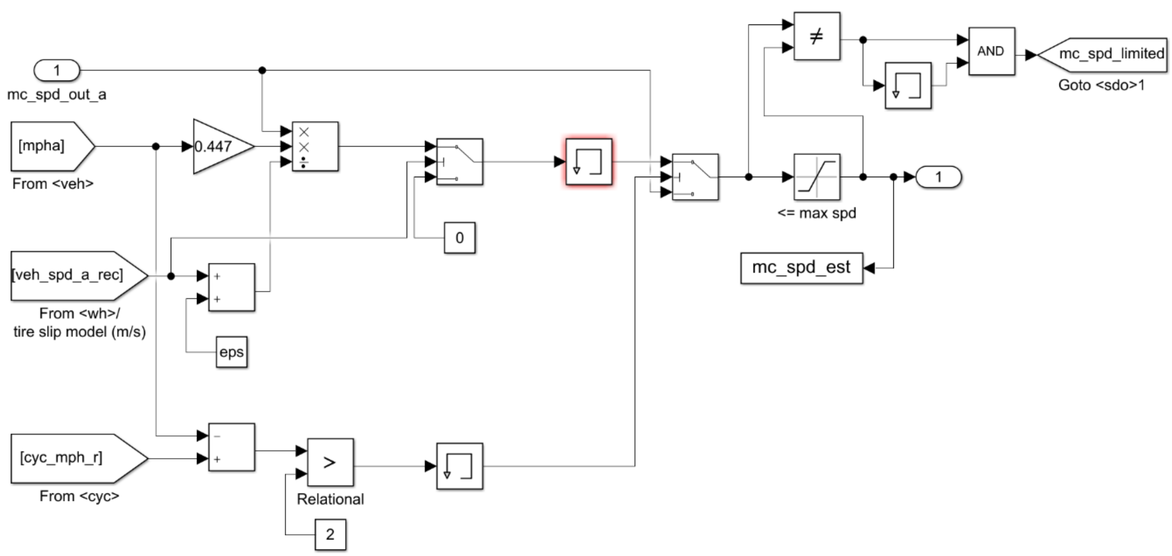

Figure 4.8 Estimation of Motor Speed Request

Torque needed to accelerate rotor inertia is the product of the derivative of speed and momentum of inertia. It is worth mentioning that it can be greater than the product of the maximum motor torque and the fractional contribution of the motor's inertia to the total vehicle inertia.

At a given speed, the maximum torque that can be produced or absorbed is obtained by indexing in lookup tables. The produced torque should be less than the maximum torque and the absorbed torque must be greater than the maximum generative torque. The torque and speed request are determined and sent to a 2D lookup table, whose row/column index input values are mc_map_spd/mc_map_trq and table data is mc_pwrin_map. The output is the power request into the electric machine from the power bus.

4.4.2.2 Available torque and speed of electric machine computation

Available torque is computed from available power by assuming that the ratio of rotor torque to input electric power is the same for the actual situation as is computed for the request. The ratio of rotor torque to input electric power is represented in Figure 4.9. The available electric power input multiply by this ratio is the available torque of the rotor. The available torque of the rotor subtracted by the torque due to inertia is the available torque of the motor.

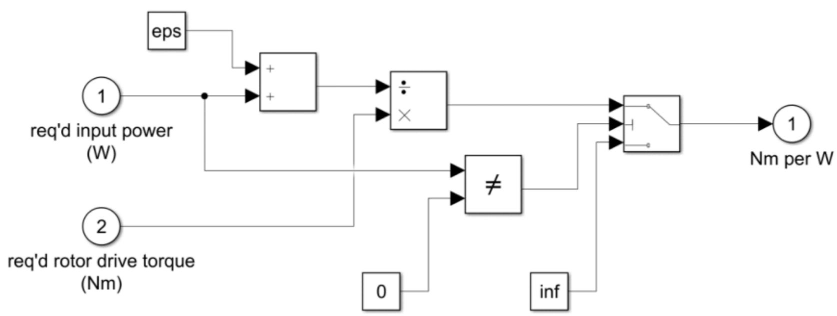

Figure4.9 Ratio to Calculate the Available Power

4.4.3 Energy storage model

The energy storage system represents the battery pack that stores electric energy on the vehicle. The model takes in the power request from the bus and outputs the achieved power, voltage, current and state of charge. The most widely used model is Rint model. The battery is represented as an ideal open circuit voltage with internal resistance connected in series, shown in Figure 4.10. The capacity of battery is fixed, and the battery is subject to a minimum voltage limit. Features of Rint model are listed below:

1. Both open circuit voltage (Voc) and internal resistance(Rint) are functions of SOC. Two maps are used to determine Rint of charging and discharging, shown in Figure 4.11. Voc and Rint are indexed by SOC and temperature.

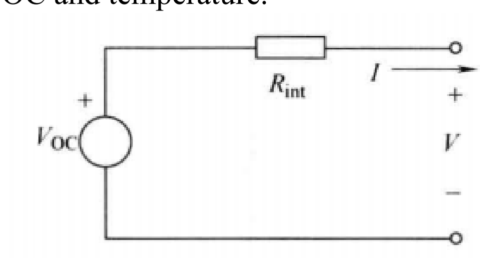

Figure 4.10 Ideal Model with Voc and Rint

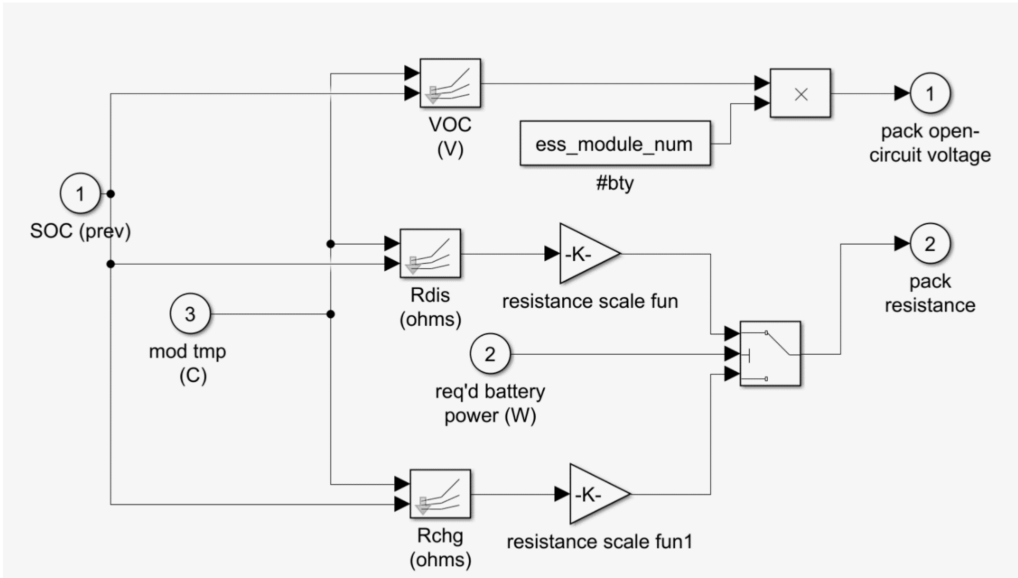

Figure 4.11 Indexing the Voc and Rint

2. The model prevents the power from exceeding limits imposed by three limits: SOC, equivalent circuit parameters, and the motor controller's minimum allowable voltage.
   The maximum power is calculated as :
   $$P_{max,bat} = V_{bus} \times \frac{Voc - V_{bus}}{R} \quad (4.12)$$
   Voc can not drop below motor's minimum voltage or battery's minimum voltage.
3. Current is determined through Kirchoff's voltage law of the equivalent circuit.
   $$RI^2 - (Voc \times I) + P = 0 \quad (4.13)$$
   The bus voltage is determined with the same approach.
   $$V_{\text{bus}} = Voc - (R \times I) \quad (4.14)$$
4. Total Ah used is the integration of the discharging current and charging current over the entire simulation time. The SOC is calculated as (Max Capacity-Ah used)/Max Capacity.
5. The power loss of the battery is the sum of loss due to internal resistance and coulombic efficiency.

4.4.4 Gearbox model

Speed reduction and torque multiplication are the main functions of a multi-speed gearbox. Again, modeling of gearbox in ADVISOR includes the forward calculation and backward calculation. It transmits torque and speed from final drive to tractive motor when calculating backward and transmits torque and speed from tractive motor to final drive in forward calculating process.

4.4.4.1 Backward calculation

In backward calculation, the model considers three effects:

1. Torque multiplication and speed reduction via the gear ratio.
2. Torque loss due to the acceleration of rotational inertia.
3. Torque loss due to the friction of the turning gears.

The three effects are described as follows:

$$gb\_trq\_in\_r \; = \; gb\_trq\_out\_r/gear\_ratio + T\_inertia + T\_loss \quad (4.15)$$

$$gb\_spd\_in\_r \; = \; gb\_spd\_out\_r \times gear\_ratio \quad (4.16)$$

where $gb\_trq\_out\_r$,$gb\_spd\_out\_r$ are the requested torque and speed at the output side of the gearbox,

$gb\_trq\_in\_r$ and $gb\_spd\_in\_r$ are the requested torque and speed at the input side of the gearbox.

T_loss is the torque loss due to friction, $T\_inertia$ is the torque loss due to inertia.

T_loss is obtained by equation 4.17 or 4.18 in tractive mode or braking mode. The efficiency (tx_eff) used in the below equation is calculated by indexing an efficiency map as a function of torque and speed.

$$T\_loss \; = \; (T\_out\_abs/gear\_ratio/tx\_eff) \times (1 - tx\_eff) \text{ (tractive mode) (4.17)}$$

$$T\_loss \; = \; (T\_out\_abs/gear\_ratio) \times (1 - tx\_eff) \text{ (braking mode) (4.18)}$$

Torque loss due to the acceleration of rotational inertia is computed as the angular speed acceleration multiplying the inertia of the gearbox.

4.4.4.2 Forward calculation

The main equations describing the forward calculation process is as follows:

$$gb\_trq\_out\_a \; = \; (gb\_trq\_in\_a \times Pout\_Pin - T\_inertia) \; \times gear\_ratio \text{ (4.19)}$$

$$gb\_spd\_out\_a \; = \; gb\_spb\_in/gear\_ratio \text{ (4.20)}$$

where $Pout\_Pin$ is the ratio of output torque and input torque.

5. Energy management strategy and results

5.1 Default power follower strategy

5.1.1 Default power follower strategy Simulink block

The built-in control strategy is a strategy of power follower. It tries to determine when to switch on/off the fuel cell and how much power the fuel cell delivers when it is on. It offers flexibility in the fuel cell operation. Therefore some variation, such as the pure thermostat control strategy, could be designed. There are 11 variables playing their roles in controlling the fuel cell output power and on/off decision which are summarized in Table 5.1.

Table 5.1 Default Control Strategy Variables

Variable	Description	Units
cs_hi_soc	Highest desired state of charge of battery	-
cs_lo_soc	Lowest desired state of charge of battery	-
cs_charge_pwr	Regulation power to adjust SOC	w
$cs\_fc\_init\_state$	Determining if the FC is initially on	-
$cs\_\max\ \_pwr$	Maximum power commanded of FC	w
$cs\_\min\ \_pwr$	Minimum power commanded of FC	w
$cs\_\max\ \_pwr\_fall\_rate$	The fastest the FC power command can decrease	w/s
$cs\_\max\ \_pwr\_rise\_rate$	The fastest the FC power command can increase	w/s
$cs\_\min\ \_off\_time$	The shortest allowed duration of FC-off period	s
$cs\_charge\_deplete\_bool$	Determining if the SOC of Battery is sustained or depleted	-
cs_fc_on	Determining if FC could be turn on	-

The top-level Simulink blocks are presents in Figure 5.1. It is worth pointing out that the power bus distribute power to fuel cell first, taking the balance from the energy from the energy storage system, which is to say:

$$P_{dem} = P_{fc} + P_{ESS} \quad (5.1)$$

As mentioned, the input of the control strategy is the raw power required by bus, denoted as (P_{raw}). P_{raw} is positive when in traction mode and negative when in regenerative mode.

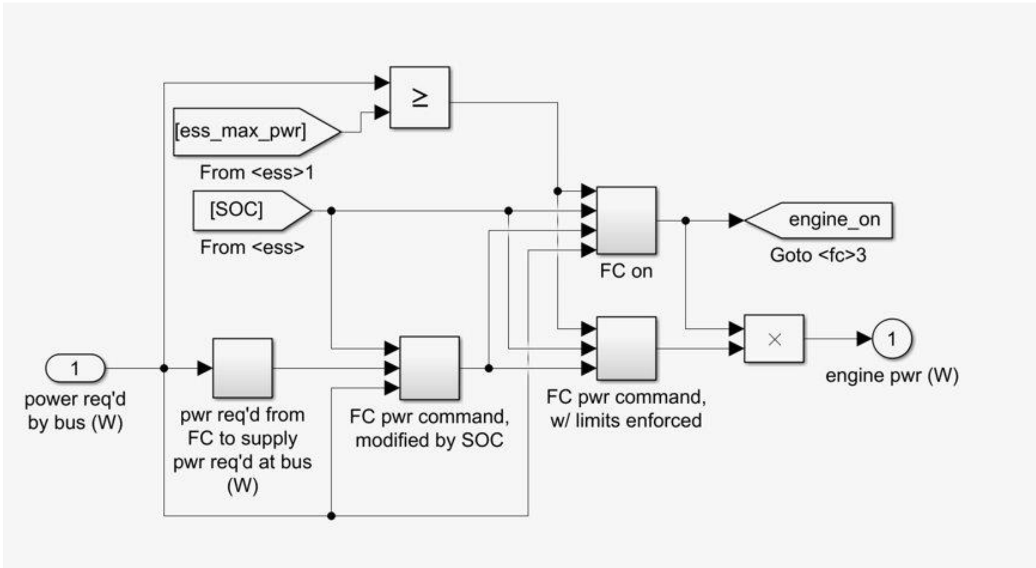

Figure 5.1 Top Level Simulink Block of Default Power follower control

The power required by bus (P_{raw}) as the input goes to the first block 'pwr req'd from FC to supply pwr req'd at bus(W)', as showed in Figure 5.2. If the vehicle is in traction mode, the output is positive and equal to P_{raw}. If it is in regenerative mode, its output is 0. The output from the first block is denoted as $P_{fc,pos}$.

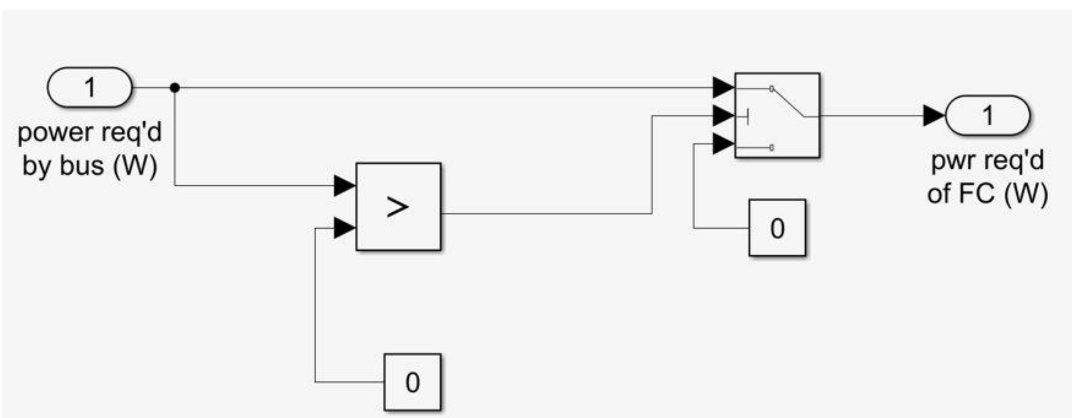

Figure 5.2 Block Detail: 'pwr req'd from FC to supply pwr req'd at bus(W)

The value $P_{fc,pos}$ is then modified by SOC, as showed in Figure 5.3. The way of balancing the SOC is by adding a regulation power, shown in equation 5.2-5.4.

$$P_{fc,soc} = \frac{(SOC^{*} - SOC)}{0.5 \times SOC_{range}} \times cs\_charge\_pwr + P_{fc,pos} \quad (5.2)$$

$$SOC^{*} = \frac{cs\_hi\_soc + cs\_lo\_soc}{2} \quad (5.3)$$

$$SOC_{range} = cs\_hi\_soc - cs\_lo\_soc \quad (5.4)$$

Where SOC^* represents the desired SOC of the battery we would like to maintain. SOC_{range} is a range using SOC upper bound subtracted by lower bound. In this way, extra power could be added into or subtracted from $P_{fc,pos}$. Thus the state of charge of the battery is maintained. For example, we define cs_hi_soc as 0.8 and cs_lo_soc as 0.4, SOC^* becomes 0.6 and SOC_{range} is 0.4. When the current SOC(t) is equal to 0.6, there is no need to balance the SOC and no balancing energy flow out of or into the battery (in traction mode); When the current SOC(t) is equal to 0.7, which is higher than the expected SOC (0.6), $P_{fc,soc}$ becomes $-0.5 \times cs\_charge\_pwr + P_{fc,pos}$, the battery is discharging with the power of $0.5 \times cs\_charge\_pwr$; When the current SOC(t) is equal to 0.5, which is lower than the expected SOC (0.6), $P_{fc,soc}$ becomes $0.5 \times cs\_charge\_pwr + P_{fc,pos}$. So the battery is recharging with the power of $0.5 \times cs\_charge\_pwr$.

In the regenerative mode, we have to consider $ess\_\max\_chg\_pwr$, which represents the max power that can be charged to battery. It is a function of SOC. We need to take the minimum value between $P_{fc,soc}$ and $ess\_\max\_chg\_pwr$ minus regenerative power.

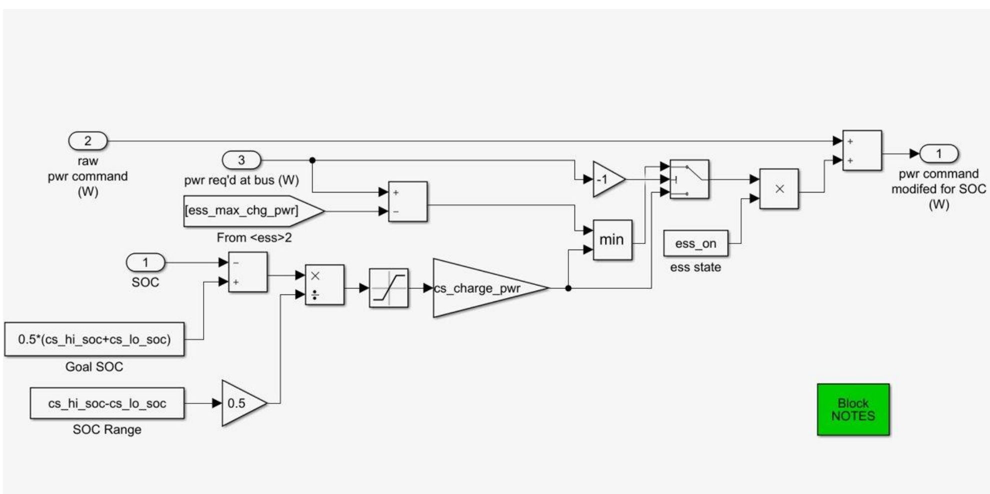

Figure 5.3 Block Detail: 'FC pwr command, modified by SOC'

$P_{fc,soc}$ is later limited by the max increase and fall rates ($cs\_\max\_pwr\_rise\_rate, cs\_\max\_pwr\_rise\_rate$), the larger the absolute value of these two rates, the more aggressive will the system response to transient load. Also, the output power is limited between $cs\_\min\_pwr$ and $cs\_\max\_pwr$. This is described in Figure 5.4.

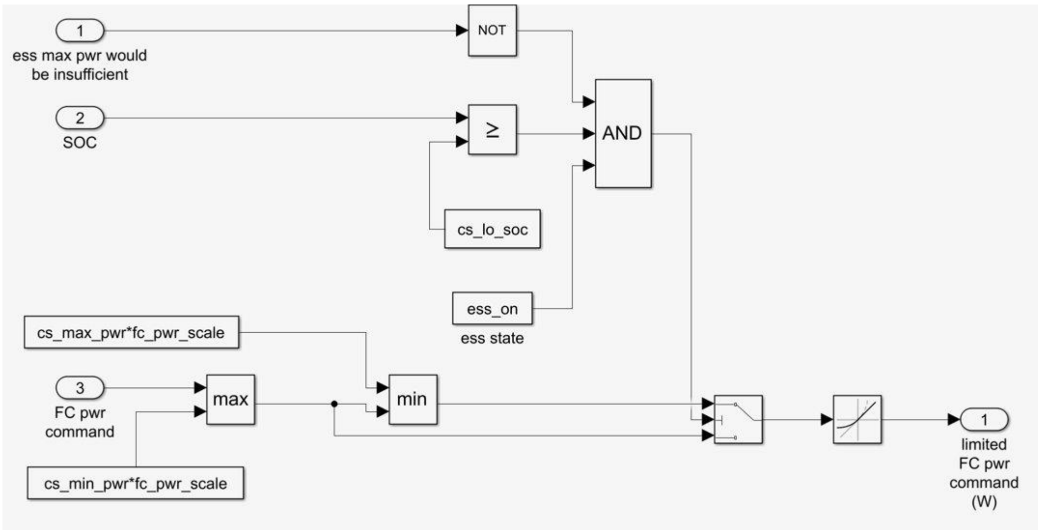

Figure 5.4 Block Detail: 'FC pwr command, w/ limits enforced'

Figure 5.5 shows how the control strategy determines the FC on/off state.

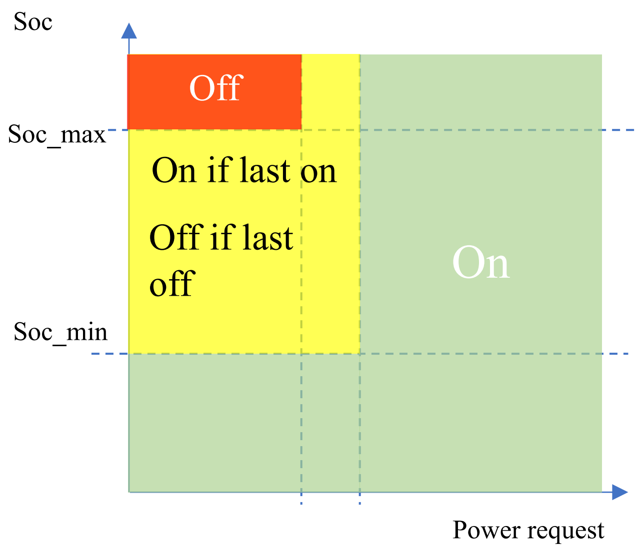

Figure 5.5 FC On/Off state

To sum up, this control strategy has the following characteristics:

- The FC output power may be adjusted by SOC, tending to bring the SOC back to the center of its operating range.
- The FC output power may be kept above some minimum value.
- The FC output power may be kept below some maximum value (which is enforced unless the SOC gets too low).
- The FC output power may be allowed to change no faster than a prescribed rate.

5.2.2 Results of default power follower strategy

5.2.2.1 UDDS drive cycle results

Energy Flow Table(kJ)

Components	In	Out	Loss	Efficiency
Fuel cell	23377	8948	14429	0.383
Battery	2250	2172	104	0.95
Energy stored in battery	-26			
Motor/controller	9509	7681	1828	0.81
Gearbox	7681	7196	486	0.94
Wheel/Axle	7196	6824	371	0.95
Aux load	958	0	958	0
Aero			1845	
Rolling			2076	
Overall efficiency				0.168
Fuel consumption(L/km)				90.3

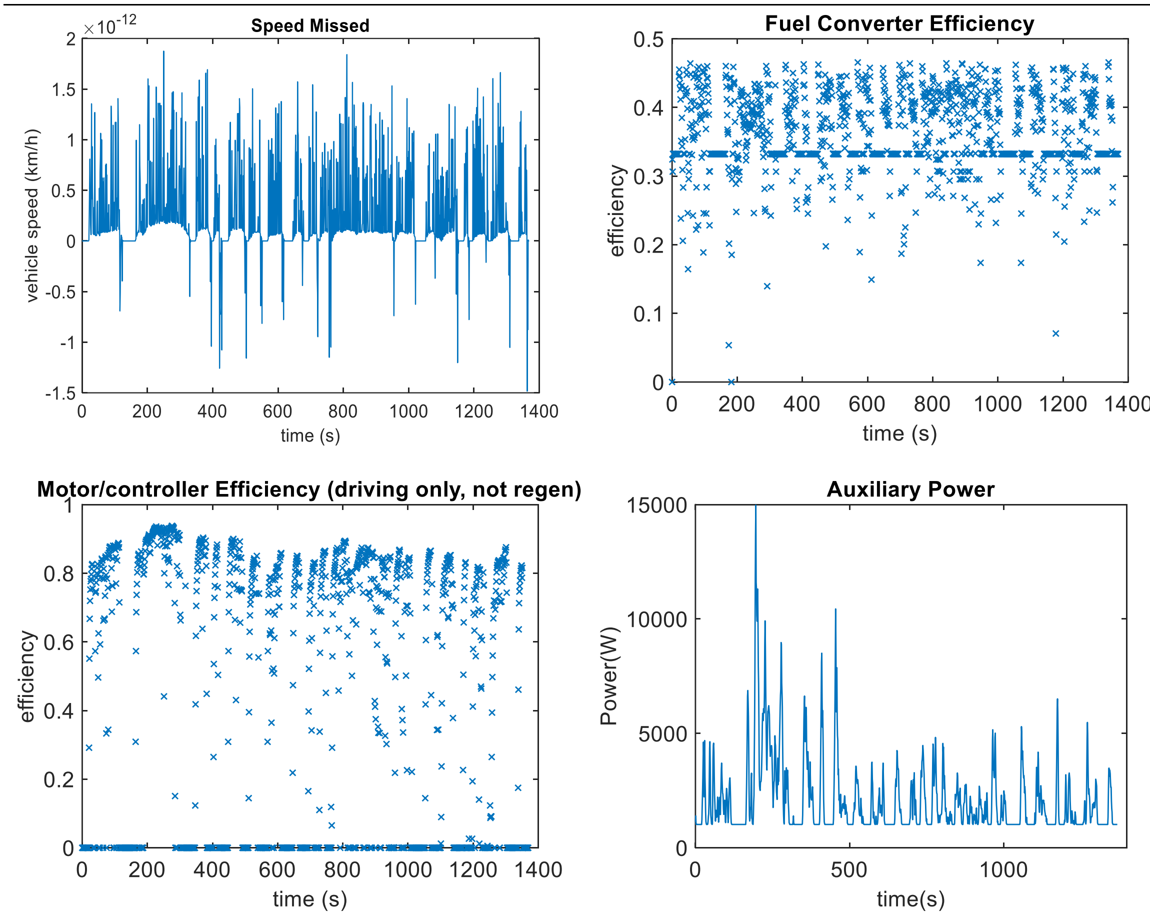

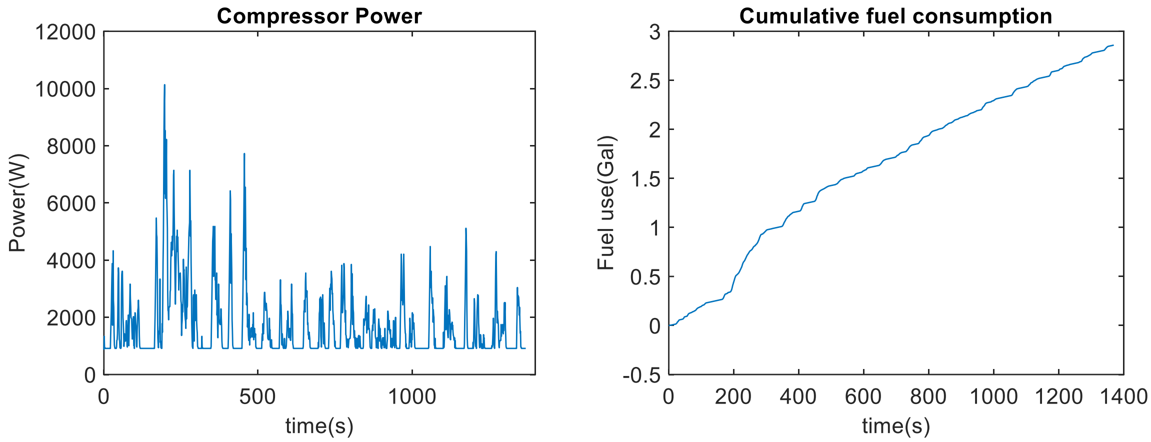

Figure 5.6 – Results of UDDS Drive Cycle: a) Speed missed b) Fuel cell efficiency c) Motor efficiency d) Auxiliary power e) Compressor power f) Cumulative fuel consumption

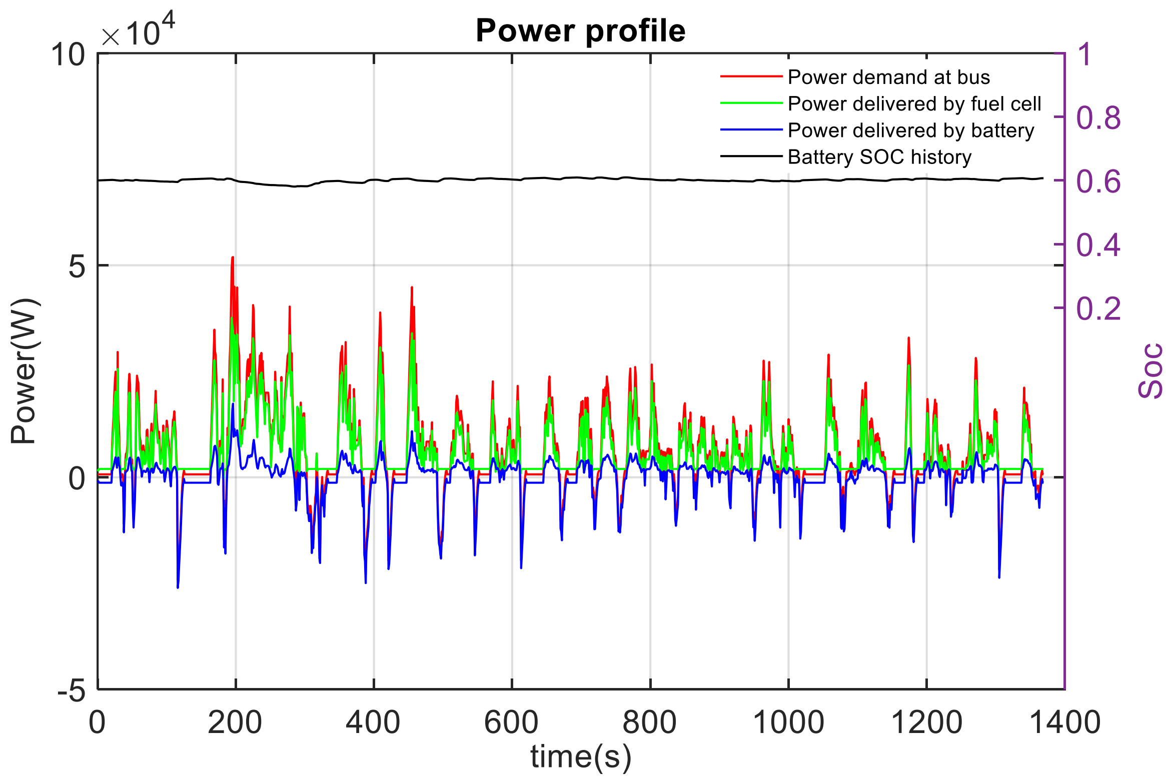

Figure 5.7 – Power Profile of UDDS Drive Cycle

5.2.2.2 NEDC drive cycle results

Energy Flow Table(kJ)

Components	In	Out	Loss	Efficiency
Fuel cell	22110	8303	13807	0.376
Battery	2701	2777	143	0.95
Energy stored in battery	-219			
Motor/controller	8639	7264	1376	0.84
Gearbox	7264	6779	485	0.93
Wheel/Axle	6779	6440	339	0.95
Aux load	829	0	829	0
Aero			2795	
Rolling			1892	
Overall efficiency				0.210
Fuel comsumption(L/km)				93.6

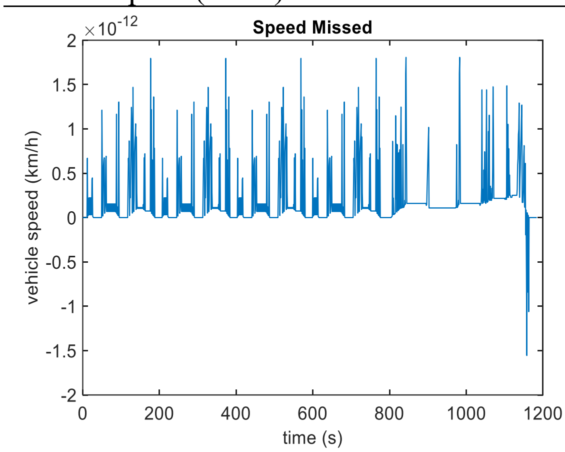

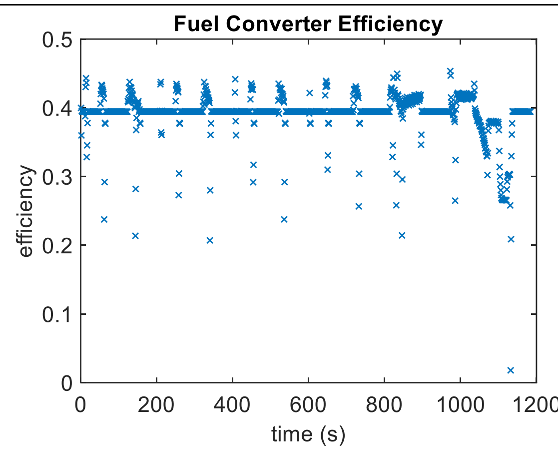

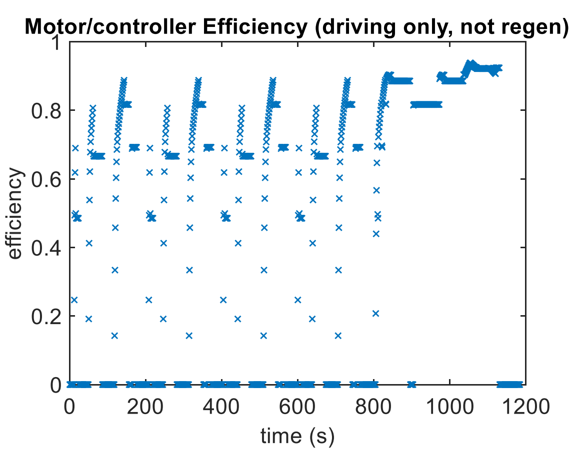

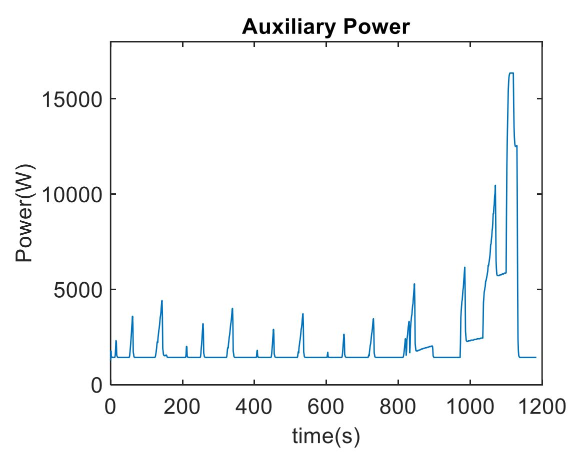

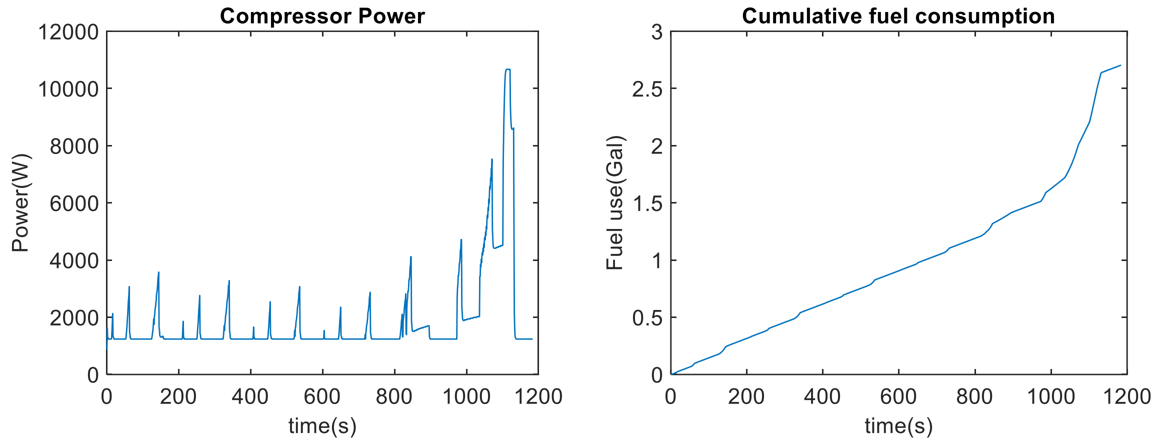

Figure 5.8 – Results of NEDC Drive Cycle: a) Speed missed b) Fuel cell efficiency c) Motor efficiency d) Auxiliary power e) Compressor power f) Cumulative fuel consumption

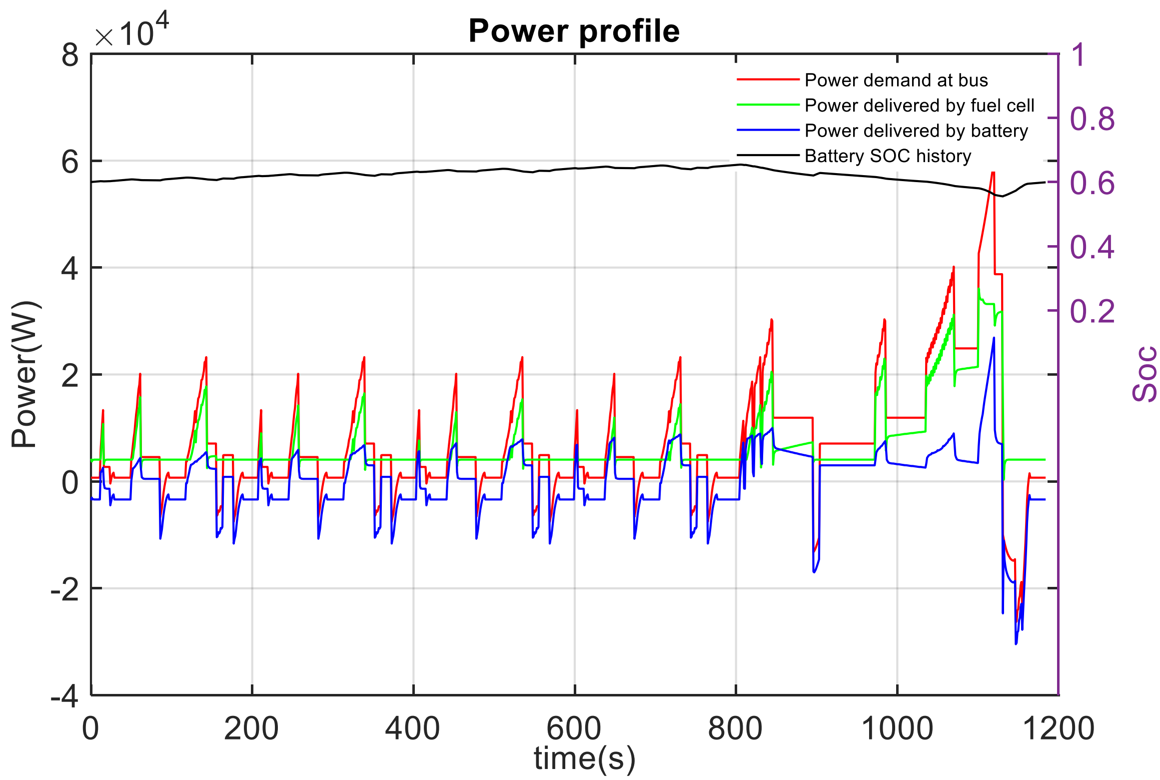

Figure 5.9 – Power Profile of NEDC Drive Cycle

5.2.2.3 WLTP drive cycle results

Energy Flow Table(kJ)

Components	In	Out	Loss	Efficiency
Fuel cell	52903	19556	33347	0.369
Battery	7105	7548	495	0.93
Energy stored in battery	-939			
Motor/controller	21070	18260	2810	0.87
Gearbox	18260	17154	1107	0.94
Wheel/Axle	17154	16406	748	0.96
Aux load	12260	0	1260	0
Aero			8407	
Rolling			4028	
Overall efficiency				0.231
Fuel comsumption(L/km)				107

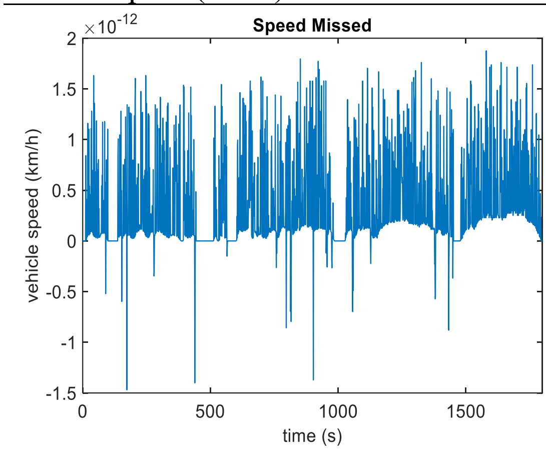

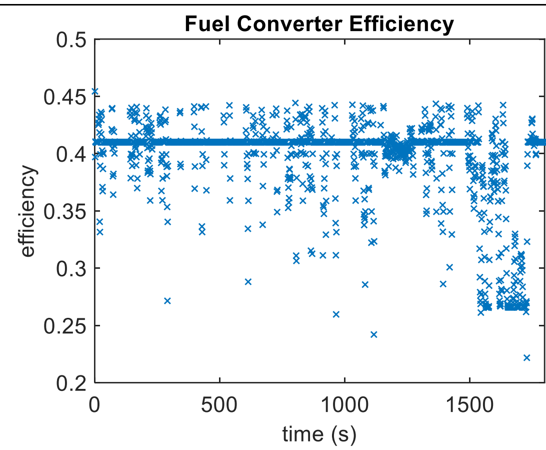

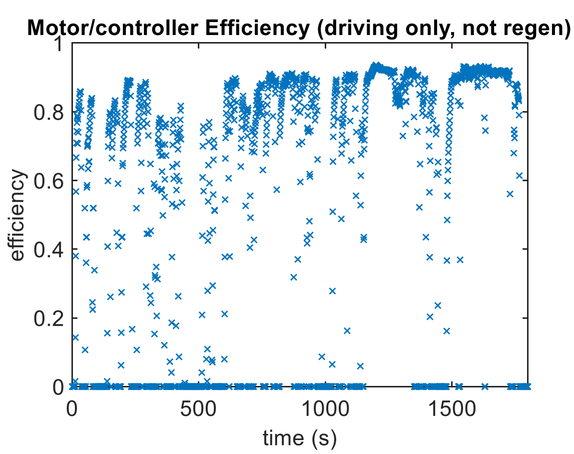

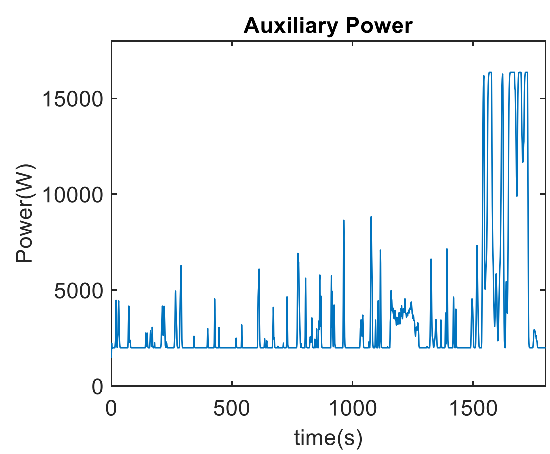

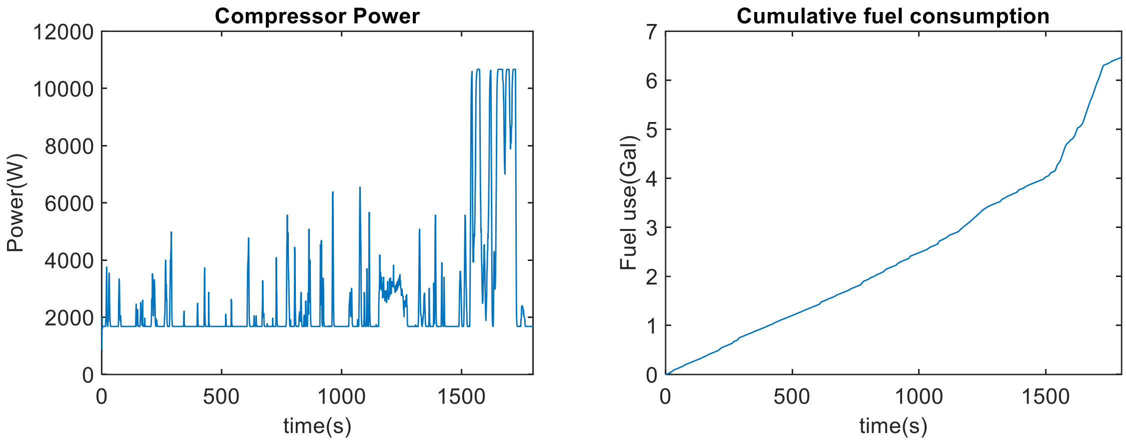

Figure 5.10 Results of WLTP Drive Cycle: a) Speed missed b) Fuel cell efficiency c) Motor efficiency d) Auxiliary power e) Compressor power f) Cumulative fuel consumption

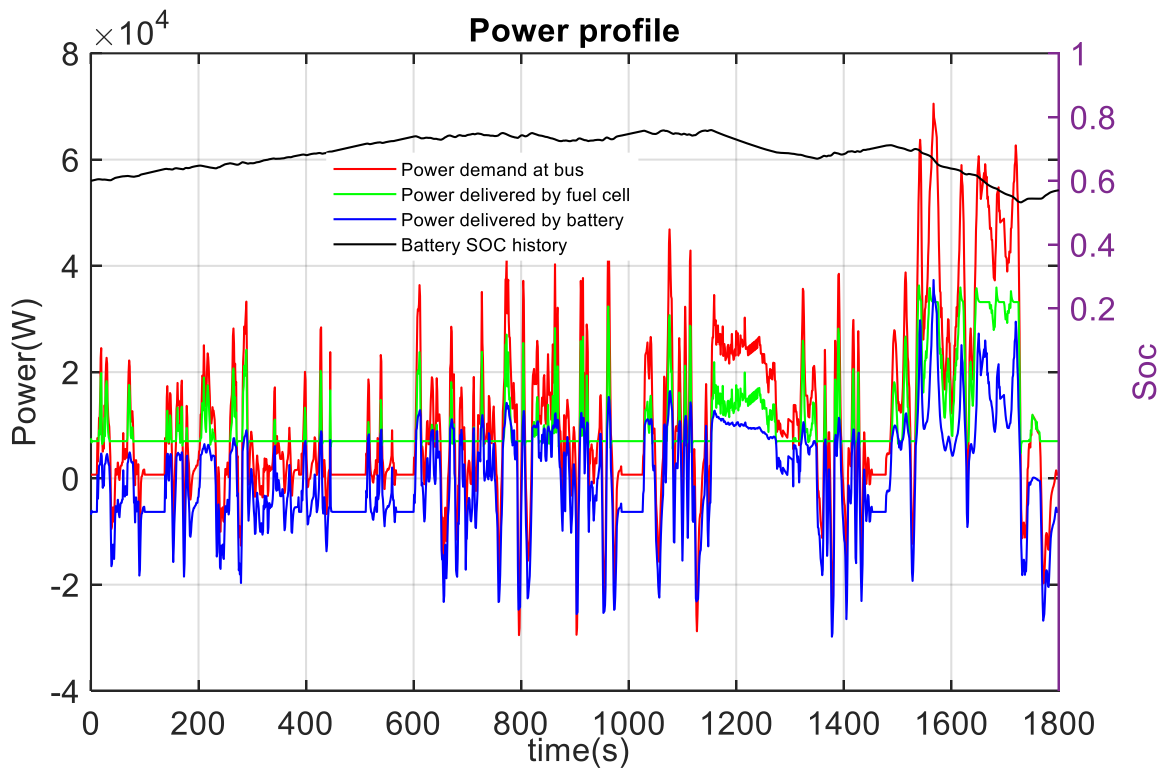

Figure 5.11 Power Profile of WLTP Drive Cycle

5.2 Proposed discretization method

5.2.1 Discretization method design

On the basis of the default control strategies, a discretization method is designed to minimizing the fuel consumption. Taking a look at the fuel cell power-efficiency curve, we can identify the region where the fuel cell is more efficient when operating, as is shown in Figure 5.12.

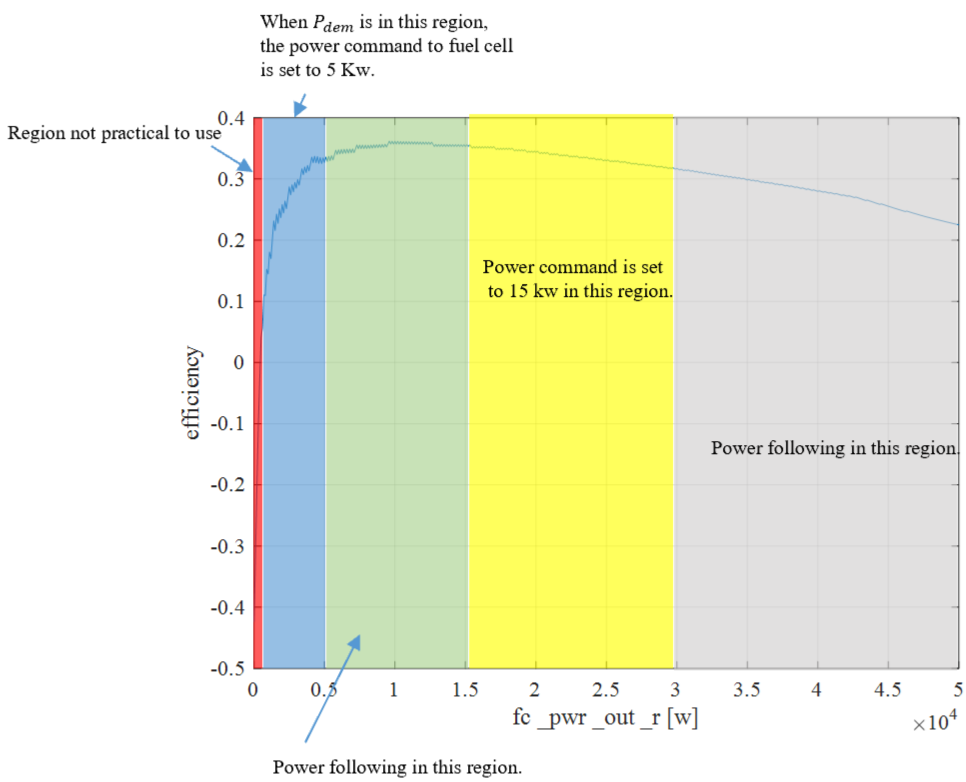

Figure 5.12 Power Efficiency Curve of Kth Fuel Cell System

In default power following control strategy, the fuel cell is either load following or at minimum power ($cs\_\min\_pwr$) and maximum power ($cs\_\max\_pwr$), which does not consider the efficiency the fuel cell operated at. The proposed discretization control strategy takes into consideration the power-efficiency curve and deliver the power according to the power demand at bus.

1. $P_{dem} < 5\ kW,\ output\ power\ 5kW$

2. $5kW < P_{dem} < 15kW,\ output\ power\ P_{dem}$

3. $15kW < P_{dem} < 30kW, output\ power\ 15kw$

4. $P_{dem} > 30kW, output\ power\ P_{dem}$

Actually, the P_{dem} is SOC corrected power according to equation 5.2. The original block 'FC pwr command, w/ limits enforced' is replaced with following blocks:

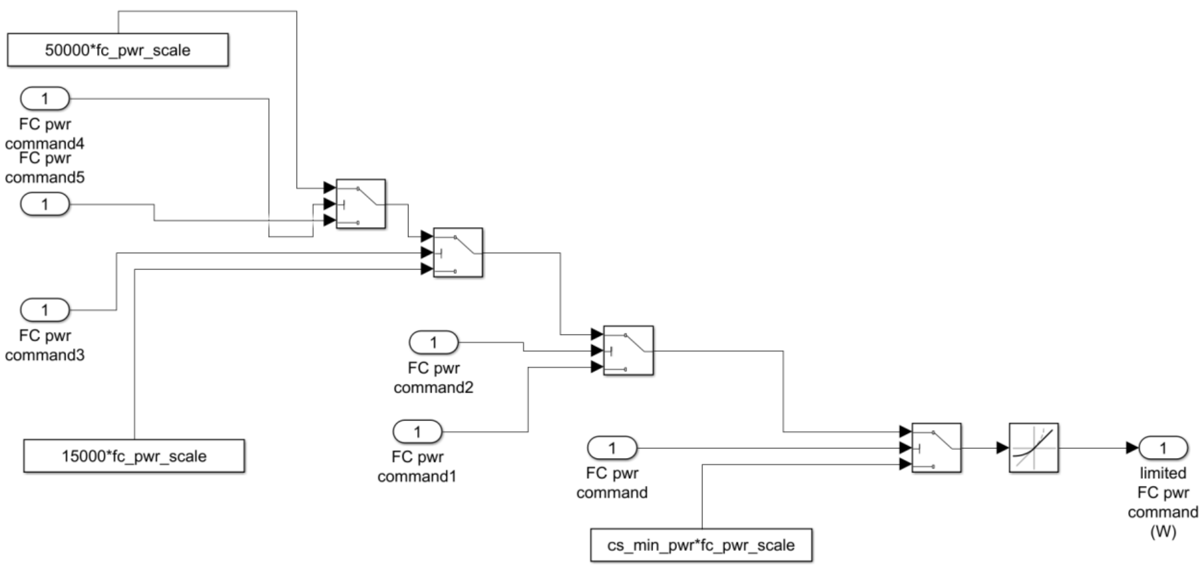

Figure 5.13 Core of Proposed Discretization Method

5.2.2 Results of discretization method

5.2.2.1 UDDS drive cycle results

Energy Flow Table(kJ)

Components	In	Out	Loss	Efficiency
Fuel cell	22365	9075	13290	0.406
Battery	4526	4325	308	0.93
Energy stored in battery	-107			
Motor/controller	9509	7681	1828	0.81
Gearbox	7681	7196	486	0.94
Wheel/Axle	7196	6824	371	0.95
Aux load	958	0	958	0
Aero			1845	
Rolling			2076	
Overall efficiency				0.174

Fuel consumption(L/km)	86.3

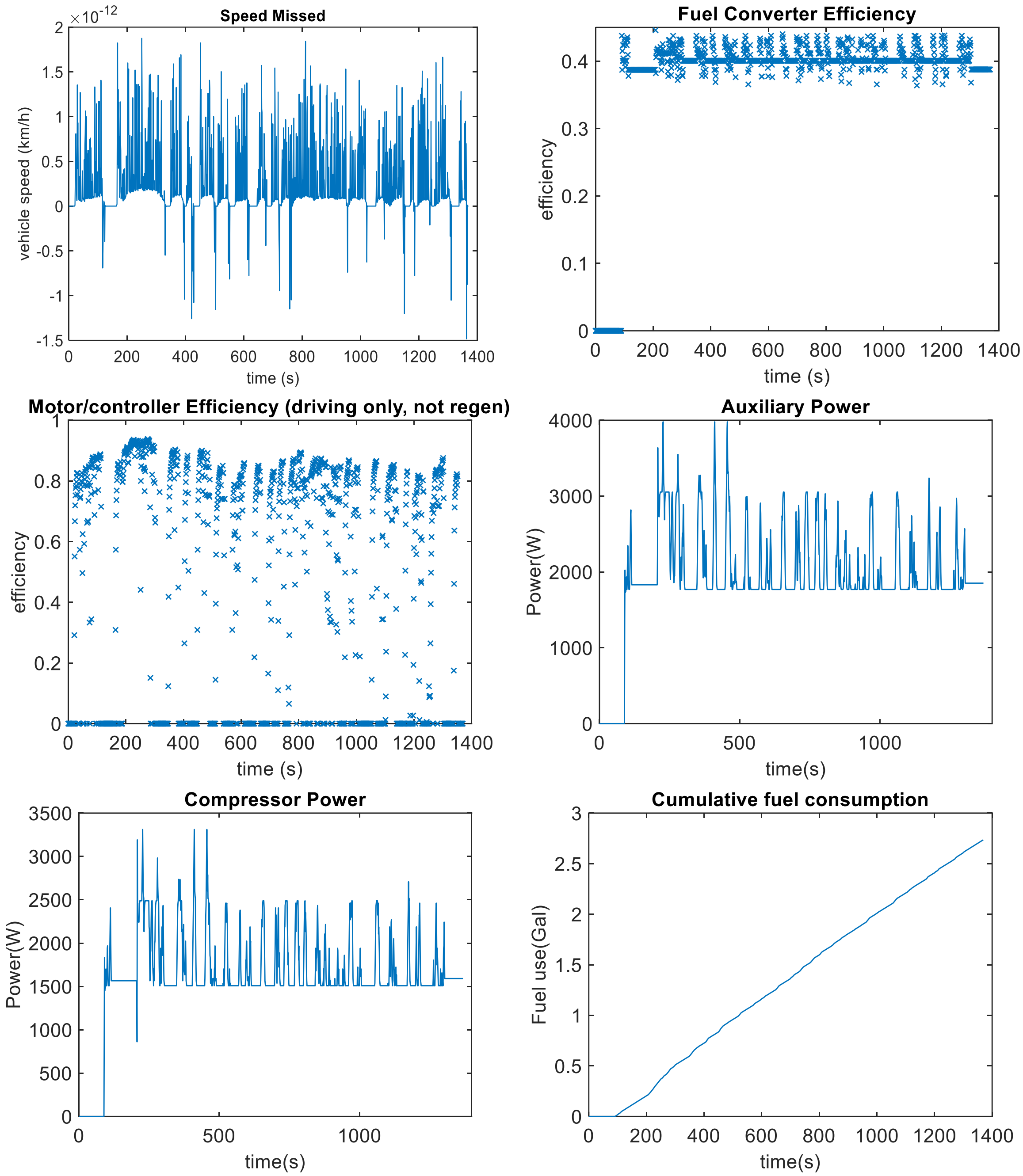

Figure 5.14 Results of UDDS Drive Cycle: a) Speed missed b) Fuel cell efficiency c) Motor efficiency d) Auxiliary power e) Compressor power f) Cumulative fuel consumption

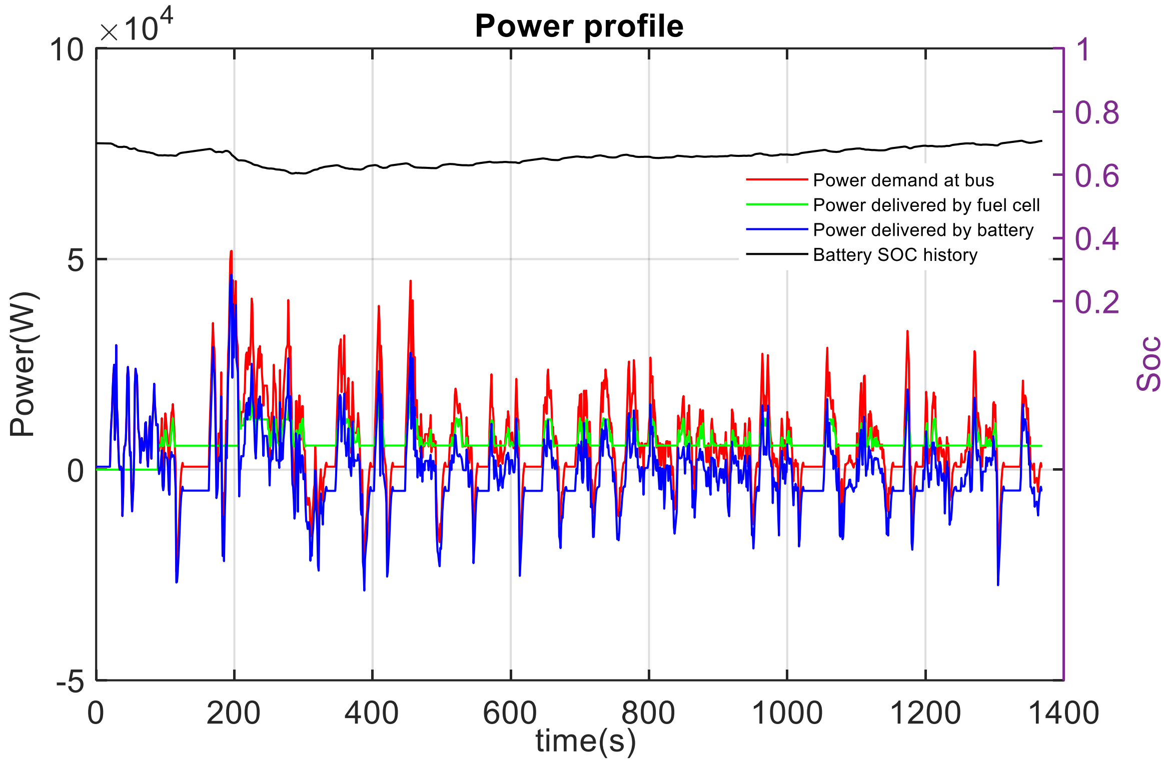

Figure 5.15 Power Profile of UDDS Drive Cycle

5.2.2.2 NEDC drive cycle results

Energy Flow Table(kJ)

Components	In	Out	Loss	Efficiency
Fuel cell	21897	8570	13327	0.391
Battery	3449	3258	217	0.94
Energy stored in battery	-26			
Motor/controller	8639	7264	1376	0.84
Gearbox	7264	6779	485	0.93
Wheel/Axle	6779	6440	339	0.95
Aux load	829	0	829	0
Aero			2795	
Rolling			1892	
Overall efficiency				0.214
Fuel comsumption(L/km)				92.7

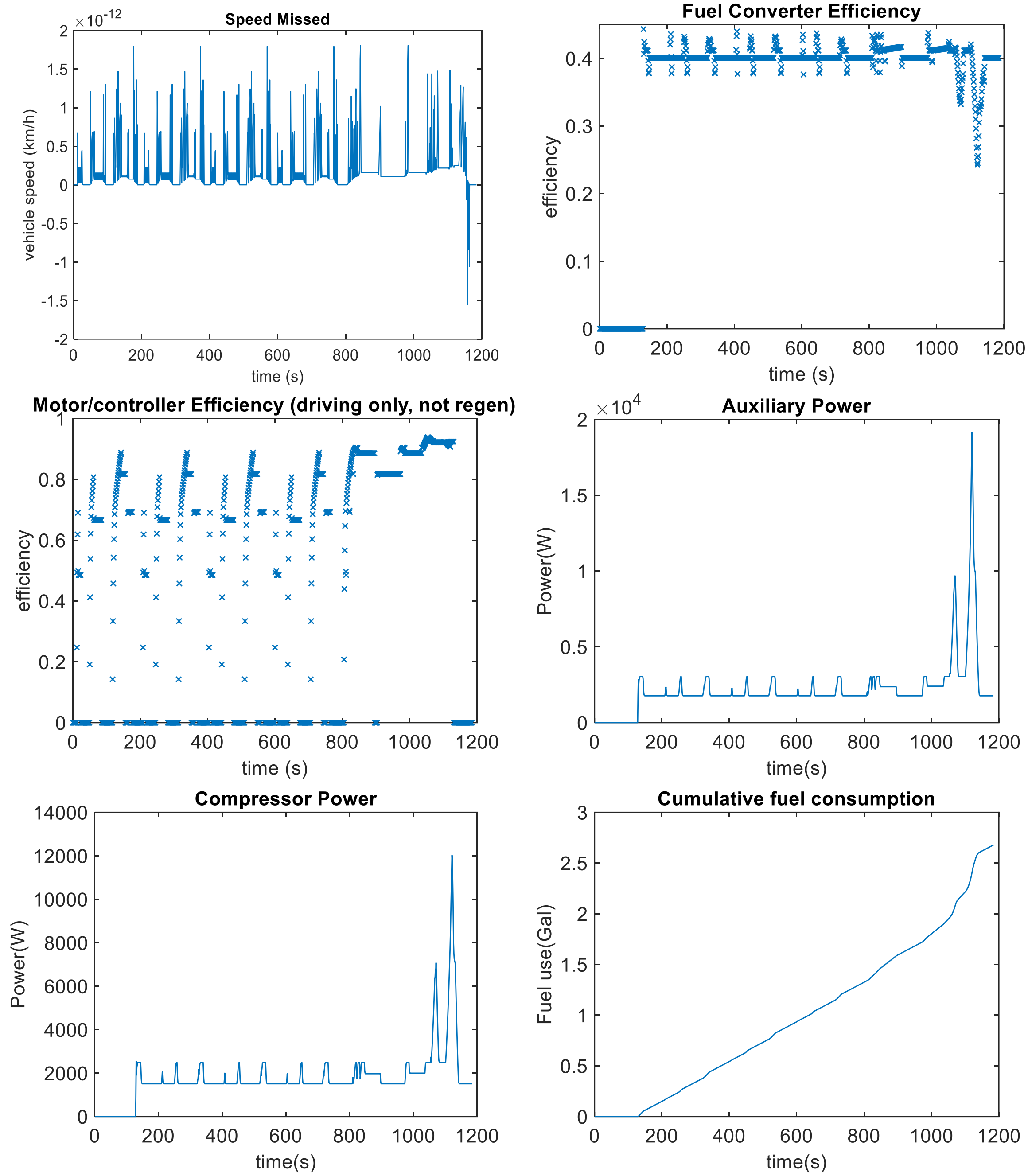

Figure 5.16 Results of NEDC Drive Cycle: a) Speed missed b) Fuel cell efficiency c) Motor efficiency d) Auxiliary power e) Compressor power f) Cumulative fuel consumption

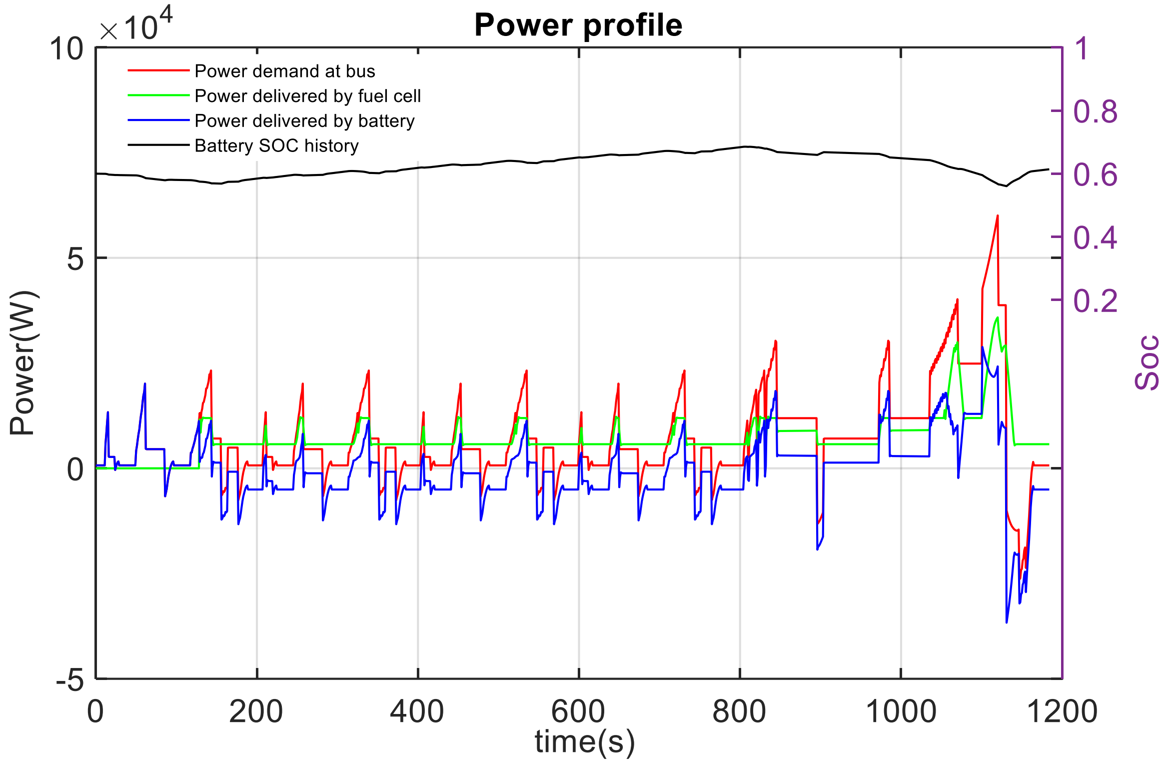

Figure 5.17 Power Profile of NEDC Drive Cycle

5.2.2.3 WLTP drive cycle results

Energy Flow Table(kJ)

Components	In	Out	Loss	Efficiency
Fuel cell	50770	18594	32177	0.366
Battery	6437	7729	562	0.92
Energy stored in battery	-1855			
Motor/controller	21070	18260	2810	0.87
Gearbox	18260	17154	1107	0.94
Wheel/Axle	17154	16406	748	0.96
Aux load	1260	0	1260	0
Aero			8407	
Rolling			4028	
Overall efficiency				0.236
Fuel comsumption(L/km)				108.6

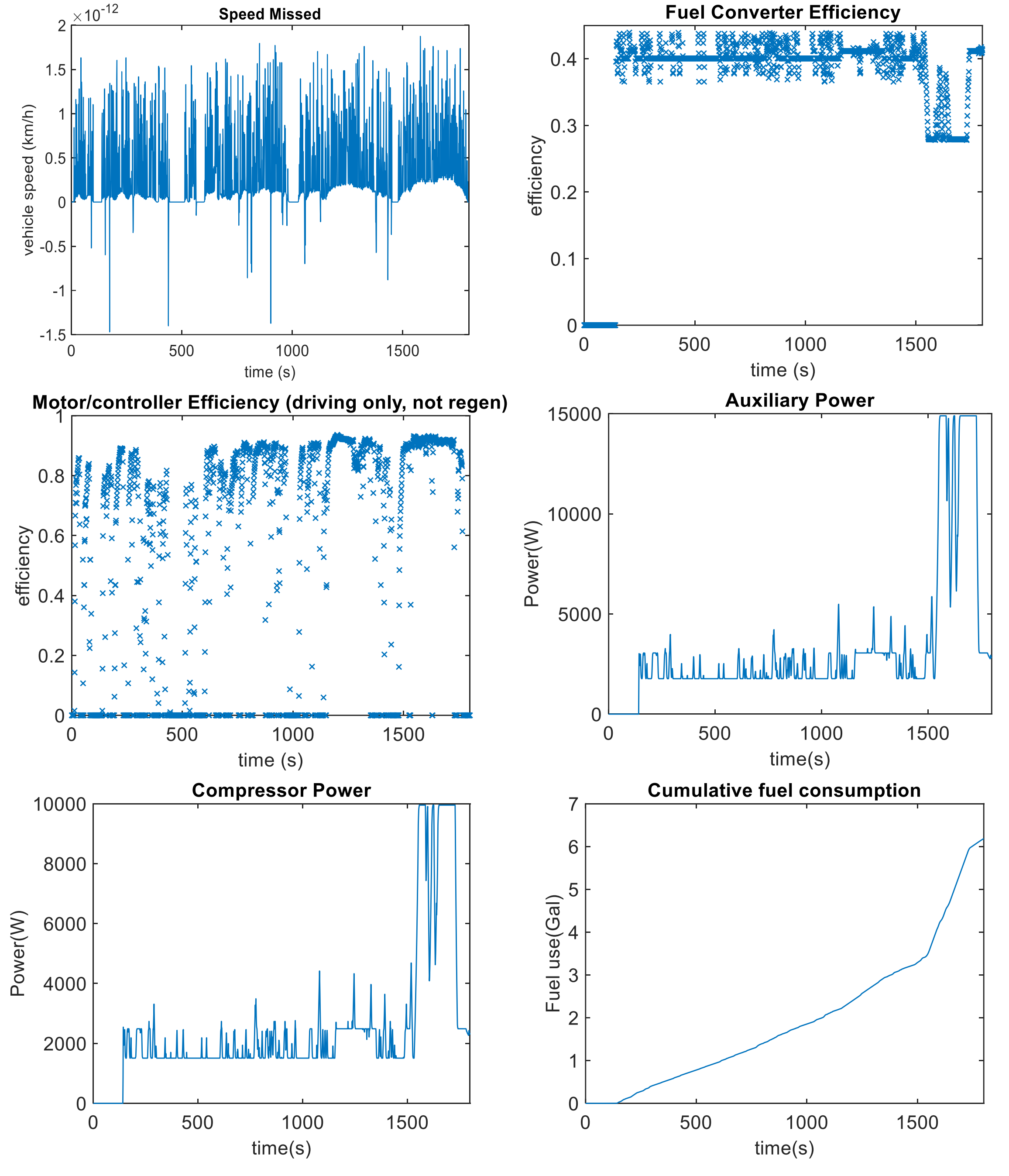

Figure 5.18 Results of WLTP Drive Cycle: a) Speed missed b) Fuel cell efficiency c) Motor efficiency d) Auxiliary power e) Compressor power f) Cumulative fuel consumption

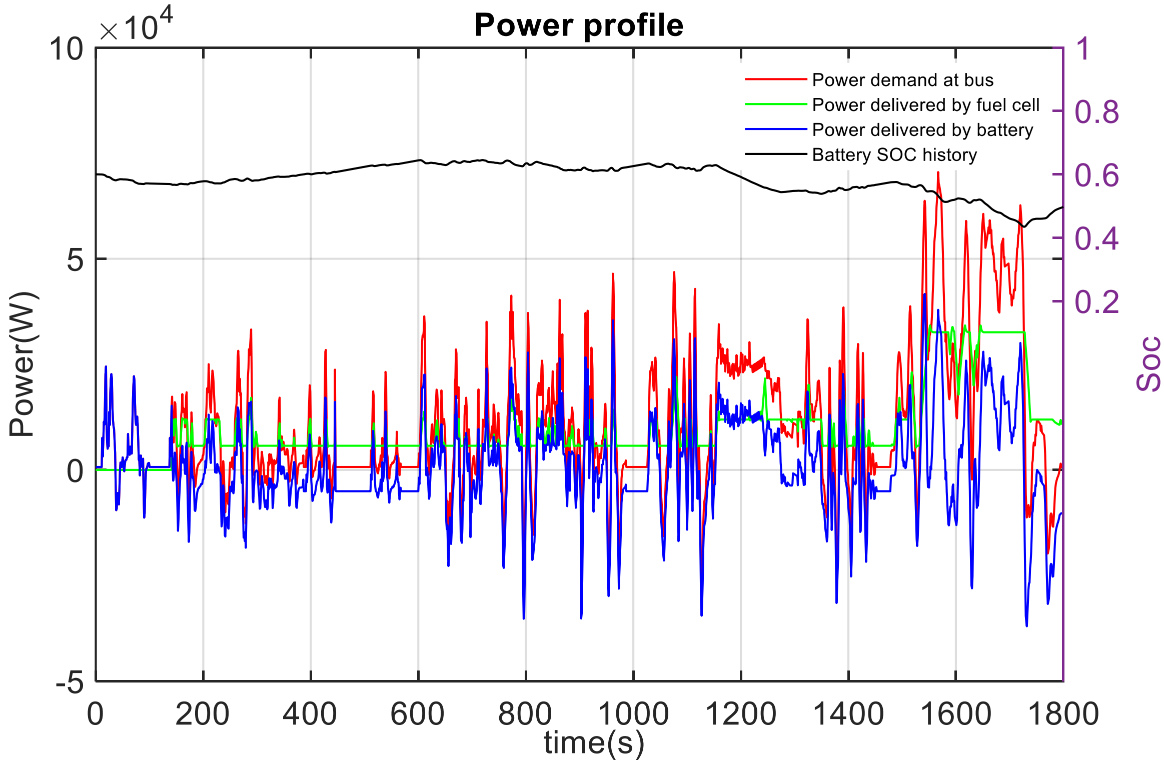

Figure 5.19 Power Profile of WLTP Drive Cycle

5.3 Proposed fuzzy logic control

5.3.1 Introduction of fuzzy logic control

Classic logic deal with variables that represents propositions (e.g. conclusion, decision) that are either true or false, but never is in between or both. However, for fuzzy logic, it uses imprecise propositions. Fuzzy set theory uses simple mathematics to make decisions consistent with process of human thinking. Fuzzy logic controllers are described by IF-THEN rules which often is based on human expertise on systems and its performance. Moreover, the membership function is somewhat subjective, depending on the designer's experience and available information.

Fuzzy control theories were first developed in the 1970s. At present, fuzzy control is widely used in many fields, such as automatic control, artificial intelligence, aerospace, rail transit, medical treatment, meteorology, finance, and so on. Its widespread application could be credited to the following advantages:

1. Fuzzy logic control system is a rule-based system and has distinguishing merits in tackling systems that are not precisely described mathematical models or highly non-linear systems.

2. It is a non-linear controller using linguistic variables, which is easy to be designed and implemented. It processes the intuition like human beings, giving it the strength to adapt to difficulties in the control.
3. It is robust, even works well with noisy inputs. It is efficient and has a fast response.
4. Concerning the designer side, it is easy to comprehend since it does not involve complex mathematical analysis. It also has a user-friendly interface, allowing designers to modify the parameters more efficiently.

The structure of a fuzzy logic controller is made of three parts: the fuzzification module, the inference engine built on rule base, and the defuzzification module, as shown in Figure 5.20.

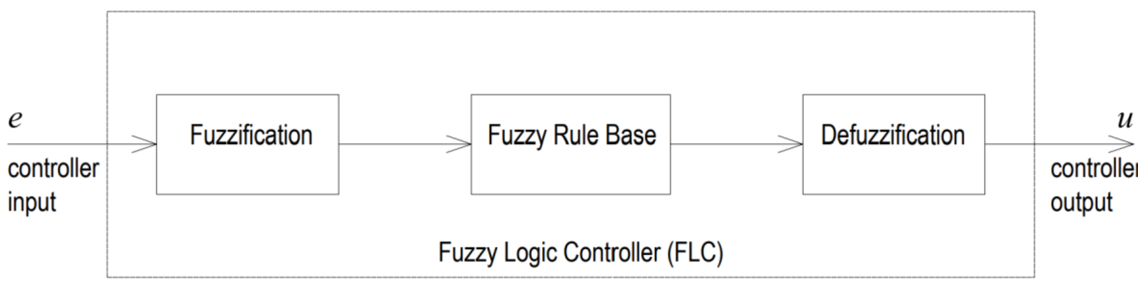

Figure 5.20 General Structure of Fuzzy Logic Controller

The fuzzification step converts the input into fuzzy subsets. The subsets include some ranges of the input and membership functions describing the degree of confidence of the belonging to a certain range. The inputs to the fuzzification module are crisp values. The outputs are membership functions and their corresponding intervals. The intervals are labeled with fuzzy terms.

The outputs of the fuzzification module are then sent to the fuzzy rule base to create control actions. To be more specific, the rule base is a set of IF-THEN rules, in the following form:

R^1 : IF controller input e_1 is E_{11} AND ... AND

controller input e_n is E_{1n}

THEN controller output u_1 is U_1

⋮

R^m: IF controller input e_1 is E_{m1} AND ... AND

controller input e_n is E_{mn}

THEN controller output u_m is U_m

Where e_n is the input, u_m is the name of the outputs, E_{mn} and U_m are the fuzzy linguistic terms. The outputs are fuzzy terms U_m.

The Defuzzification Module:

The defuzzification module is a process to determine the crisp value of the outputs. Commonly used defuzzification methods are center-of-gravity methods, center-of-sums, mean-of-maxima, and so on.

5.3.2 Fuzzy logic controller design

The fuzzy logic control in this paper has two input variables and one output variable. The input variables are battery SOC and the power demand at bus (P_{dem}). The output is the power request to fuel cell ($P_{fc,r}$). The power required from energy storage system (P_{ess}) can be calculated by subtracting the power achieved ($P_{fc,a}$) by fuel cell from the power demand at bus (P_{dem}).

Figure 5.21 shows the Simulink block used in the design:

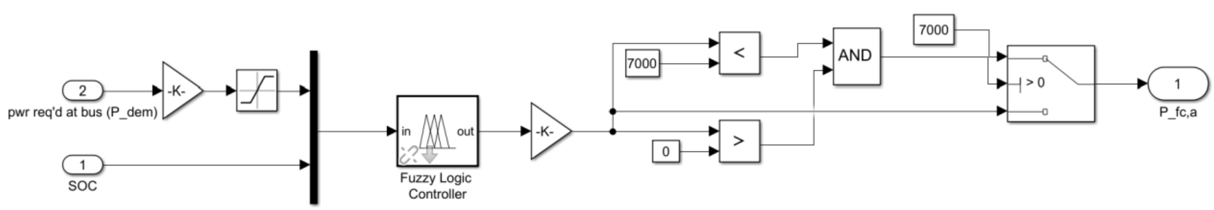

Figure 5.21 Simulink Block of FLC

The range of input variables and output variable are pre-assigned as:

$$0 \leq SOC \leq 1$$

$$0 \leq P_{dem} \leq 50\ kW$$

$$0 \leq P_{fc,r} \leq 45\ kW$$

The linguistic terms used are given as follows:

Table 5.2 Linguistic Terms of FLC

SOC	P_{dem}	$P_{fc,r}$
L: Low	ZO: Zero	ZO: Zero
M: Medium	SS: Super Small	NZ: Near Zero
H: High	S: Small	SS: Super Small
	M: Medium	S: Small
	MB: Medium Big	M: Medium
	B: Big	MB: Medium Big
	SB: Super Big	B: Big
	MAX: Maximum	SB: Super Big
		MAX: Maximum

The performance of fuzzy logic controller is determined by the number and shape of the membership functions and the rule base, which are critical to improve the fuel cell efficiency and maintaining state of charge. The member functions associated with each input and output fuzzy variables are showed in the following figure:

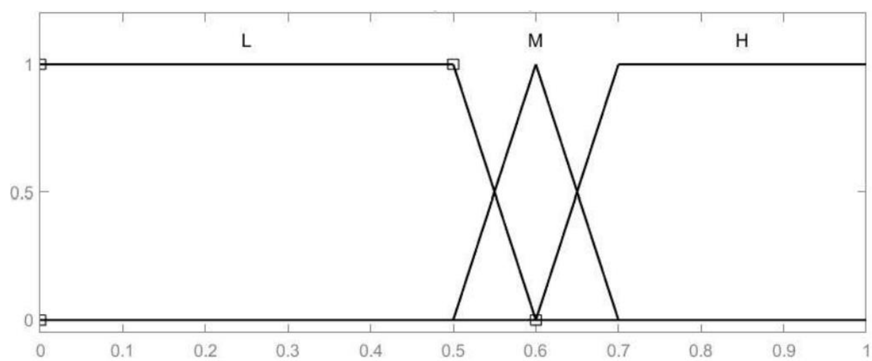

Figure 5.22 Membership Function of Input Variable 'SOC'

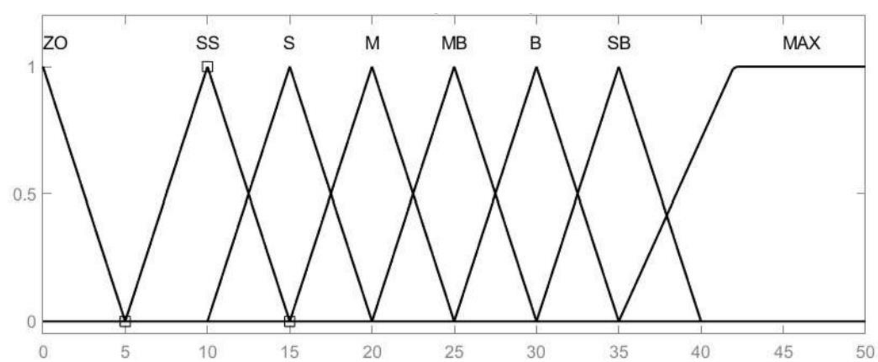

Figure 5.23 Membership Function of Input Variable 'P_{dem}'

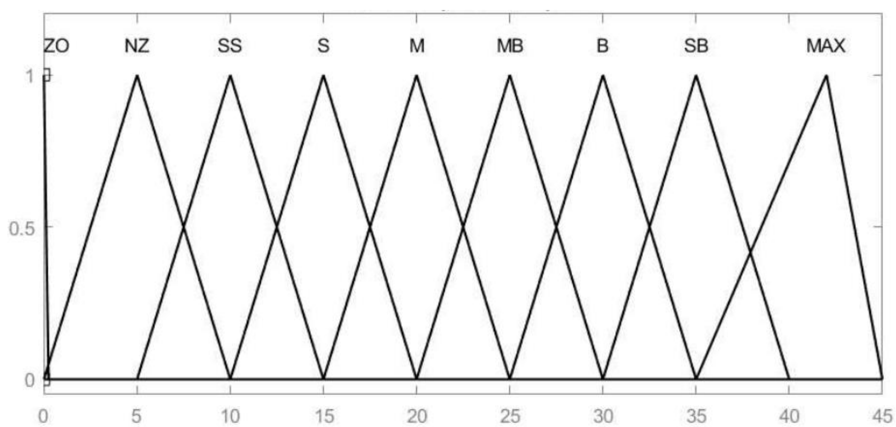

Figure 5.24 Membership Function of Input Variable '$P_{fc,r}$'

The rule base selected are summarized as follows:

Table 5.3 Rule Base of FLC

		P_{dem}							
	$P_{fc,r}$	ZO	SS	S	M	MB	B	SB	MAX
SOC	L	NZ	S	M	MB	B	SB	MAX	MAX
	M	ZO	SS	S	M	MB	B	SB	MAX
	H	ZO	ZO	SS	S	M	MB	B	SB

Table 5.3 illustrates the rules of the fuzzy logic controller and can be interpreted as:

IF SOC is L, P_{dem} is ZO/SS/S/M/MB/B/SB/MAX,

THEN $P_{fc,r}$ is NZ/S/M/MB/B/SB/MAX/MAX;

IF SOC is M, P_{dem} is ZO/SS/S/M/MB/B/SB/MAX,

THEN $P_{fc,r}$ is ZO/SS/S/M/MB/B/SB/MAX;

IF SOC is H, P_{dem} is ZO/SS/S/M/MB/B/SB/MAX,

THEN $P_{fc,r}$ is ZO/ZO/SS/S/M/MB/B/SB;

A more intuitive rule surface is displayed in Figure 5.25.

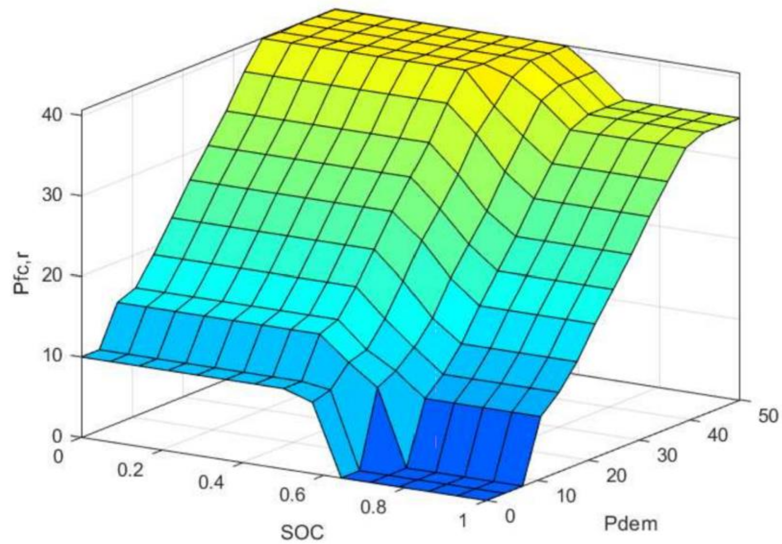

Figure 5.25 Rule Surface of FLC

5.3.3 Results of proposed fuzzy logic control

5.3.3.1 UDDS drive cycle results

Energy Flow Table(kJ)

Components	In	Out	Loss	Efficiency
Fuel cell	21607	8859	12748	0.41
Battery	2200	2210	106	0.95
Energy stored in battery	-116			
Motor/controller	9509	7681	1828	0.81
Gearbox	7681	7196	486	0.94
Wheel/Axle	7196	6824	371	0.95
Aux load	958	0	958	0
Aero			1845	
Rolling			2076	
Overall efficiency				0.180
Fuel consumption(L/km)				83.4

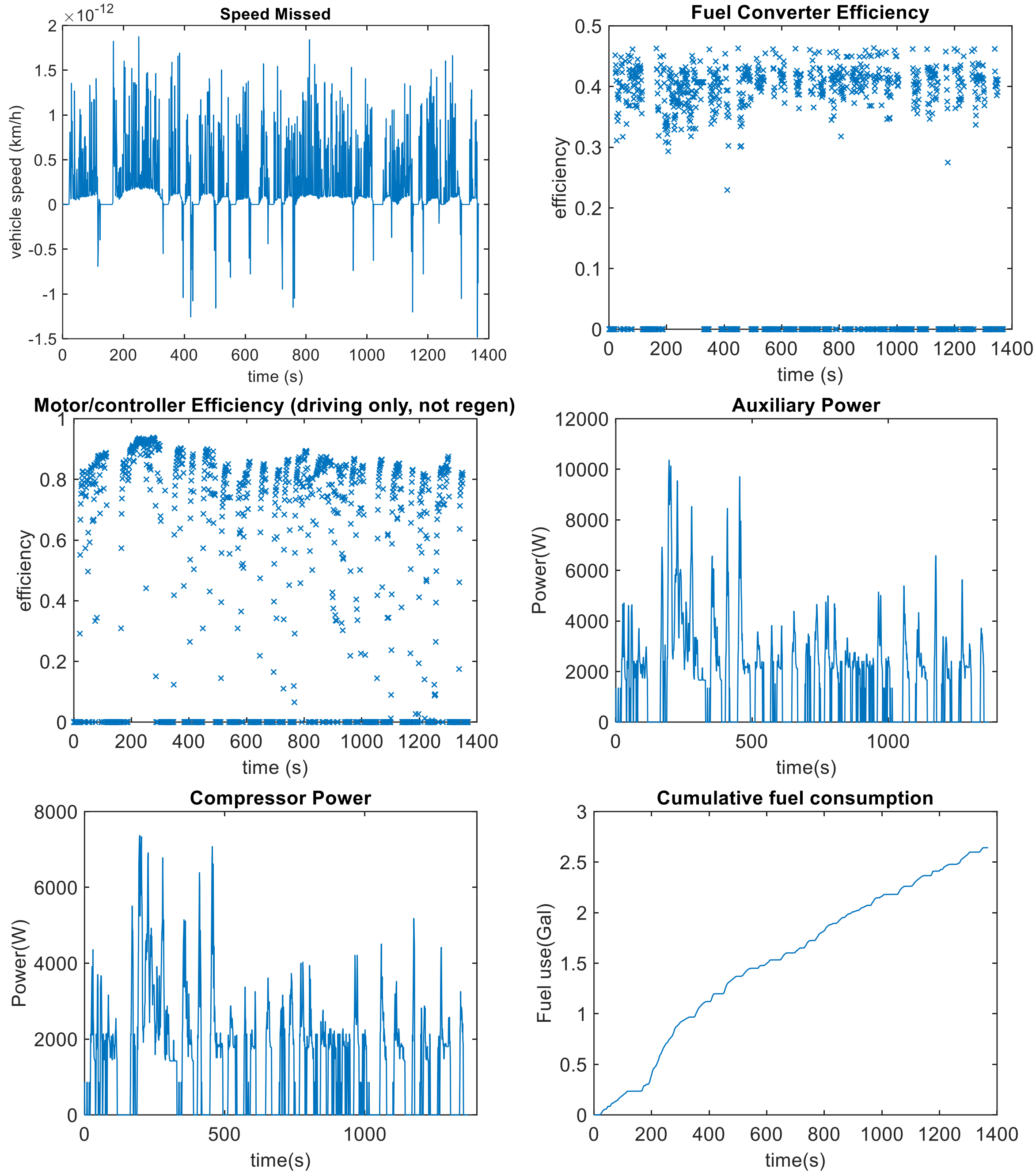

Figure 5.26 Results of UDDS Drive Cycle: a) Speed missed b) Fuel cell efficiency c) Motor efficiency d) Auxiliary power e) Compressor power f) Cumulative fuel consumption

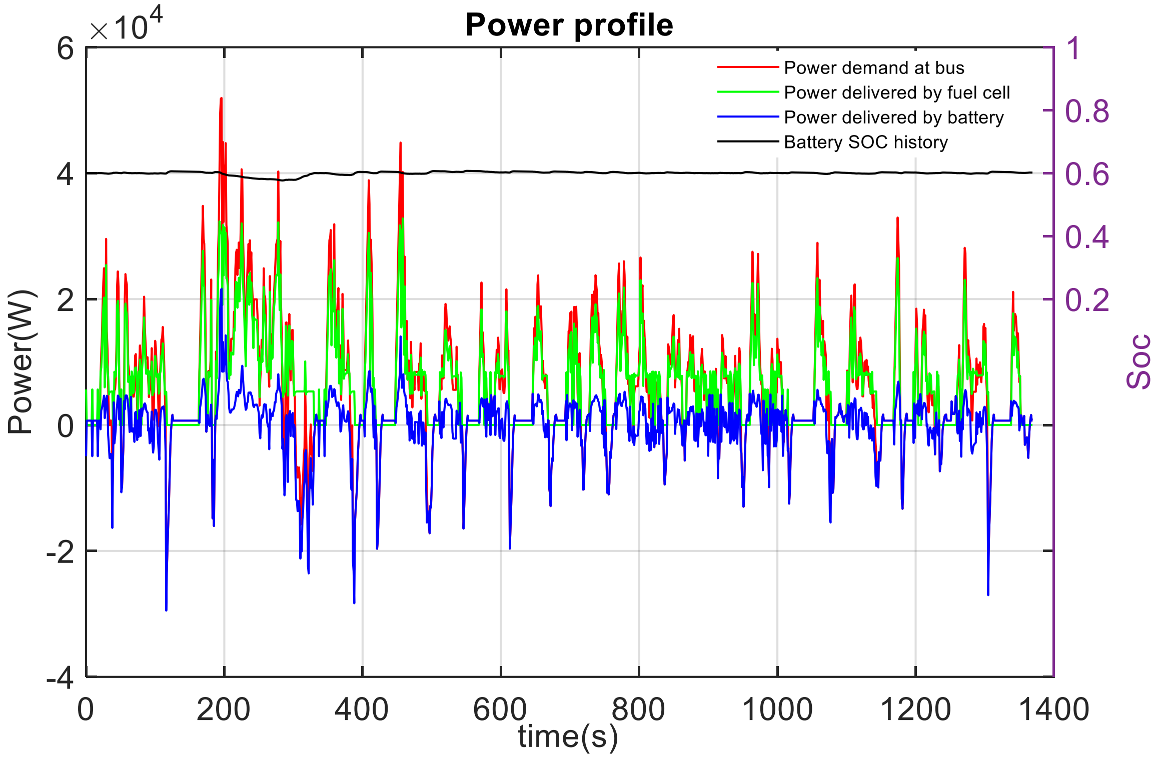

Figure 5.27 Power Profile of UDDS Drive Cycle

5.3.2.2 NEDC drive cycle results

Energy Flow Table(kJ)

Components	In	Out	Loss	Efficiency
Fuel cell	20436	8098	12338	0.396
Battery	1767	2048	117	0.94
Energy stored in battery	-398			
Motor/controller	8639	7264	1376	0.84
Gearbox	7264	6779	485	0.93
Wheel/Axle	6779	6440	339	0.95
Aux load	829	0	829	0
Aero			2795	
Rolling			1892	
Overall efficiency				0.225
Fuel comsumption(L/km)				90

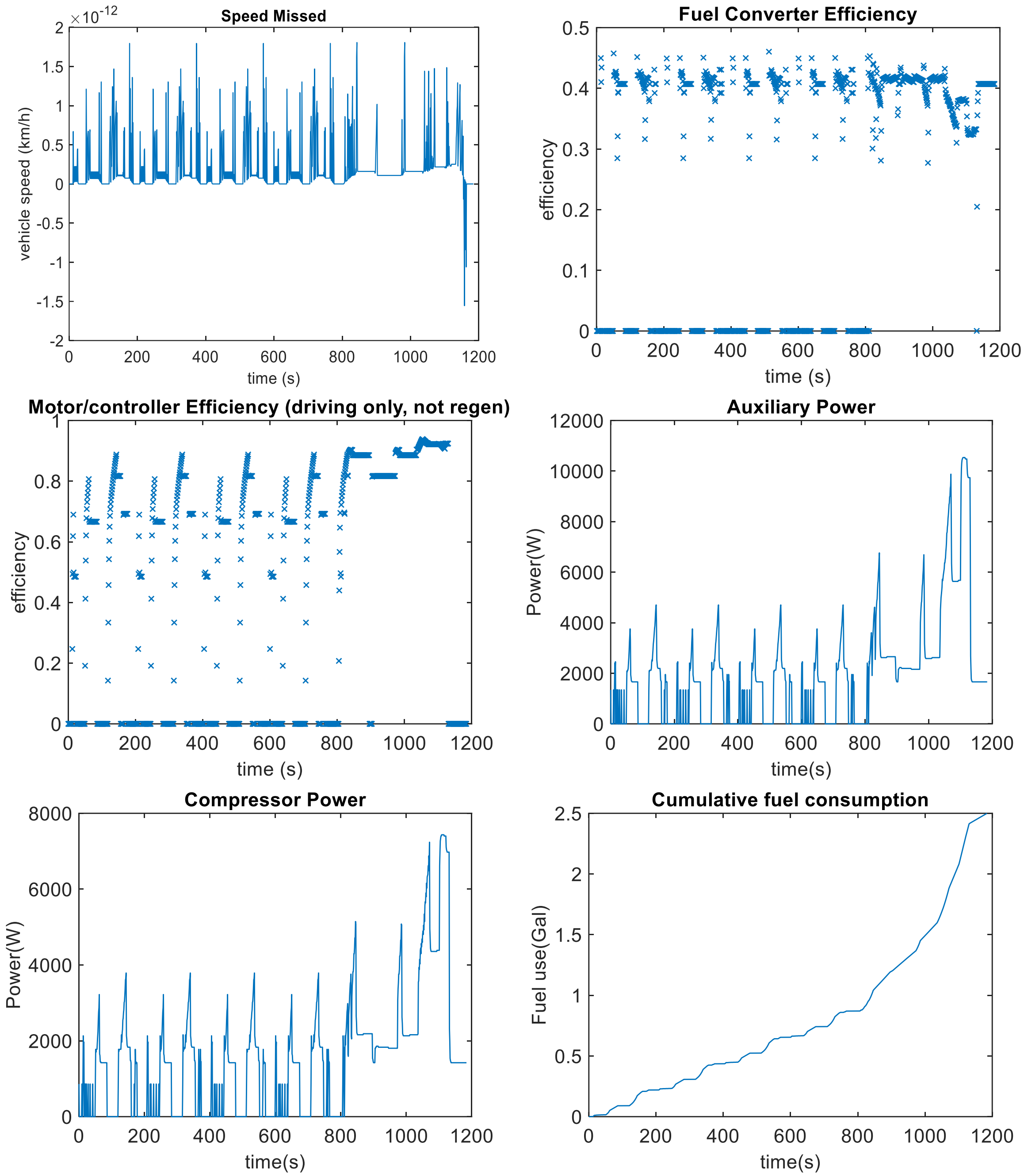

Figure 5.28 Results of NEDC Drive Cycle: a) Speed missed b) Fuel cell efficiency c) Motor efficiency d) Auxiliary power e) Compressor power f) Cumulative fuel consumption

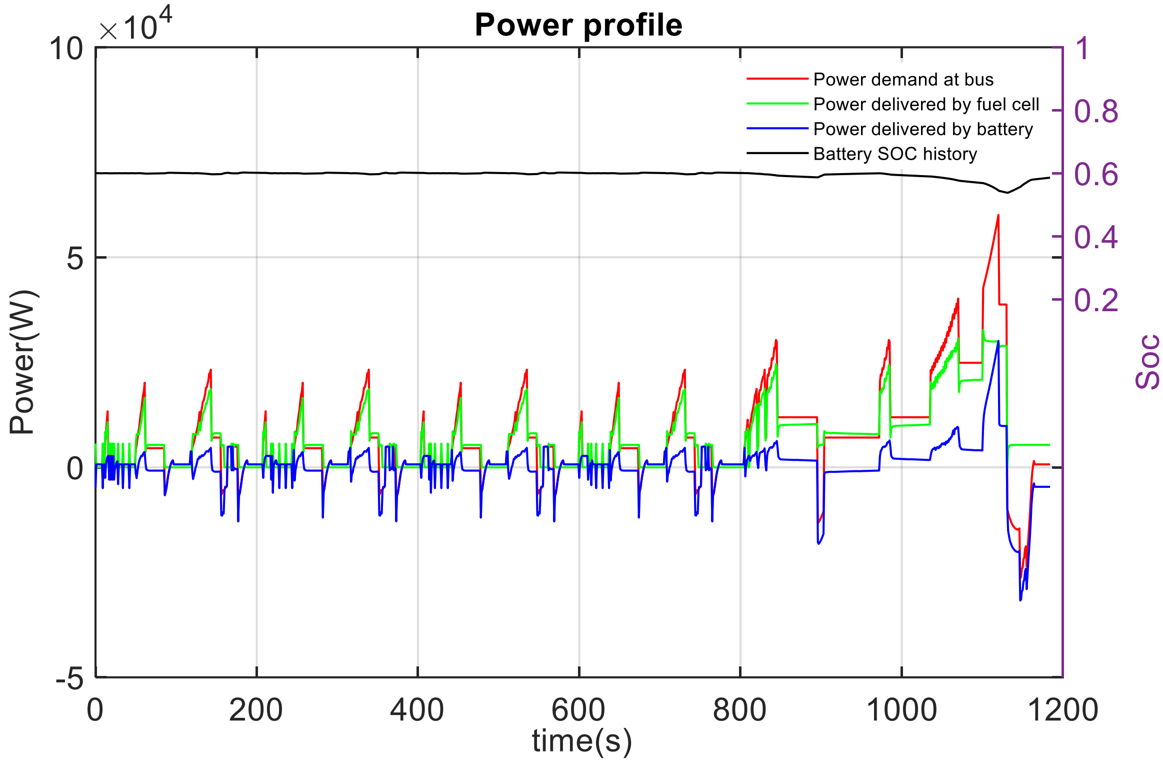

Figure 5.29 Power Profile of NEDC Drive Cycle

5.3.2.3 WLTP drive cycle results

Energy Flow Table(kJ)

Components	In	Out	Loss	Efficiency
Fuel cell	46183	17556	28627	0.380
Battery	3539	5869	337	0.93
Energy stored in battery	-2668			
Motor/controller	21070	18260	2810	0.87
Gearbox	18260	17154	1107	0.94
Wheel/Axle	17154	16406	748	0.96
Aux load	1260	0	1260	0
Aero			8407	
Rolling			4028	
Overall efficiency				0.255
Fuel comsumption(L/km)				104.2

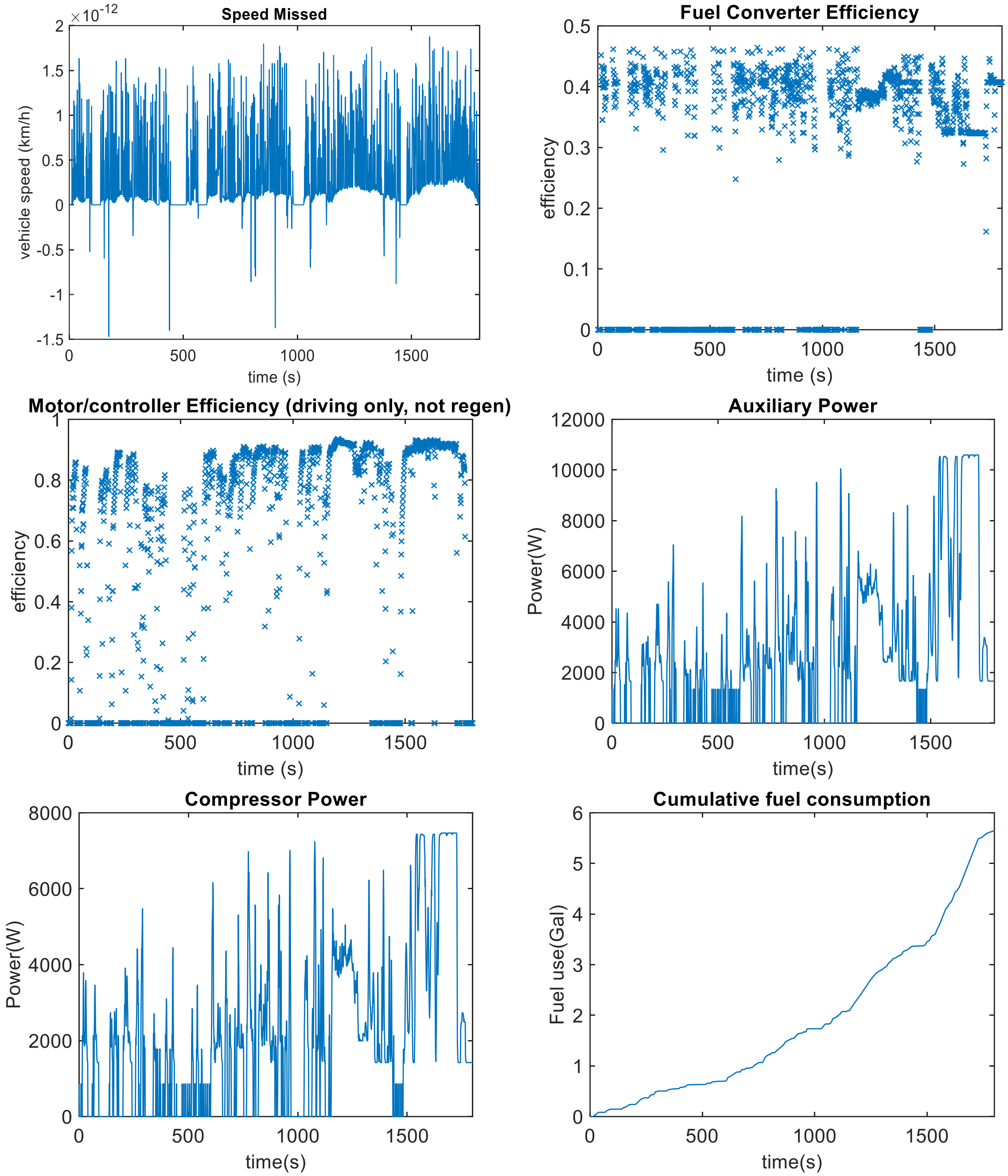

Figure 5.30 Results of WLTP Drive Cycle: a) Speed missed b) Fuel cell efficiency c) Motor efficiency d) Auxiliary power e) Compressor power f) Cumulative fuel consumption

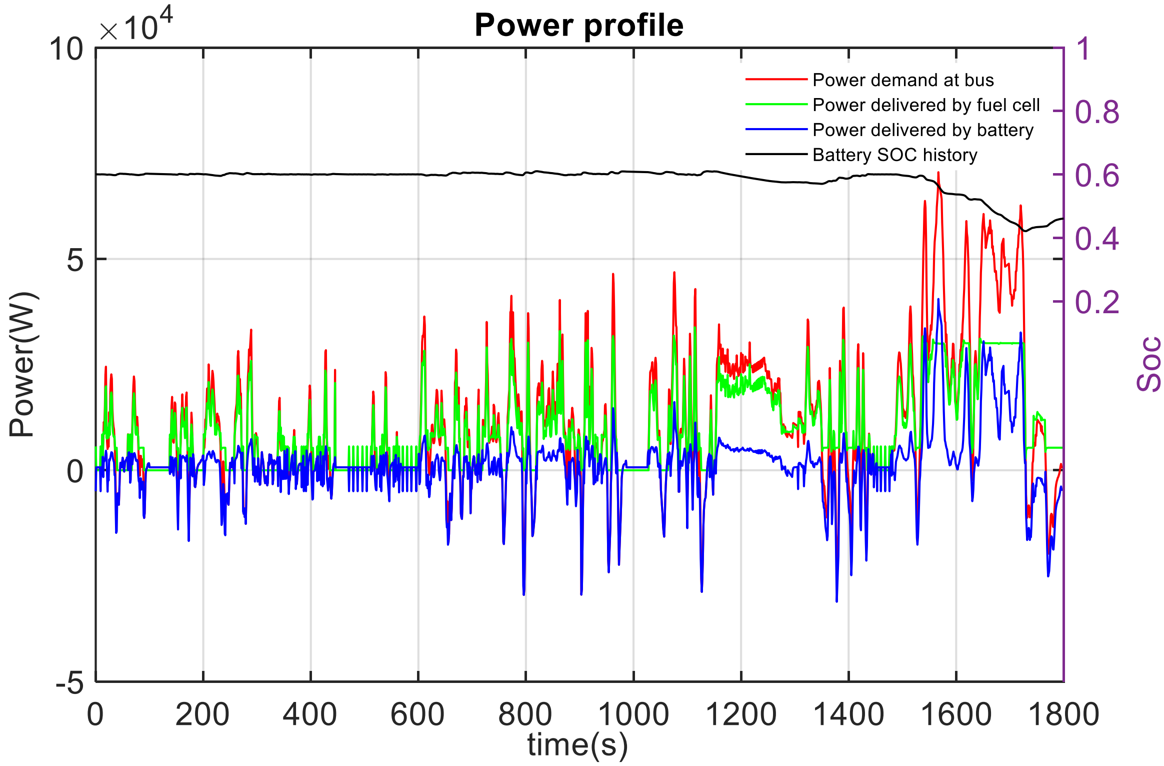

Figure 5.31 Power Profile of WLTP Drive Cycle

5.4 Summary of results

All the control strategies listed above are able to meet the power requirement and the vehicle can meet the speed trace of different drive cycles. The SOC of is are maintained in the range of expected value and can be recovered after running multiple drive cycles.

Table 5.4 Summary of Fuel Cell Results

	UDDS		NEDC		WLTP	
	Fuel cell efficiency	Fuel economy(L/100km)	Fuel cell efficiency	Fuel economy(L/100km)	Fuel cell efficiency	Fuel economy(L/100km)
PF	0.383	90.3	0.376	93.6	0.368	107
DM	0.406	86.3	0.391	92.7	0.369	108.6
FLC	0.410	83.4	0.396	90	0.380	104.5

Table 5.4 shows the efficiency and fuel economy of the fuel cell, where PF stands for default power follower control, DM stands for discretization method, FLC stands for fuzzy logic control.

Among those control strategies, the fuzzy logic control has the best efficiency and fuel economy. The FLC improves the fuel cell efficiency by 3 percent in UDDS drive cycle, 2 percent in NEDC cycle, 1.3 percent in WLTP cycle. The proposed discretization method outperforms the PF in UDDS and NEDC cycle, while approximately identical in WLTP cycle. The FLC could save about 7 liters fuel when vehicle covers 100 km in UDDS and NEDC cycle, while 3.5 liters in WLTP cycle. With discretization method, the fuel economy is reduced in UDDS and NEDC cycle, however, it undergoes an a slightly increase in WLTP cycle.

6.Two-speed transmission optimization

6.1 Introduction of two-speed transmission

Almost FCVs, including Toyota Mirai, Hyundai Nexo, Honda Clarity, adopt a configuration in which electric motor and final drive are connected via a fixed, single-speed gearbox. This is due to many reasons: first, in terms of characteristic of traction motor, it exhibits a relatively high constant torque from zero to base angular speed, and later enters into a region characterized by constant power in higher angular speed. The traction motor can output sufficient torque when vehicle accelerates from low speed and, due to wide range of angular speed of motor, the top speed could also be achieved by single fixed speed ratio. Second, concerning efficiency of traction motor, it is less sensitive to speed and torque when compared with the efficiency of traditional combustion engine.

However, having a better efficiency over ICE doesn't mean that the traction is operating at its optimal region. Researches within recent years show improvements in efficiency and performance of motor is possible.Walker et al. conducted a research on two-speed transmission of pure electric vehicle, and results show that the installing of two-speed gearbox improve the performance of acceleration and grade climbing [19]. Alexei et al. investigated two-speed gearbox in electric delivery step vans. Pareto optimization method based on GA is used to design the optimum gear ratio pairs using AVL Cruise. The minimum acceleration time from standstill to 100 km/h of 17.05 s and minimum energy consumption of 4.77 kWh is achieved with two-speed transmission [20]. The impact of the two-speed gearbox on Nissan Leaf was investigated by Ahmed et al. and found the efficiency of the motor is increased to 90.25%, while the one with 1-speed transmission is 88.05% [21]. The research was done by Ren et al. in various drive cycles with a variable ratio gearbox. The conclusions are that it is possible to improve overall energy consumption levels by more than 5 % with a variable ratio gearbox[22].

In 2012, one of the world leaders in transmission technology, Oerlikon Graziano, in collaboration with Vocis Driveline Control, reported the results of a case study on a two-speed system for EVs. These results clearly demonstrate the advantages of the two-speed transmission when compared to a single-speed model used in EVs via four main characteristics: acceleration time, maximum climbing grade, maximum speed, and energy consumption.

Looking at the commercial implementation of the two-speed transmission, it is worth mentioning the Porsche Taycan. Below in Figure 6.1 shows the system layout of the rear axle. It has two PMS motors; In the front axle, the motor is coupled with a one-speed transmission with a gear ratio of 8.05. In the rear, the motor is coupled with two-speed transmission with a first gear ratio of 15.563 and a second gear ratio of 8.05. The gearshift strategies of Taycan are:

1.Maximum driving efficiency:

Second gear is used as often as possible.

2.Maximum drive off performance:

Engaged in the first gear.

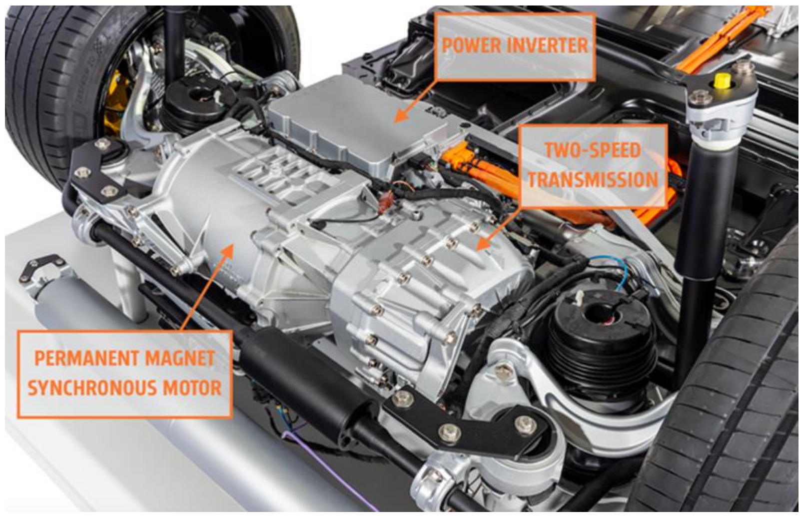

Figure 6.1 Rear Axle of Tycan

For compact class vehicle, ZF has a two-speed gearbox that claimed to have an improvement in energy conversion efficiency, which extends the driving range by 5% for each battery charge. "An even better efficiency at the sweet spot of the efficiency map in combination with the 2-speed gearbox leads to an efficient system layout", said Stephan Demmerer, Head of ZF Advanced Engineering e-Mobility. Figure 6.2 showed the product.

Figure 6.2 Two-speed Gearbox by ZF

A Canadian company called inmotive provides the two-speed transmission (Ingear). A simulation report is present on their official website. In the simulation, for the 1-speed, 9.665 gear ratio is used. The 2-speed transmission module uses a combination of 5:1 high gear ratio and 10:1 low gear ratio. The simulation indicates that the EV extends 7.1% range on the WLTP drive cycle with the two-speed transmission.

Based on the above discussion, we can draw the conclusion that improving motor efficiency by integrating a two-speed transmission is a feasible way. In the below sub-chapters, the gear ratio, shifting strategy, and results about the motor efficiency will be investigated.

6.2 Two speed transmission simulation

The aim of integrating a two-speed transmission is to improve the motor efficiency by allowing the traction motor to operate in a more efficient region. The efficiency of the traction motor is a function of speed and torque, represented by an efficiency map. The shifting could change the overall ratio of powertrain and influence the torque and speed request to motor, thus changing the operating point in the efficiency map of motor. In this way, an improvement in motor efficiency is possible to achieve.

The selection of gear ratio has to meet some requirements in different driving conditions according to the below equation 6.1.

$$F_t = F_f + F_w + F_i + F_j \quad (6.1)$$

Where the F_t is the traction force, F_f is the rolling friction, F_i is the force due to inclined road, F_j is the inertia force due to acceleration. Substituting with the detailed force expressions yields:

$$\frac{Ti\eta_T}{r} = mgf\cos\alpha + \frac{C_d A u^2}{21.15} + mg\sin\alpha + \delta m \frac{du}{dt} \quad (6.2)$$

Where T is toque delivered by motor, i is overall ratio, η_T is average powertrain efficiency, r is the effective rolling radius of tire, α is road inclination angle, δ is equivalent mass inertial coefficient, C_d is drag coefficient, A is frontal area, u is the velocity of the vehicle. In Table 6.1 shows the parameters needed to define the gear ratio.

Table 6.1 Parameters of the Simulated Vehicle

Parameters	Values
m (additional 14 kg)	1975 kg
C_d	0.44
A	2.66 m^2
f	0.015
u_{max}	140 km/h
n_p	12997 rpm
T_{max}	203 Nm
r	0.343 m
φ	0.75
η_T	0.92
C_w	0.55

Ratio design for grade: The design of the first gear ratio is important for the capability of climbing an inclined road. It must ensure the vehicle to enter or leave steep driveway and parking structures. It is defined in a scenario where the vehicle is exerting max torque to climb an inclined road with the angle α (tanα =30%) at the speed of 30 km/h. The expression is given in inequation 6.3.

$$\frac{i_1 T_{max}\eta_T}{r} \geq mgf cos\alpha + \frac{C_d A u^2}{21.15} + mg sin\alpha \quad (6.3)$$

Solving the inequation:

$$i_1 \geq 11$$

Ratio design for top speed: Vehicle top speed is critical for customer acceptance. It is achieved when the motor is operating at its maximum speed and the second gear is engaged. The output rotational speed must be larger than the rotational speed of the wheel at maximum vehicle speed. This is given in inequation 6.4. 0.377 is present due to in the equation we use the rpm, km/h rather than the international units rad/s, m/s.

$$i_2 - 0.377\frac{n_p r}{u_{max}} \leq 0 \quad (6.4)$$

Solving the inequation:

$$i_2 \leq 12$$

Ratio design considering tire adhesion: The adhesion limit is the force required for the wheels to transit rolling to sliding. For front-drive vehicles, it is a function of weight distribution and tire static friction coefficient. Inequation 6.5 indicates that the maximum torque of transmission output must be lower than the road can provide.

$$\frac{i_1 T_{max} \eta_T}{r} \leq C_w m g \varphi \quad (6.5)$$

Solving inequation:

$$i_1 \leq 19.9$$

Continuity: The difference between two gear ratio i_1, i_2, can not be too big, in order to switch smoothly from i_1 to i_2, or i_2 to i_1.

$$1.4 \leq \frac{i_1}{i_2} \leq 1.8$$

The range of ratios for i_1, i_2 are determined. Another important variable is the shifting speed, i.e., the speed where the second speed is engaged. Here we define the shifting speed as 40 km/h.

The gear ratio pairs are simulated in UDDS cycle and the trend can be seen in Table 6.2. So the gear ratio(19.8,11) is selected where the most efficiency is obtained.

Table 6.2 Motor Efficiency as a Function of Ratio Pair

		Gear 1									
Efficiency		11	12	13	14	15	16	17	18	19	19.8
Gear 2	11	0.81	0.82	0.82	0.83	0.83	0.84	0.84	0.84	0.85	0.85
	10	0.81	0.82	0.82	0.83	0.83	0.84	0.84	0.84	0.84	0.85
	9	0.8	0.81	0.82	0.82	0.83	0.83	0.83	0.84	0.84	0.84
	8	0.8	0.81	0.81	0.82	0.82	0.83	0.83	0.83	0.83	0.84
	7	0.79	0.8	0.81	0.81	0.82	0.83	0.83	0.83	0.83	0.83
	6	0.79	0.8	0.8	0.81	0.81	0.82	0.82	0.82	0.82	0.82
	5	0.78	0.78	0.79	0.8	0.8	0.8	0.81	0.81	0.81	0.81
	4	0.76	0.77	0.78	0.78	0.79	0.79	0.79	0.79	0.79	0.8
	3	0.74	0.75	0.75	0.76	0.76	0.76	0.77	0.77	0.77	0.77

6.3 Results and discussion

The evaluation of the effect of two-speed transmission is conducted using fuzzy logic control in UDDS cycle and NEDC cycle. Table 6.3 shows the impact on motor efficiency and fuel economy compared with the one-speed transmission. We can see that efficiency of the motor is increased by 4 percent in UDDS cycle and 2 percent in NEDC cycle, resulting in the fuel consumed by the fuel cell decreasing remarkably. Both in NEDC and UDDS cycle, the operating points of the motor are moving to the right part where the efficient region locates, as are shown in Figure 6.3 and Figure 6.4.

Table 6.3 Results of Two-speed Transmission

	Efficiency of motor		Fuel economy(L/100 km)	
	UDDS	NEDC	UDDS	NEDC
One-speed transmission with fuzzy logic controller	0.81	0.84	83.4	90
Two-speed transmission with fuzzy logic controller	0.85	0.86	78.3	85.3

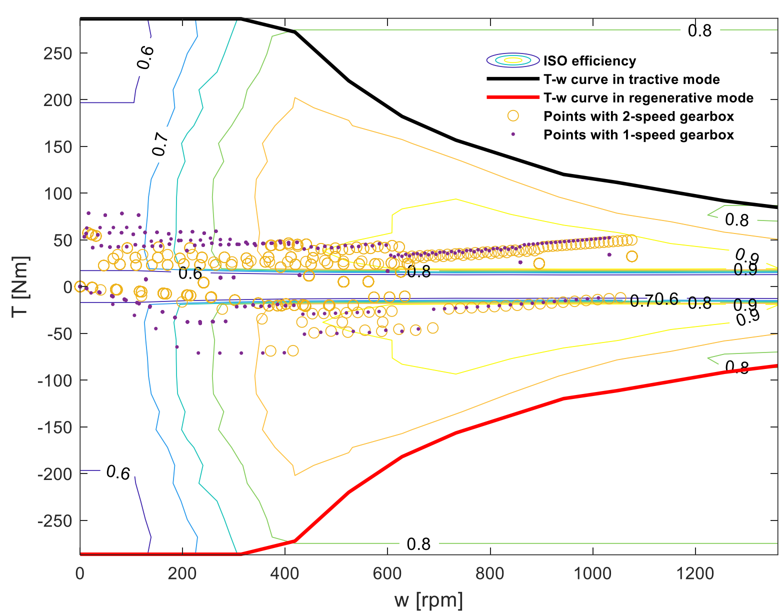

Figure 6.3 Operating Points of Motor in NEDC Cycle

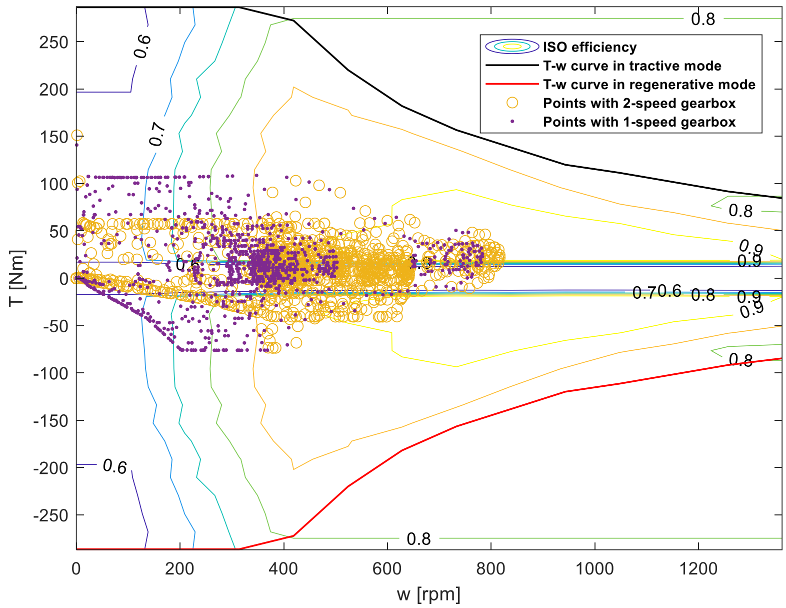

Figure 6.4 Operating Points of Motor in UDDS Cycle

7. EMS applied on Toyota Mirai

7.1 Driving intention prediction

The driving intention is a short-term action taken by the driver in the next few seconds. The driving intention of the driver in this paper are defined as eight classes, which are labeled as follows:

1. Deceleration
2. No speed
3. Low-speed cruise
4. Low-speed acceleration
5. Intermediate-speed cruise
6. Intermediate-speed acceleration
7. High-speed cruise
8. High-speed acceleration

A multiclass support vector machine is developed to predict the driving intention at the current time instant t, denoted as $DI(t)$. The $DI(t)$ is predicted based on the velocity sampled data in the previous period with a window size of 10s. To put it in another way, we use the velocities of the vehicle at $[t-9,t]$ as an input to the multiclass SVM and obtain the driving intention within $[t-9,t]$. Later, we assume that the driving intention at time t is the same as the driving intention within the time $[t-9,t]$.

The multiclass SVM has to be trained before implemented to predict the DI. The training data is constructed first: the velocity points are sampled from 11 drive cycles, which are ARB02, HL07, HWFET, IM240, IM240, REP05, SC03, UNIF01, US06, WLTP, FTP. The data sequence of velocity is collected with a window size of 10s, where the window is sliding with the step size of 1s. Figure 7.1 shows the procedure. The scale of the window size in the figure is not the same as it actually is. It is plotted in this way so that the window of sampling can be seen clearly. We can see that the sampling window has a length of 10 seconds and slides along the horizontal axis with the step size of 1 second.

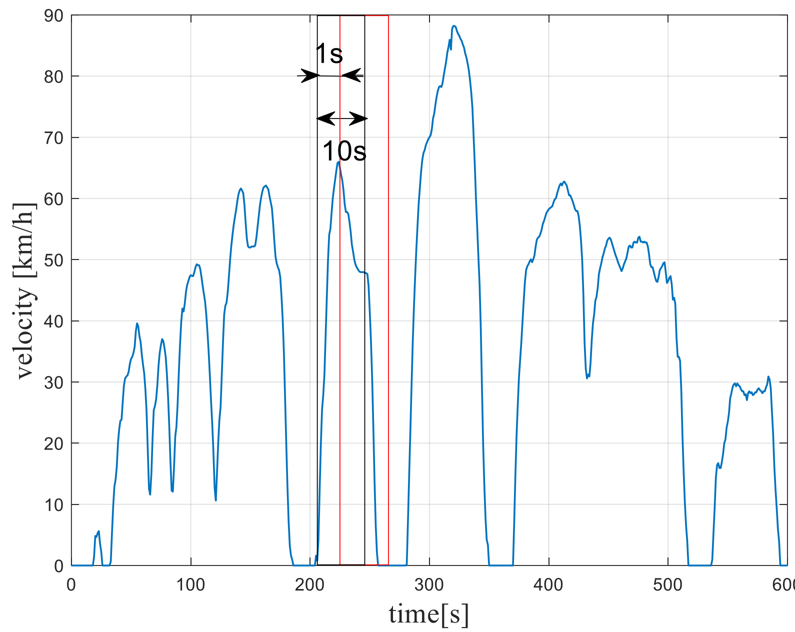

Figure 7.1 Example of Sampling the Training Data from SC03

After sampling from all the drive cycles, the training data have the size of 13081x10, which means the velocities of ten seconds are stored in one row. Each row is labeled with its corresponding class(1-8) listed above.

When training the SVM models, we use the so called 'one vs rest' method. Eight binary class classifiers are created. The test data set is sampled from WVUINTER and UDDSHDV. The accuracy of the classifiers is 97.75%.

7.2 Combining the DI prediction with Fuzzy logic

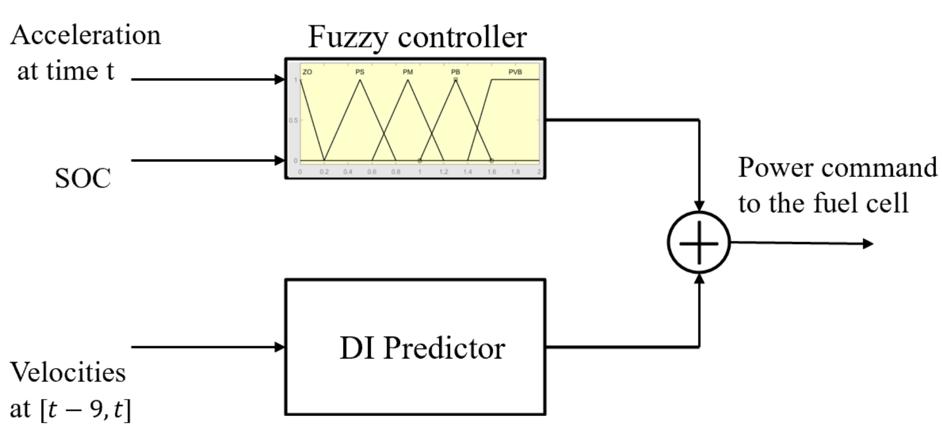

Figure 7.2 Fuzzy Controller with DI Prediction

Figure 7.2 shows the schematic diagram of the fuzzy controller with DI prediction. The DI predictor takes in the velocities at $[t-9, t]$, whose size is 10×1. The SVM models in the DI predictor identify the driving intention. The DI predictor output the base power according to the driving intention, as is shown in Table 7.1.

Table 7.1 Driving Intention and its Corresponding Output Power

Label	Driving Intention	Base power (kW)
1	Deceleration	0
2	No speed	0
3	Low-speed cruise	3
4	Low-speed acceleration	5
5	Intermediate-speed cruise	6
6	Intermediate-speed acceleration	8
7	High-speed cruise	15
8	High-speed acceleration	20

The fuzzy controller uses the acceleration at time t, denoted as a(t), and SOC(t) as inputs. The member function of a(t) is defined as follows:

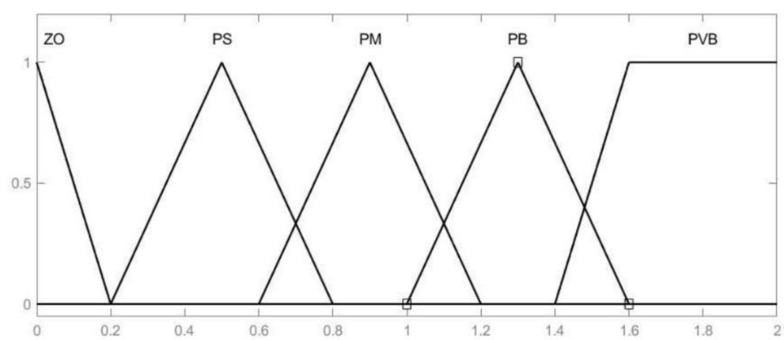

Figure 7.3 Membership Function of $a(t)$

The membership function of the Battery's SOC is as follows:

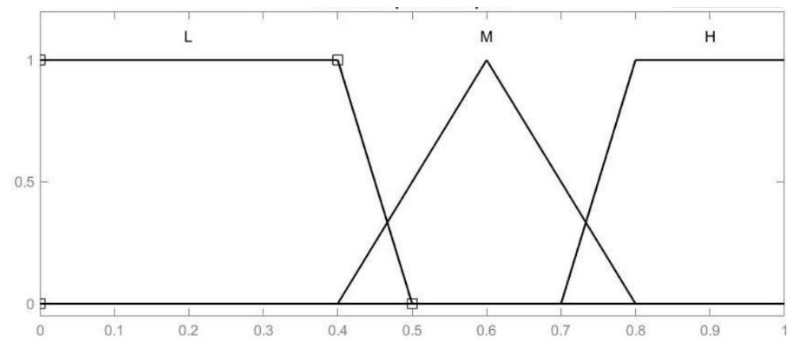

Figure 7.4 Membership Function of SOC

Rule base is illustrated in Table 7.2.

Table 7.2 Rule Base of Fuzzy Controller in Mirai

				a(t)		
	$P_{fc,r}$	ZO	PS	PM	PB	PVB
SOC	L	SS	S	M	MB	B
	M	ZO	SS	S	M	MB
	H	ZO	ZO	SS	S	M

The output membership function is shown in Figure 7.5.

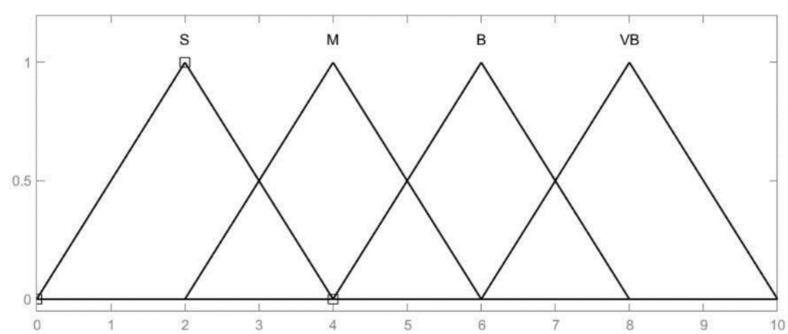

Figure 7.5 Membership Function of Output Power Command (in kW)

The output power command of the fuzzy controller added by the base power output of DI predictor is the power command to the fuel cell.

7.3 Results and discussion

7.3.1 UDDS drive cycle results

Energy Flow Table(kJ)

Components	In	Out	Loss	Efficiency
Fuel cell	17227	8918	8309	0.52
Battery	4249	4201	300	0.93
Energy stored in battery	-252			
Motor/controller	9509	7681	1828	0.81
Gearbox	7681	7196	486	0.94
Wheel/Axle	7196	6824	371	0.95
Aux load	958	0	958	0
Aero			1845	
Rolling			2076	
Overall efficiency				0.224
Fuel consumption(L/km)				66.5

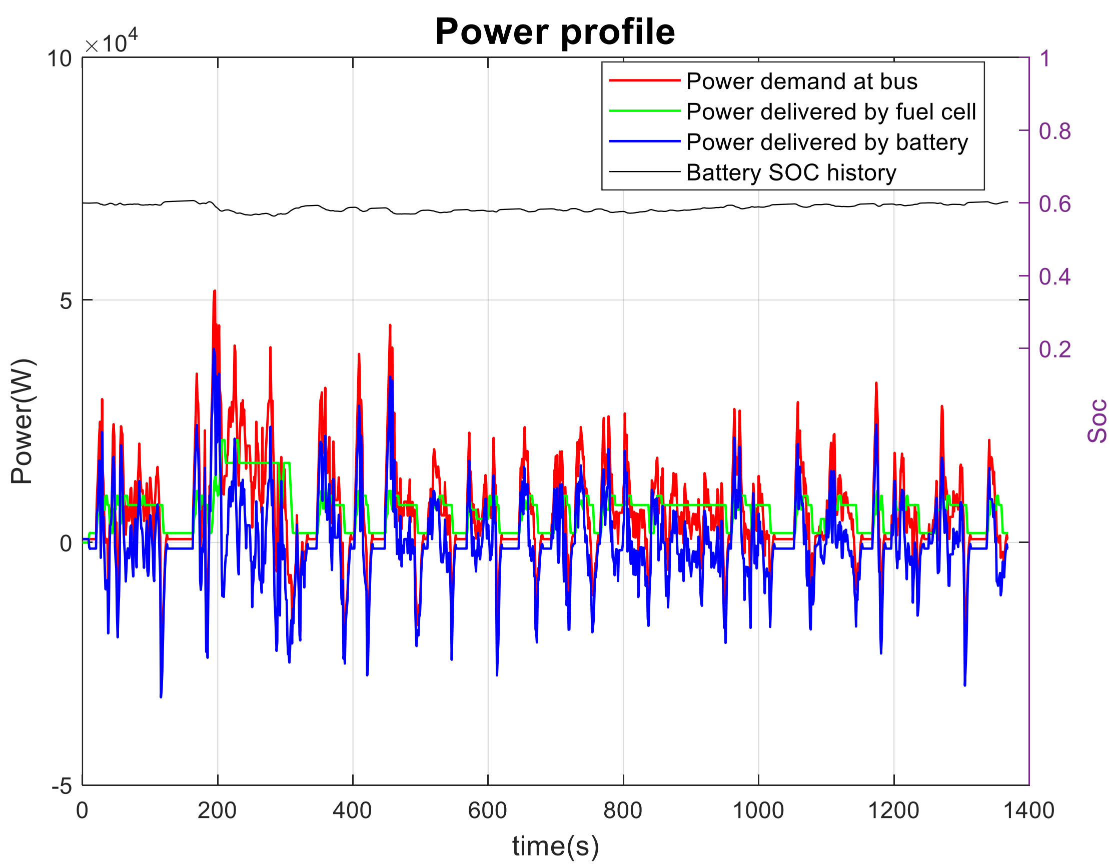

Figure 7.6 Power Profile in UDDS Drive Cycle

7.3.2 NEDC drive cycle results

Energy Flow Table(kJ)

Components	In	Out	Loss	Efficiency
Fuel cell	15679	8297	7382	0.53
Battery	3211	3293	236	0.93
Energy stored in battery	-319			
Motor/controller	8639	7264	1376	0.84
Gearbox	7264	6779	485	0.93
Wheel/Axle	6779	6440	339	0.95
Aux load	829	0	829	0
Aero			2795	
Rolling			1892	
Overall efficiency				0.293
Fuel comsumption(L/km)				66.4

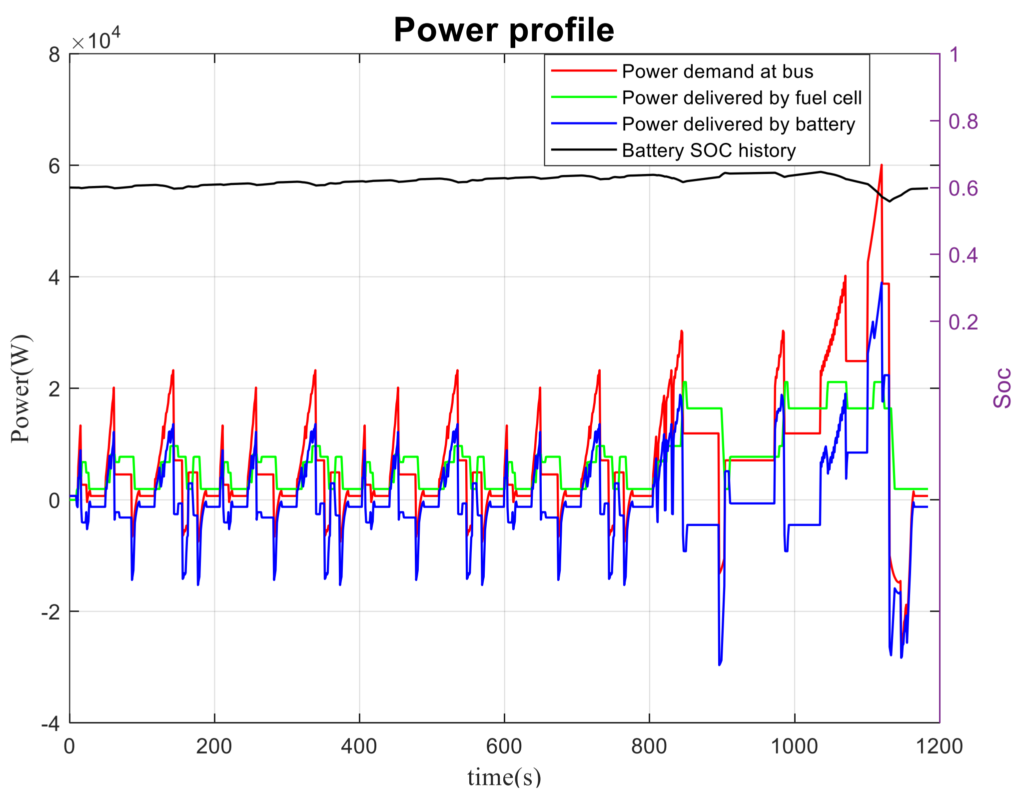

Figure 7.7 Power Profile in NEDC Drive Cycle

8. Conclusion and future work

In summary, the works were conducted to simulate the SUV with the KTH fuel cell model and the Toyota Mirai fuel cell. In the simulation of SUV with the KTH model, three control strategies were established and compared in terms of efficiency and fuel economy of the fuel cell. The baseline is the power follower control. It is found that the fuzzy logic control outperforms the power follower control with a resulting increment of efficiency by 3 percent in UDDS cycle and NEDC cycle, 2 percent in WLTP cycle. The fuzzy logic control could save about 7 liters of fuel when the vehicle covers 100 km in UDDS and NEDC cycle, while 3.5 liters in WLTP cycle. The discretization method outperforms the power follower in UDDS and NEDC cycle while approximately identical in WLTP cycle. With the two-speed gearbox integrated into the driveline, the efficiency of motor improves by 4 percent in UDDS cycle and 2 percent in NEDC cycle. This leads to the overall fuel economy improve to 78.3 L/100km in UDDS cycle and 85.3 L/100km in NEDC cycle. The two-speed gearbox and fuzzy logic control have a significant impact when compared to the baseline with fuel economy of 90.3 L/100km in UDDS cycle and 93.6 L/100km in NEDC cycle. In simulating the SUV with the Toyota Mirai fuel cell, a driving intention prediction is realized with multiclass SVM. This driving intention prediction was combined with another fuzzy logic control. The efficiency of the Mirai fuel cell could reach up to 0.52 in UDDS cycle and 0.53 in NEDC cycle. A more smooth power profile of the fuel cell is achieved. Among all the control strategies, the SOC of the battery is kept between the desired range.

Concerning the future work, despite the efficiency of the fuel cell efficiency is increased in proposed control strategies, the limits of how much we can improve, remain unknown. Thus, it is necessary to explore the global optimal by applying the dynamic programming algorithm to the control strategy. Additionally, the next step is to validate the results in a bench test or in a vehicle prototype.

Reference

[1] Fuel Cell and Hydrogen Joint Undertaking. FCH JU Projects, https://www.fch.europa.eu/page/fch-ju-projects

[2] Measures for the Parallel Administration of the Average Fuel Consumption and New Energy Vehicle Credits of Passenger Vehicle Enterprises, http://www.gov.cn/xinwen/2017-09/28/content_5228217.htm

[3] Prime Minister of Japan and His Cabinet, Japan Revitalization Strategy, http://japan.kantei.go.jp/96_abe/documents/2013/1200485_ 7321.html

[4] Ministry of Economy, Trade and Industry, Strategic Energy Plan, https://www.enecho.meti.go.jp/en/category/others/basic_plan/pdf/ 4th_strategic_energy_plan.pdf

[5] Venturi, M., Sang, J., Knoop, A., & Hornburg, G. (2012). Air supply system for automotive fuel cell application. *SAE Technical Papers*.

[6] Barbir, F. (2012). PEM fuel cells: theory and practice. Academic press.

[7] Friess BR, Hoorfar M. Development of a novel radial cathode flow field for PEMFC. *Int J Hydrogen Energy 2012;37:7719-29*

[8] Bae I, Kim B, Kim D, Kim H, Oh K. In-plane 2-D patterning of microporous layer by inkjet printing for water management of polymer electrolyte fuel cell. *Renew Energy 2020;146:960-7.*

[9] Lin R, Diao X, et al. Optimized microporous layer for improving polymer exchange membrane fuel cell performance using orthogonal test design. *Appl Energy 2019;254:113714.*

[10] Jung UH, Jeong SU, Park KT, Lee HM, Chun K, ChoiD W, Kim S. Improvement of water management in air-breathing and air-blowing PEMFC at low temperature using hydrophilic silica nano-particles. *Int J Hydrogen Energy 2007;32:4459-65.*

[11] Yumiya, H., Kizaki, M., & Asai, H. (2015). Toyota fuel cell system (TFCS). *World Electric Vehicle Journal, 7(1), 85-92*.

[12] Cheng W, Ou Y et al. (2008). Selection and application of motor for fuel cell vehicle (Chinese edition). *J renewal electric vehicle.*

[13] Miller JM. Energy storage system technology challenges facing strong hybrid, plug-in and battery electric vehicles. *Veh Power Propuls Conference 2009. VPPC '09. IEEE; 2009. p. 4–10.*

[14] A. Burke, B. Jungers, C. Yang, J. Ogden Battery electric vehicles: an assessment of the technology and factors influencing market readiness. *Public Interes Energy Res Progr Calif Energy Comm (2007), pp. 1-24*

[15] Miller JM, Bohn T, Dougherty TJ, Deshpande U. Why hybridization of energy storage is essential for future hybrid, plug-in and battery electric vehicles. *2009 IEEE Energy Convers. Congr. Expo. ECCE 2009; 2009. p. 2614–20.*

[16] B. Scrosati, J. Garche Lithium batteries: status, prospects and future

J Power Sources, 195 (2010), pp. 2419-2430, 10.1016/j.jpowsour.2009.11.048

[17] S. Gurski, Cold start effects on performance and efficiency for vehicle fuel cell system, MSc Thesis, Virginia Polytechnic Institute and State University, 2002.

[18] K. Johansson (Haraldsson), Modelling of a proton exchange membrane fuel cell system for automotive applications, Licentiate of Engineering Thesis, Royal Institute of Technology, Stockholm, Sweden, 2001

[19] Walker, P. D., Abdul Rahman, S., Zhu, B., & Zhang, N. (2013). Modelling, simulations, and optimisation of electric vehicles for analysis of transmission ratio selection. *Advances in Mechanical Engineering, 2013.*

[20] Morozov, A., Humphries, K., Zou, T., Martins, S., & Angeles, J. (2015). Design and optimization of a drivetrain with two-speed transmission for electric delivery step van. *2014 IEEE International Electric Vehicle Conference, IEVC 2014*.

[21] Abdelrahman, A. S., Algarny, K. S., & Youssef, M. Z. (2017). Optimal gear ratios selection for a nissan leaf: A case study of ingear transmission system. *2017 IEEE Energy Conversion Congress and Exposition, ECCE 2017*, *2017-January, 2079–2085.*

[22] Ren, Q., Crolla, D. A., & Morris, A. (2009). Effect of transmission design on Electric Vehicle (EV) performance. *5th IEEE Vehicle Power and Propulsion Conference, VPPC '09, 1260–1265.*